LIBRARY
Michigan State
University

This is to certify that the

dissertation entitled

Crystallographic Studies of Lipid Metabolism Proteins:
The Enzymes SQD1 and PGHS-1

presented by

Michael John Theisen

has been accepted towards fulfillment
of the requirements for

___Ph.D.___ degree in __Biochemistry__ and
Molecular Biology

Major professor

Date __11/6/2001__

PLACE IN RETURN BOX to remove this checkout from your record.
TO AVOID FINES return on or before date due.
MAY BE RECALLED with earlier due date if requested.

DATE DUE	DATE DUE	DATE DUE

CRYSTALLOGRAPHIC STUDIES OF LIPID METABOLISM PROTEINS:
THE ENZYMES SQD1 AND PGHS-1

By

Michael John Theisen

A DISSERTATION

Submitted to
Michigan State University
in partial fulfillment of the requirements
for the degree of

DOCTOR OF PHILOSOPHY

Department of Biochemistry and Molecular Biology

2001

ABSTRACT

CRYSTALLOGRAPHIC STUDIES OF LIPID METABOLISM PROTEINS:

THE ENZYMES SQD1 AND PGHS-1

By

Michael John Theisen

Lipids are important for cellular function, both as constituents of membranes and as precursors of signaling molecules. The work described here has involved crystallographic studies of two enzymes which function in lipid metabolism. Besides revealing new information about the enzymes themselves, the two projects highlight the challenges of conducting crystallographic studies with integral membrane proteins (*e.g.* PGHS-1), as compared to soluble proteins (*e.g.* SQD1).

Prostaglandin H_2 synthase-1 (PGHS-1), an integral membrane protein of the endoplasmic reticulum and nuclear envelope, catalyzes the committed step in formation of prostanoids. Its isoform, PGHS-2, performs the same reaction and is a key target of new pharmaceuticals designed to control inflammation, arthritis and possibly cancer. Although the crystal structure of PGHS-1 was solved in 1994, technical difficulties were slowing further progress. Therefore, the methods supporting structural biology (protein purification, crystallization and crystal mounting) were modified to reduce the

expendi

These i

PGHS-

photos

SQDB

sulfoq

protei

enzyn

unrea

of the

occur

hypo

"cata

disto

rely

bond

dete

T14

the

mut

expenditure of time and labor, while increasing the likelihood of success at each step. These improved techniques have begun to bear fruit in the form of more and better PGHS-1 crystal structures.

The sulfolipid sulfoquinovosyldiacylglycerol (SQDG) is nearly ubiquitous among photosynthetic organisms. SQDG production depends on a conserved enzyme, termed SQDB in bacteria and SQD1 in plants, which converts UDP-glucose and sulfite to UDP-sulfoquinovose. In this work, the crystal structure of SQD1 was determined. The overall protein fold confirmed its membership in the short-chain dehydrogenase/reductase (SDR) enzyme family. In the crystal structure, SQD1 binds both NAD^+ and UDP-glucose in an unreacted, "poised" state. This pause in the catalytic cycle may be due to misorientation of the nicotinamide ring of NAD^+, and presumably prevents untoward reactions from occurring before the sulfur donor has bound. Several amino acid residues were hypothesized to be important for the function of SQD1, particularly His183 and a "catalytic triad" of Thr145, Tyr182 and Lys186. All SQD1 structures have significant distortion of the Tyr182 phenol ring, which may support the theory that SDRs generally rely on an O_η-deprotonated tyrosine to initiate catalysis.

Thr145 is hypothesized to accelerate catalysis forming by low-barrier hydrogen bonds (LBHBs) to UDP-glucose and/or reaction intermediates. A T145A mutant had no detectable activity *in vitro*, using UDP-glucose and inorganic sulfite as substrates. T145A protein, treated with UDP-glucose and sulfite, was crystallized. Unexpectedly, the product UDP-sulfoquinovose was observed in the active site, demonstrating that the mutant enzyme retains residual activity. A number of future experiments are suggested.

DEDICATION

This work is dedicated to

my parents,

who taught me how to get along in the world,

my wife Jie,

who gave me a happy future,

and my daughter Rachel,

who is teaching me patience.

sacr

her

Penr

fini

fro

on

du

N

A

a

ACKNOWLEDGEMENTS

This work would not have been possible without help, encouragement and sacrifices from many people. First, I thank my wife and fellow biochemist, Jie Qian, for her constant support and advice, as well as love. I am grateful to my family in Pennsylvania and neighboring states, who patiently endured our six-year absence while I finished my doctorate. A big 谢谢 is due to my mother-in-law, Guifang Qian, who came from China and spent almost nine months providing child care, thus freeing me to work on this dissertation.

My advisor, Dr. R. Michael Garavito, provided financial and scientific support during my time in his laboratory. Several of my colleagues in the lab, Dr. Anne M. Mulichak, Dr. Opinya A. Ekabo, Ms. Melissa S. Harris, Dr. Michael G. Malkowski, Ms. Amy Scharmen and Mr. Micheal Dumond were especially important sources of advice and assistance.

My collaborators on the SQD1 project were Dr. Christoph Benning (also a member of the guidance committee) and members of his lab: Dr. Sherrie L. Sanda, Dr. Bernd Essigmann and Mr. Bart Leonard. Dr. Stephan L. Ginell and other staff at the Structural Biology Center, Advanced Photon Source, Argonne National Laboratory, collaborated in collecting the data used for the high-resolution SQD1 structure.

Dr. Alexander Tulinsky (also a former member of the guidance committee) and members of his lab, Dr. Jorge L. Ríos-Steiner, Dr. Raman Krishnan and Dr. Robert St. Charles, generously helped me with the theory and practice of crystallography. The other

PGHS

Int

E
S
C

Ma

Re

TABLE OF CONTENTS

LIST OF TABLES

LIST OF FIGURES

KEY TO SYMBOLS AND ABBREVIATIONS

Å, Ångström (10^{-10} m)
3αHDH, 3-α-hydroxysteroid dehydrogenase/carbonyl reductase
7αHDH, 7-α-hydroxysteroid dehydrogenase
AA, arachidonic acid
ADH, alcohol dehydrogenase
AGME, ADP-L-glycero-D-mannoheptose 6′-epimerase
APR1, adenosine-5′-phosphosulfate reductase 1f
APS, adenosine-5′-phosphosulfate
A. thal., Arabidopsis thaliana
ATS, ATP sulfotransferase
AuCN, KAu(CN)$_2$

BCA, bicinchoninic acid
Bis-Tris,
βKR, β-keto acyl carrier protein reductase
3α20βHDH, 3α,20β-hydroxysteroid dehydrogenase
17βHDH, 17β-hydroxysteroid dehydrogenase-I
20βHDH, 20-β-hydroxylsteroid dehydrogenase
β-OG, β-octyl glucoside
BSA, bovine serum albumin

C$_9$M, nonyl maltoside
C$_{10}$E$_7$, heptaethylene glycol monodecyl ether
C$_{10}$M, decyl maltoside
cBDH, *cis*-biphenyl-2,3-dihydrodiol-2,3-dehydrogenase
CGD, CDP-glucose 4,6-dehydratase
CR, carbonyl reductase
C. test., Comamonas testosteroni

DAG, diacylglycerol
DEAE, diethylaminoethyl
DEDTC, diethyldithiocarbamate
D. leb., Drosophila lebanonensis
D. mel., Drosophila melanogaster
DMSO, dimethyl sulfoxide
DPR, liver dihydropteridine reductase
dTGD, dTDP-glucose 4,6-dehydratase

E. coli, Escherichia coli
EDTA, ethylenediamine tetraacetic acid
EGF, epidermal growth factor
EMTS, ethylmercurithiosalicylate

ER.

F_c, s
F_u, s
FPL

g. th
GD
GM
GM
GSF
GSS

3HC
HEF
15H
HPL

IC,
IPTC

kDa.

MBI
mBE
MDE
MES

NAD
NAD
NE,
Ni-N
NMS
NSA

PAPS
PEG
PEG
PG, p
PGD,
PGE,
PGF,
PGG,
PGH,
PGHS
PGHS

ER, endoplasmic reticulum

F_c, structure factor amplitude, calculated
F_o, structure factor amplitude, observed
FPLC, fast protein liquid chromatography

g, the acceleration of gravity of Earth, at sea level
GDH, glucose dehydrogenase
GMD, GDP-mannose 4,6-dehydratase
GMER, GDP-4-keto-6-deoxymannose 3,5-epimerase 4-reductase (GDP-fucose synthase)
GSH, glutathione, reduced form
GSSG, glutathione, crosslinked oxidized form

3HCDH, 3-hydroxyacyl-CoA dehydrogenase
HEPES, 4-(2-hydroxyethyl)-1-piperazine-ethanesulfonic acid
15HPDH, 15-hydroxyprostaglandin dehydrogenase
HPLC, high pressure/performance liquid chromatography

IC_{50}, the concentration of inhibitor which results in half-maximal enzyme activity
IPTG, isopropyl-β-D-thiogalactoside

kDa, kiloDalton

MBD, membrane binding domain
mBDH, *meso*-2,3-butanediol dehydrogenase
MDH, mannitol 2-dehydrogenase
MES, 4-morpholineethanesulfonic acid

NAD^+, nicotinamide adenine dinucleotide, oxidized form
NADH, nicotinamide adenine dinucleotide, reduced form
NE, nuclear envelope
Ni-NTA, nickel-nitrilotriacetic acid
NMSDR, nucleotide-sugar modifying SDR
NSAID, nonsteroidal anti-inflammatory drug

PAPS, 3′-phosphoadenosine-5′-phosphosulfate
PEG 4000, polyethylene glycol of 4000 average molecular weight
PEG MME 550, polyethylene glycol monomethyl ether of 550 average molecular weight
PG, phosphatidyl glycerol
PGD_2, prostaglandin D_2
PGE_2, prostaglandin E_2
$PGF_{2\alpha}$, prostaglandin $F_{2\alpha}$
PGG_2, prostaglandin G_2
PGH_2, prostaglandin H_2
PGHS-1, prostaglandin H_2 synthase-1
PGHS-2, prostaglandin H_2 synthase-2

PGI. pr
PHMBS
PR. pte

RMSD.
rpm. re
RSM. r
RSV. r

S. ent..
SDR. s
SDS-P
SQD1.
SQDG
SR. se
S. typh

tetraH
TLC.
TMPD
TR-I.
TR-II
triHN
Tris. t
TxA₂

UDP.
UDP.
UO₂A
UGE

Z. th

PGI$_2$, prostaglandin I$_2$
PHMBS, para-hydroxymercuribenzenesulfonate
PR, pteridine reductase

RMSD, root mean squared deviation
rpm, revolutions per minute
RSM, ram seminal microsome
RSV, ram seminal vesicle

S. ent., *Salmonella enterica*
SDR, short-chain dehydrogenase/reductase
SDS-PAGE, sodium dodecyl sulfate polyacrylamide gel electrophoresis
SQD1, UDP-sulfoquinovose synthase
SQDG, 6-sulfo-α-D-quinovosyl diacylglycerol
SR, sepiapterin reductase
S. typh., *Salmonella typhimurium*

tetraHNR, 1,3,6,8-tetrahydroxynaphthalene reductase
TLC, thin-layer chromatography
TMPD, N,N,N′,N′-tetramethyl-*p*-phenylenediamine
TR-I, tropinone reductase-I
TR-II, tropinone reductase-II
triHNR, 1,3,8-trihydroxynaphthalene reductase
Tris, tris(hydroxylmethyl)aminomethane
TxA$_2$, thromboxane A$_2$

UDP-glucose, uridine-5′-diphospho-α-D-glucose
UDP-sulfoquinovose, uridine-5′-diphospho-α-D-sulfoquinovose
UO$_2$Ac, uranyl acetate.
UGE, UDP-galactose 4′-epimerase

Z, the number of molecules in the asymmetric unit of a crystal

Pr

blood clo

(1). In a

lung and

formatio

H_2 (PGH

by non

acetami

in resp

cellular

separat

is alter

specifi

PGI_2, a

with

forma

versio

functi

Introduction

Prostanoids and PGHS in human biology

Prostanoids play a major role in regulating physiological phenomena as diverse as blood clotting, gastric and renal homeostasis, parturition, inflammation, fever and pain (1). In addition, prostanoid formation is implicated as a cause of cancers of the colon, lung and breast, of arthritis and possibly of Alzheimer's disease. The committed step in formation of all prostanoids in the conversion of arachidonic acid (AA) to prostaglandin H_2 (PGH$_2$) by prostaglandin H_2 synthase (PGHS). Clinically, PGHS catalysis is inhibited by nonsteroidal anti-inflammatory drugs (NSAIDs) such as aspirin, ibuprofen, acetaminophen, Meloxicam, Celebrex and Vioxx.

The pathway of prostanoid biosynthesis (Figure 1) begins when phospholipases, in response to transduced signals, cleave at the *sn2* position of phospholipids in the cellular membranes to release AA. AA is then taken up by PGHS, which has two separate, heme-dependent catalytic activities: 1) cyclooxygenase (after which the enzyme is alternatively named) and 2) peroxidase. The product, PGH$_2$, is converted by various specific synthases to a number of bioactive products, including PGD$_2$, PGE$_2$, PGF$_{2\alpha}$, PGI$_2$, and TxA$_2$. The specific prostanoids made vary with cell type.

Two isoforms of PGHS are known to exist, both catalyzing the same reaction, but with differences in protein expression, kinetic parameters, and downstream product formation. PGHS-1, the best studied isoform, is described as the "house-keeping" version because it is constitutively expressed in most tissues and regulates normal functions like renal homeostasis, gastric acid secretion and the participation of platelets in

1
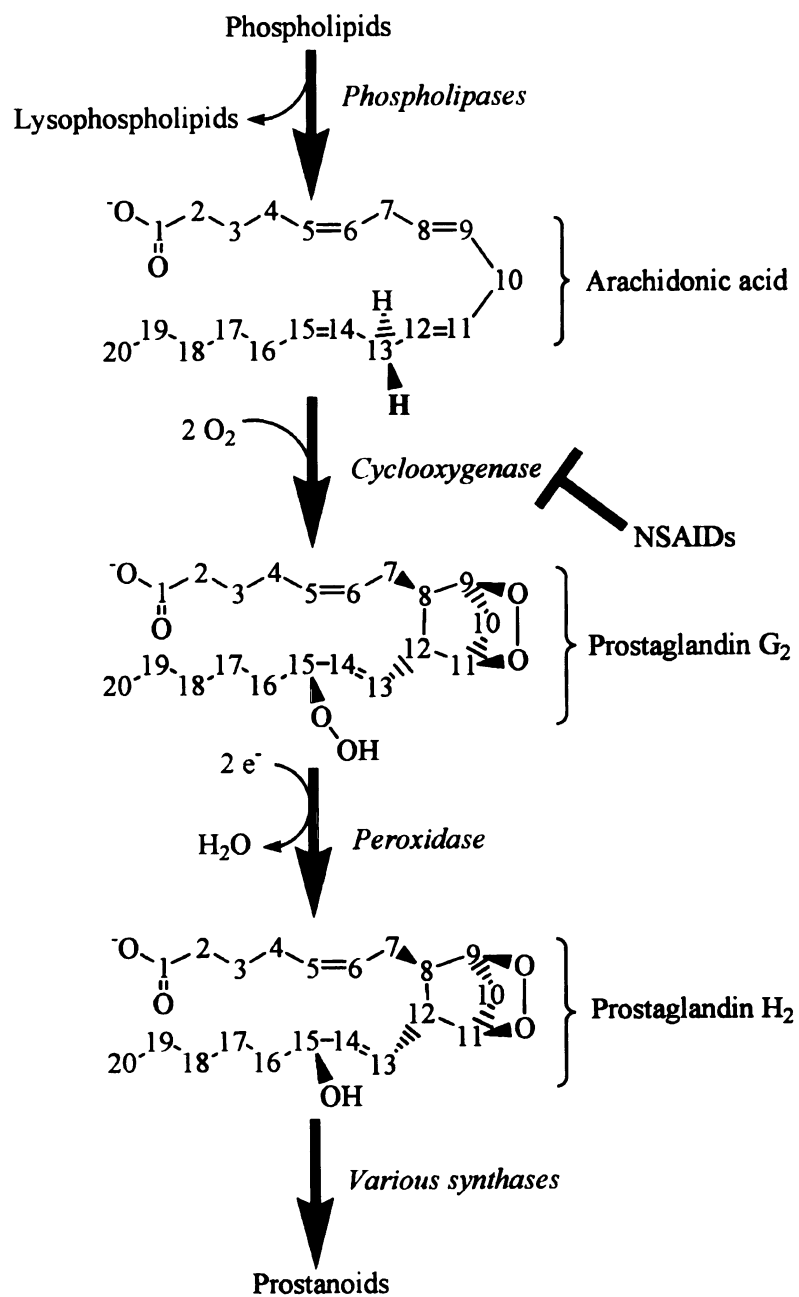
Figure 1. The pathway of prostanoid biosynthesis.

blood cl

induced l

tetradeca

proteins.

cleavage

two to

conditio

substrat

subcell:

localize

differe

vitro st

of hyd

the sar

cataly

colon

colon

PGH

Inhib

for p

inflar

disea

blood clotting. In contrast, PGHS-2 is normally absent from most tissues, but can be induced by a number of extracellular factors such as lipopolysaccharide (LPS) or 12-O-tetradecanoylphorbol 13-acetate (TPA) (1). Both isoforms are integral membrane proteins, having in their mature forms an apparent molecular weight of 72 kDa, after cleavage of an N-terminal endoplasmic reticulum-targeting signal and glycosylation of two to four asparagine residues (2). PGHS exists as a dimer under nondenaturing conditions and has never been isolated as an active monomer. These differences in substrate activation and downstream product formation cannot be easily rationalized by subcellular localization or compartmentation, since both isoforms seem to be similarly localized to the endoplasmic reticulum (ER) and nuclear envelope (NE) (3). Instead, differential substrate utilization by PGHS-1 and PGHS-2 may provide an explanation. *In vitro* studies have shown that PGHS-2 is more active than PGHS-1 at low concentrations of hydroperoxide or arachidonic acid (4-6). Thus, while both isoforms may be present at the same time and place, under the right conditions it is possible that only PGHS-2 may catalyze a greater fraction of substrate conversion.

Long-term prophylactic ingestion of aspirin greatly reduces the risk of developing colon cancer. It has been found that PGHS-2 is often overexpressed in cancers of the colon, lung and breast. PGHS-2 is inhibited by aspirin, though to a lesser degree than PGHS-1. Therefore, it is suspected that PGHS-2 may be involved in tumorigenesis. Inhibitors selective for PGHS-2, such as Vioxx, Celebrex and Meloxicam, hold promise for prevention and treatment of cancer, besides their current uses in ameliorating inflammation and symptoms of arthritis. Because of the role of PGHS in metabolism and disease, and because of the pharmacological significance of NSAIDs, understanding the

mechanisr

The PGH

A

shown in

heme. ra

the prote

the cyc!

autoinac

events.

largely

is retur

in vivc

abstrac

AA m

attacks

C12. a

by dor

The pi

where

mechanism of PGHS catalysis is an important goal relevant to human health.

The PGHS catalytic mechanism

A model of the PGHS catalytic mechanism, modified from that of Ruf *et al.*, is shown in Figure 2. An initial round of peroxidase catalysis is thought to form a ferryloxy heme, raising the iron oxidation state from +3 to +4 and producing a π-cation radical on the protoporphyrin ring. The radical then migrates to the O_η of Tyr385, where it supports the cyclooxygenase reaction; the radical also may be responsible for time-dependent autoinactivation of the enzyme, which apparently results from untoward crosslinking events. After this point, the cyclooxygenase and peroxidase activities can cycle in a largely independent fashion. To be ready for subsequent peroxidase reactions, the heme is returned to the +3 state by electron additions from a reducing substrate, whose identity *in vivo* is unknown. The tyrosyl radical initiates the cyclooxygenase reaction by abstracting the pro-*S* hydrogen atom from C13 of bound AA. The resulting radical on AA migrates to C11 and is attacked by a molecule of oxygen. The dioxygen in turn attacks C9 and forms an endoperoxide bridge. Next, a bond is made between C8 and C12, and a second molecule of dioxygen adds at C15. Finally, the radical is neutralized by donation of a hydrogen atom from the O_η of Tyr385, yielding a C15-hydroperoxide. The product of the cyclooxygenase reaction, PGG_2, binds at the peroxidase active site, where the hydroperoxide on C15 is reduced to an alcohol, giving the final product, PGH_2.

Figure 2. The Ruf model of PGHS catalysis. The enzyme initially exists in the Resting State. The plane of the protoporphyrin ring, which coordinates the heme iron, is represented by a trapezoid. The side chain of Tyr385 is shown. Electrons donated by the reducing substrate are given the symbol "e⁻".
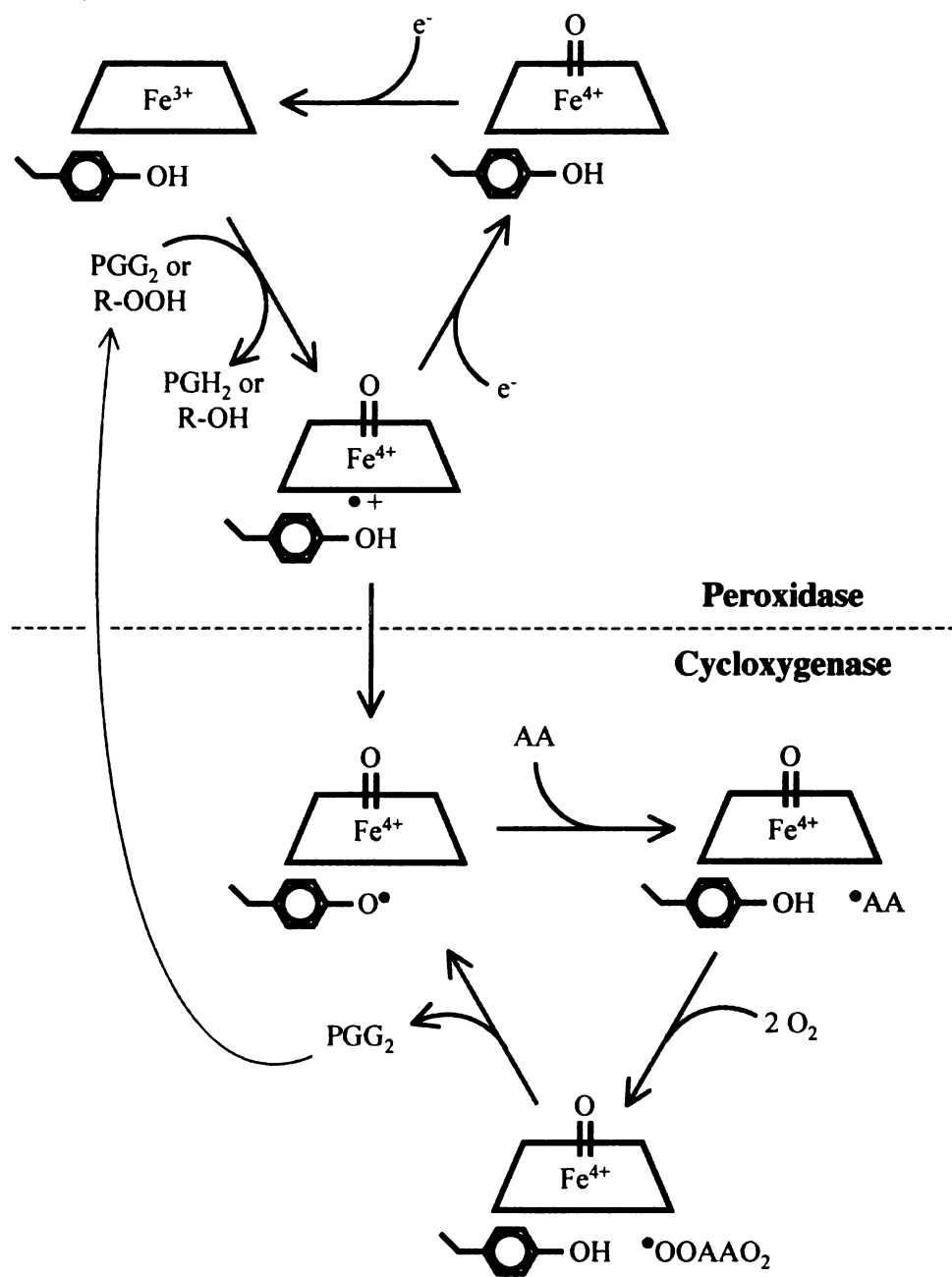
Figure 2

Pr

membra

bilayer.

biology.

Furtherm

such as

human

the Prot

in und

structur

al. and

contain

which

cycloo

monor

the fir

subdiv

growt

domai

solubl

which

Protein are classified as integral membrane proteins (hereafter simply called "membrane proteins") if detergent is required to disrupt their association with a lipid bilayer. Many membrane proteins, including PGHS, have important functions in human biology, for example in signal transduction as pores, ion channels and receptors. Furthermore, a large fraction of pharmaceuticals are targeted against membrane proteins such as G protein-coupled receptors. It is widely believed that approximately 20 % of human genes code for membrane proteins, yet only about 1 % of structures available at the Protein Data Bank are of this type. Considering the value of crystallographic studies in understanding soluble protein function, the relative dearth of membrane protein structures represents a serious handicap to researchers in this field.

The crystal structure of ovine PGHS-1 was solved to 3.5 Å resolution by Picot *et al.*, and later refined to 3.1 Å resolution (PDB entry 1CQE) (7). The asymmetric unit contains a dimer of PGHS-1 molecules (Figure 3). Each monomer binds a single heme, which physically separates the cyclooxygenase and peroxidase active sites. The cyclooxygenase sites in this complex were occupied by the inhibitor flurbiprofen. Each monomer consists of 576 amino acid residues, ordered from residue 32 to residue 583 in the first monomer, and from to 31 to 583 in the second. The monomer structure can be subdivided into three domains, arranged from the N- to the C-terminus: 1) an epidermal growth factor (EGF)-like domain involved in the dimer interface, 2) a membrane binding domain (MBD) and 3) a large, solvent-exposed domain with structural homology to soluble peroxidases. The MBD is composed of a spiral of four amphipathic helices, which create a hydrophobic surface that apparently anchors PGHS in only one leaflet of

the lipi

membr

also fo

and he

deterge

from t

Howev

cycloc

PGHS

crysta

purifi

for s

crysta

struct

cyclo

chlor

batch

purifi

PEG.

pertu

succe

of the

the lipid bilayer, in contrast to transmembrane proteins which traverse both leaflets of the membrane (7,8). Besides integrating PGHS into the membrane, the helices of the MBD also form a channel leading into the cyclooxygenase active site. In addition to the protein and heme, several asparagine-linked sugar residues and β-octyl glucoside (β-OG) detergent molecules were observed in the crystal structure. Crystal structures of PGHS-2 from two species are also available, and are very similar to that of PGHS-1 (9,10). However, subtle but significant differences in the volume and shape of the cyclooxygenase active site have allowed the development of drugs that inhibit only PGHS-2, and not PGHS-1.

As with other membrane proteins, a major obstacle to comprehensive crystallographic studies of PGHS-1 was the greater time and effort required for purification, crystallization and collection of diffraction data, compared to what is typical for soluble proteins. For example, the original purification procedure gave crystallization-quality about two thirds of the time. The crystals used for the original structure determination, and for subsequent studies of complexes with different cyclooxygenase inhibitors, were grown using polyethylene glycol 4000 and sodium chloride as precipitants. Under these conditions, about half of the crystallizable protein batches gave crystals of diffraction quality. Thus, only about every third cycle of purification and crystallization resulted in useable diffraction data. These PEG4000/NaCl crystals were sensitive to physical manipulation and to chemical perturbation. As a result, they could not be stored for extended periods and had a low success rate for collection of X-ray diffraction data. Conditions allowing cryoprotection of the crystals for data collection had not been identified, effectively eliminating the

8

Figure 3. The crystal structure of ovine PGHS-1. The asymmetric unit, containing a dimer of PGHS molecules, is shown. The protein backbone of Monomer A is represented by orange tubes, while that of monomer B is dark blue. The heme atoms in each monomer are depicted as red spheres, while those of the inhibitor flurbiprofen, bound in the cyclooxygenase channel, are green. Sugar and β-octyl glucoside molecules, shown as stick models, are colored by element type (gray=carbon, red=oxygen, blue=nitrogen). Space-filling models of dimyristoyl phosphatidyl glycerol (not observed in the crystal structure), colored by element type (as above, and purple=phosphorus), have been placed to suggest the interaction of PGHS-1 with one leaflet of a membrane bilayer. Since the depth to which the MBD is inserted is not precisely known (8), the position of the phospholipids is only approximate. This and other molecular images were prepared with one or more of the following programs: Swiss-Pdb Viewer 3.7b2 (11), POV-Ray 3.1, POV-Ray 3.5, spock 1.0b170 (12), Raster3D 2.6b (13) and SETOR 2001 (14). Images in this dissertation are presented in color.
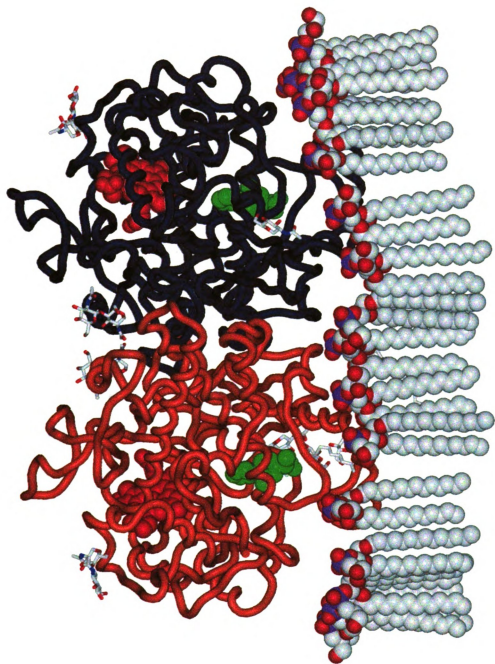
Figure 3

possi

prote

PGH

colle

whil

the

poss

with

crys

com

crys

inte

com

ana

bin

acti

fina

PGl

bet

possibility of using of synchrotron radiation, whose high intensity quickly destroys protein crystals at ambient temperature.

Objectives of the PGHS project

The initial goal of this project was to improve all of the experimental stages of PGHS-1 crystal structure determination, *i.e.* purification, crystallization and data collection. For purification, we wanted to increase speed, specific activity and yield, while reducing lipid contamination. For crystallization, we wanted to reproduce readily the original crystals, as well as identify newer, more tractable crystallization regimes and possibly develop new, better-ordered crystal forms. Because soaking or cocrystallization with a ligand could easily disorder any one particular type of crystal, having multiple crystal forms could also increase the chances of solving the structure of a protein/ligand complex. Lastly, diffraction data quality was to be improved by cryoprotecting the crystals to largely eliminate radiation damage. Additionally, cryoprotection would allow intense synchrotron X-rays to be used, so that higher-resolution data might be obtainable.

Another original goal in studying PGHS-1 was to solve the structures of complexes with peroxidase inhibitors. While extensive structural and biochemical analysis of cyclooxygenase inhibition had been done, relatively little was known about binding or reaction of ligands in the peroxidase active site. Understanding the peroxidase activity is important because of its role in initial enzyme activation, in formation of the final product PGH_2, and potentially in the activation of procarcinogenic compounds. PGHS-1 uses hydroperoxides less avidly than PGHS-2, and any point of difference between the two isoforms is an opportunity to design an isozyme-specific inhibitor with

11

potent

Ekabc

PGHS

actual

AHA

AHA

PGHS

in a p

mode

(15). I

cause

reduce

the st

correl

optim

homo

(RR)

substr

use cy

oxyge

compl

ovine

potential therapeutic applications. To begin studying peroxidase inhibition, Dr. Opinya Ekabo had synthesized a series of arylhydroxamic acid (AHA) derivatives that inhibited PGHS-1 peroxidase activity to varying degrees. These AHA peroxidase inhibitors actually are tightly-binding reducing substrates that react poorly. The ability of each AHA inhibitor to act as a reducing substrate was inversely correlated with its IC_{50}. These AHA inhibitors have a constant hydroxamic acid portion, which can act to reduce the PGHS heme, and a variable, nonreactive hydrophobic portion, which is believed to bind in a protein pocket adjacent to the site of the peroxidase reaction. A similar binding mode of AHA inhibitors is seen in the structurally related enzymes myeloperoxidase (15), horseradish peroxidase (16) and *Arthromyces ramosus* peroxidase (17,18).

Our hypothesis was that differential binding by the hydrophobic part of the AHAs causes misalignment of the reactive hydroxamic acid portion, thus impairing its ability to reduce the heme, while still blocking access by hydroperoxide substrates. By comparing the structures of a series of complexes, and observing trends in binding pattern that correlated with inhibitory efficacy, we hoped to identify the binding mode that led to optimal ligand/heme reactivity. These PGHS-1/AHA structures were to be compared to homologous PGHS-2/AHA complexes, and also to dynamic data from resonance Raman (RR) spectroscopy, to understand why the two isoforms are differently activated by substrates. In addition to mimicking substrate binding with AHAs, another goal was to use cyanide as a model for oxygen binding to the heme iron. In fact, since AHAs and oxygen can bind simultaneously to PGHS, it was conceivable that PGHS/AHA/cyanide complexes could be obtained. Cyanide has since been shown to bind the heme iron of ovine PGHS-1 perpendicular to the protoporphyrin plane (19). A final potential objective

was t

Proje

protei

level

PGHS

struct

was to crystallize and solve the structure of apo-PGHS, *i.e.* enzyme missing the heme. Projects such as these, which involve purifying and crystallizing large amounts of protein, and which require collection of many X-ray diffraction datasets, demand a high level of technical support. Through a group effort, the experimental methods for PGHS-1 crystallography have been greatly improved, providing continued benefits to structural biology studies of PGHS-1.

Measure

ability

carried

contain

equine

tetram

2.86

samp

obse

The

32°

whi

sec

the

bi

C

d

v

b

Materials and Methods

Measurement of peroxidase activity

To monitor PGHS catalytic competence, for example during purification, the ability of the enzyme to degrade hydrogen peroxide (H_2O_2) is measured. The assay is carried out at ambient temperature. An aliquot (usually 1 to 100 μL) of solution containing PGHS is added to a cuvette containing buffer (95 mM Tris, pH 8.0), 1.75 μM equine hemin (from a stock dissolved in dimethyl sulfoxide, DMSO) and 105 mM tetramethylphenyldiamine (TMPD, from a stock dissolved in DMSO) in a total volume of 2.86 mL. Two minutes of incubation at room temperature are necessary for the protein sample to achieve 95% of maximal incorporation of exogenous hemin (personal observation). The contents of the cuvette at this point are used as an absorbance blank. The reaction is initiated by mixing in 100 μL of 9 mM H_2O_2 (prepared that day from a 32% stock) giving a final H_2O_2 concentration of 0.3 mM. The absorbance at 611 nm, which is the absorption maximum of oxidized TMPD, is monitored for a period of twenty seconds. As a control, several assays in the absence of protein are also done to determine the rate of TMPD oxidation due solely to the presence of hemin, called the "activity blank".

The initial rate in absorbance units per second is estimated with Hewlett-Packard Chemstation software using nonlinear curve fitting. One unit of peroxidase activity is defined as the amount of enzyme required to reduce 1 μmole of hydrogen peroxide to water in 1 minute at room temperature. The rate in AU/s is converted to standard units by subtracting the value of the "activity blank", then multiplying by 7.5. This calculation

is deri

U

wher

enti

val

hep

res

non

do

the

res

ac

is derived as follows:

$$U_c = \frac{(Ap - Ab)\, v\, d}{2\, \varepsilon}\ (60\ \text{sec/min})\ (10^6\ \mu\text{mol/mol})$$

where U_c is the total activity in the cuvette

A_p is the initial slope of the absorbance at 611 nm in AU/s (with protein),

A_b is the initial slope of the absorbance at 611 nm in AU/s for the activity blank,

v is the volume in the cuvette (0.003 L),

d is the path length of light through the sample (1 cm), and

ε is the molar extinction coefficient of oxidized TMPD (12000 AU cm L mol^{-1}).

Because two molecules of TMPD are necessary for one peroxidation cycle, the entire equation is divided by 2.

A specific activity of 40 U/mg for PGHS-1 in β-OG is considered pure, but this value may be somewhat different in other detergents; for example, it is typically higher in heptaethyleneglycol monodecyl ether ($C_{10}E_7$). A complicating factor in interpreting the results of the peroxidase assay is that PGHS has high K_m's for H_2O_2 and TMPD. Because nonsaturating concentrations of H_2O_2 and TMPD are used, the assay described above does not always follow Michaelis-Menten kinetics. When the concentration of PGHS in the cuvette is high, the substrates are rapidly depleted, which slows the reaction and results in an underestimation of the true amount of activity present. Dilution of very active protein samples prior to assay should partially alleviate this potential inaccuracy.

Determination of protein concentration by the Bradford assay

In early work, protein concentration was estimated with the Bradford assay (Bio-Rad). For this assay, standards are prepared using bovine serum albumin (BSA) in the range of 0 to 20 µg in a volume of 200 µL. Samples of the protein of interest are similarly prepared. To each standard and sample, 800 µL of Bradford reagent are added and mixed. In a modification of the usual Bradford assay protocol, the absorbance of the mixture at both 594 nm (A_{594}) and 466 nm (A_{466}) is measured spectrophotometrically (20). The ratio A_{594}/A_{466} is plotted *versus* BSA concentration to form a standard curve, from which the concentration of protein in the samples is estimated by interpolation.

Determination of protein concentration by the bicinchoninic acid (BCA) assay

In later work, protein concentration was estimated with the bicinchoninic acid (BCA) assay kit from Pierce, again using BSA as a standard. The BCA assay has the advantages over the Bradford assay of a larger dynamic range, less sensitivity to interference by detergents and greater stability of absorbance readings over time. As described in the manufacturer's instructions, 50 volumes of Reagent A (containing bicinchoninic acid) are mixed with 1 volume of Reagent B (containing $CuSO_4$) to give the Working Reagent, which has a green color. Standards are prepared by mixing each of a series of 100 µL samples, containing 0 to 200 µg of BSA, with 2.0 mL of the Working Reagent. Samples containing PGHS are set up at the same time and in the same manner as the standards, and all of the test tubes are incubated in a 37°C water bath for 30 minutes. The tubes are removed and cooled to room temperature. Those samples where protein is present will have a purple color. Quantitative measurements of absorbance at

16

562 nm

concent

Chemst

automa

Detern

presur

Stand

standa

total

μL c

unca

thoro

to cc

gent

volu

in 1

is a

mir

det.

ver

pho

562 nm (A_{562}) are taken spectrophotometrically. A standard curve of A_{562} vs. BSA concentration is plotted, and a best-fit line is derived by the Hewlett-Packard Chemstation software using a quadratic equation. The concentration of PGHS is automatically estimated by interpolation from the BSA standard curve.

Determination of phospholipid concentration by the Ames phosphate assay

The Ames phosphate assay can be used to measure total phosphate content, which presumably provides an estimate of the amount of phospholipids present (21,22). Standards are made up from stock solutions of KH_2PO_4 or phosphatidyl choline. Each standard or sample, having a volume of 10-100 μL and no more than 80-90 nanomoles of total phosphate, is pipetted into a *very clean*, acid-washed Pyrex or Kimax vial, and 30 μL of 10% (w/v) $Mg(NO_3)_2 \cdot 6H_2O$ in 95% ethanol is added. The contents of the uncapped vials are carefully dried by heating over a Bunsen burner flame, then thoroughly ashed in the flame until no more brown fumes are seen. The vials are allowed to cool, then 300 μL of 0.5 M HCl is added to each. The vials are sealed and boiled gently for 15 minutes. Next, a fresh batch of Color Reagent is made by combining 1 volume of 10% (w/v) ascorbic acid with 6 volumes of 0.42% (w/v) $(NH_4)_6Mo_7O_{24} \cdot 4H_2O$ in 1 M H_2SO_4; the Color Reagent is kept on ice. To each vial, 0.7 mL of Color Reagent is added and mixed by vortexing. The vials are heated in a 45°C water bath for 20 minutes, then cooled. The absorbance at 820 nm (A_{820}) of the solution in each vial is determined spectrophotometrically using a quartz cuvette. A standard curve of A_{820} *versus* phosphate concentration is constructed for the KH_2PO_4 standards, and the phosphate concentration in the samples is estimated by interpolation from the standard

curve.

Detectio

microp

asolecti

The pl

dried i

sampl

by m

revea

com

atop

1.3

Dr

ch

v

o

c

curve.

Detection of lipids and detergents by thin layer chromatography (TLC)

Glass or aluminum plates, coated with silica (Sigma), are used for TLC. Using a micropipette, a plate is spotted with samples and with standards such as recrystallized soy asolectin (Associated Concentrates), egg lecithin phosphatidic acid (Sigma) and KH_2PO_4. The plate is developed with $CHCl_3:CH_3OH:NH_4OH$ (65:35:5;v/v) in a glass chamber, dried in an oven, and then treated by one or more methods to reveal the chromatographed samples and standards. Chemicals for identifying samples can be sprayed onto the plate by means of a glass atomizer (Aldrich). Exposing a plate to iodine vapor temporarily reveals many compounds as brown marks. To permanently reveal all carbonaceous compounds, the plate may be sprayed with 50% (v/v) H_2SO_4 and charred in a Pyrex dish atop a hot plate. Phospholipids can be detected specifically by spraying the plate with 1.3% (w/v) molybdenum oxide in 4.2 M H_2SO_4 (Sigma), producing blue spots. The Dragendorff reagent, which reacts with alkaloids and nitrogen, is used to detect the choline group of phosphocholine. The Dragendorff reagent is prepared by mixing 1 volume of Solution A (1.7% (w/v) bismuth oxinitrate in 20% (v/v) acetic acid), 1 volume of Solution B (aqueous potassium iodide) and 4 volumes of acetic acid, then adding water or ethyl acetate to a total of 20 volumes. Finally, free amino groups, as in phosphatidyl serine, are revealed by 0.2 % (w/v) ninhydrin in 95% ethanol.

Sodium dodecyl sulfate polyacrylamide gel electrophoresis (SDS-PAGE)

For analysis of protein samples by sodium dodecyl sulfate polyacrylamide gel

ele

the

acr

wit

run

San

(2.5

0.0(

ther

the

incu

meth

with

(40°

Puri

(Oxf

thawe

thawe

region

mM T

temper

electrophoresis (SDS-PAGE), discontinuous gels are used. The stacking gel containing the sample wells is composed of 5% (w/v) polymerized acrylamide with 0.13% bis-acrylamide crosslinker, while the resolving gel is 10% (w/v) polymerized acrylamide with 0.27% bis-acrylamide crosslinker. Gels are placed in a Hoefer SE250 apparatus and running buffer (25 mM Tris, 192 mM glycine, 0.1% (w/v) SDS, pH 8.3) is added. Samples are prepared by adding 3 volumes of sample to 1 volume of 4X sample buffer (2.5 mL Upper Buffer, 8% (w/v) SDS, 8% (v/v) β-mercaptoethanol, 40% (w/v) glycerol, 0.008% (w/v) Bromophenol Blue) and heating for five minutes in a boiling water bath, then loaded into the wells of the gel. The samples are drawn electrophoretically through the gel with a potential of 100 V and at maximum current. The protein is visualized by incubation in staining buffer (0.25% (w/v) Coomassie Brilliant Blue R250, 45.5% (v/v) methanol, 9.2% (v/v) glacial acetic acid) at ambient temperature for 30 minutes or longer, with agitation. Nonspecific staining is removed with repeated washes in destain buffer (40% (v/v) methanol, 10% (v/v) glacial acetic acid). Gels are photographically recorded.

Purification of PGHS-1 ram seminal microsomes from ram seminal vesicles

Ram seminal vesicles (RSVs) are obtained from Oxford Biomedical Research (Oxford, Michigan) and stored at -80°C. Prior to use, approximately 350 g of RSVs are thawed sufficiently so that they can be cut with a razor blade or knife. The partially thawed, pinkish-yellow RSVs are trimmed of fat, connective tissue and any discolored regions, then cut into small cubes and covered with ice-cold homogenization buffer (50 mM Tris, 5 mM EDTA, 1 mM NaN_3, 5 mM DEDTC, adjusted to pH 8.0 at room temperature). All subsequent steps are carried out at 4°C or on ice. The trimmed vesicles

and hom

give a t

pellet

(micros

layers (

the m

resusp

DEDT

8.0 a

perch

mem

minu

micr

mM

Elvo

ass

mL

sto

tin

O

w

and homogenization buffer are blended in two 90 second stages with a Waring Blendor to give a thin, homogenous pink paste, which is centrifuged for 10 minutes at 12,000g to pellet cellular debris. The pink supernatant, containing disrupted membranes (microsomes) and soluble cellular components, is cleared of fat by straining through four layers of cheesecloth. The filtrate is ultracentrifuged for 75 minutes at 200,000g to pellet the microsomes, and the clear supernatant solution is discarded. The pellet is resuspended in extraction buffer (50 mM Tris, 1 mM EDTA, 1 mM NaN_3, 0.1 mM DEDTC, 0.1 M sodium perchlorate ($NaClO_4$, from a freshly made stock), adjusted to pH 8.0 at room temperature), using a motor-driven Potter-Elvehjem homogenizer. The perchlorate strips peripheral membrane proteins from the microsomes, but leaves integral membrane proteins. The resuspended material is ultracentrifuged at 200,000g for 75 minutes to pellet the microsomes, and the supernatant solution is discarded. The pelleted microsomes are quickly resuspended in storage/solubilization buffer (20 mM Tris, 0.05 mM EDTA, 0.1 mM DEDTC, adjusted to pH 8.0 at room temperature) with the Potter-Elvehjem homogenizer to dilute the oxidizing perchlorate. Peroxidase activity is assayed, and the resuspended microsomes are typically diluted to a total volume of 60 mL, split into three batches of 1200-1300 U each, then flash-frozen in liquid nitrogen and stored at -80°C. The activity of frozen microsomes declines slowly but steadily over time, becoming significant less after about six months of storage.

Optimization of detergent extraction of PGHS-1 from ram seminal microsomes

Detergents were obtained from Anatrace (Maumee, Ohio), except $C_{10}E_7$, which was purchased from Fluka (Buchs, Switzerland); ram seminal microsomes had been

prepared

stored at

Further

combine

concent

were st

micros

supern

gauge

the ar

chrom

protei

Mich

by d

remo

then

3.75

dete

foan

the

prepared previously and kept at -80°C. Tubes of ram seminal microsomes (RSMs), stored at -80°C, were rapidly thawed in room temperature water baths, with stirring. Further work was carried out at 4°C or on ice. Small aliquots of thawed RSMs were combined with detergent stock solutions and buffer in various ratios so that the concentrations of both protein and detergent were systematically varied. The mixtures were stirred vigorously, but without foaming, for 20 minutes to extract PGHS-1, and the microsomes were pelleted by microultracentrifugation at 200,000g for one hour. The supernatant solution, containing solubilized membrane proteins, was characterized to gauge the success of the extraction. Peroxidase activity was determined as a measure of the amount of PGHS-1 present. Lipid contamination was estimated by thin-layer chromatography (TLC) and by the Ames phosphate assay, both described above. Total protein concentration was measured by the Bradford assay, described above.

Purification of solubilized PGHS-1 from ram seminal microsomes:

All chromatography resins were purchased from Pharmacia (Kalamazoo, Michigan). For each purification, a fresh 0.1 M stock of flurbiprofen (Sigma) is prepared by dissolving in absolute ethanol. On the first day, an aliquot of frozen microsomes is removed from storage at −80°C, rapidly thawed in a stirred room temperature water bath, then placed on ice. A 26.25 mL volume of storage/solubilization buffer (see above) and a 3.75 mL aliquot of 10% (w/v) $C_{10}E_7$ is added to give a final volume of 50 mL and a final detergent concentration of 0.75%. This mixture is stirred on ice, vigorously but without foaming, for 30 minutes. The solution is ultracentrifuged at 200,000g for 90 minutes and the pellet is discarded. The supernatant solution is loaded at 2 mL/min directly onto a 2.6

× 40 cr

mM T

tempe

fractic

of Bu

Buffe

mM

rest

as B

frac

per

cer

co

fil

l

r

C

a

× 40 cm DEAE-Sepharose FastFlow column, previously equilibrated with Buffer A (10 mM Tris, 10 mM Bis-Tris, 1 mM NaN_3, 0.1% (w/v) $C_{10}E_7$, adjusted to pH 8.5 at room temperature). Sample and buffers are loaded at 2 mL/min; the eluent is collected in 8mL fractions throughout the procedure. The column is first washed with an additional 50 mL of Buffer A, then PGHS-1 is eluted with a linear gradient from 100% Buffer A to 100% Buffer B (40 mM Tris, 40 mM Bis-Tris, 20 mM NaCl, 1 mM NaN_3, 0.05 mM EDTA, 0.1 mM DEDTC, 0.1% (w/v) $C_{10}E_7$, adjusted to pH 6.5 at room temperature). Finally, the rest of the proteins are eluted with a gradient from 100% Buffer B to 40% Buffer C (same as Buffer B, but with 500 mM NaCl), followed by a step gradient to 100% Buffer C. The fractions are pooled based on the amount of enzymatic activity in each, as determined by peroxidase activity. The pooled fractions are concentrated with Millipore Ultrafree centrifugal concentrators with a nominal molecular weight cutoff of 50 kDa. The concentrated material is loaded at 1 mL/min onto a 1.6 × 70 cm Sephacryl 300-HR gel filtration column, previously equilibrated with elution buffer (20 mM Tris, 50 mM NaCl, 1 mM NaN_3, 0.1 mM EDTA, 0.1 mM DEDTC, 0.1% (w/v) $C_{10}E_7$, adjusted to pH 8.0 at room temperature). The protein is eluted overnight with the same buffer at 0.2 mL/min. On the second day, the active fractions are pooled and concentrated as described above, and an aliquot of 30% (w/v) β-OG is added to a final concentration of 0.9% (w/v). To complete the exchange of $C_{10}E_7$ for β-OG, the solution is loaded onto a 1.6 cm × 40 cm S200-HR gel filtration column, previously equilibrated with elution buffer (20 mM potassium phosphate, 50 mM NaCl, 1 mM NaN_3, 0.1 mM EDTA, 0.1 mM DEDTC, 0.1 mM flurbiprofen, 0.3% (w/v) β-OG, adjusted to pH 7.4 at room temperature). The protein is eluted with the same buffer at a flow rate of 0.2 mL/min, and leaves the column

just afte

above.

presenc

stock ir

to reco

Slide-a

(20 m\`

room

conce

result

save

ident

Proc

diff

Cal

All

cry

ma

of

pi

sp

just after the void volume. Active fractions are pooled and concentrated as described above. The amount of apoenzyme is estimated by comparing peroxidase activity in the presence and absence of exogenous hemin. An amount of equine hemin (from a 4 mM stock in DMSO) equal to the amount of apoenzyme, with a 10 to 100% excess, is added to reconstitute PGHS to the holoenzyme form. The reconstituted enzyme is loaded into a Slide-a-Lyzer dialysis cassette (Pierce) and dialyzed against 250 mL of dialysis buffer (20 mM HEPES, 20 mM NaCl, 1 mM NaN₃, 0.1 mM flurbiprofen, 0.5% β-OG, pH 7.0 at room temperature) for approximately 24 hours, at 4°C and with stirring. The protein concentration of the dialyzed material should be 10-20 mg/mL. An aliquot of the resulting material is immediately used for initial crystallization screens, while the rest is saved on ice until the optimal crystallization conditions for the current batch have bee identified.

Production of PGHS-1 crystals under the original conditions

Crystallization experiments were conducted using the hanging drop vapor diffusion method in Linbro tissue culture plates (Hampton Research, Laguna Niguel, California). A ring of vacuum grease was placed around the top of each well in the plate. All drop stock and reservoir solutions were prepared prior to setting up the crystallization. Drop stock solutions typically contained 0.4% (w/v) β-OG and otherwise matched the least concentrated reservoir in each row of the crystallization tray. Two μL of purified, dialyzed PGHS-1 at a concentration of approximately 10 mg/mL were pipetted onto a round, 22 mm diameter cover slip (siliconized to minimize drop spreading). An equal volume of appropriate drop stock solution was added to the protein

drop and mi

placed over

solution. T

the ring of

Screening

Cry

kits (Tabl

contains 5

CSII cont

diffusion

crystalliz

each Crys

Crystalli

C

Cryscher

solutions

range of

contain

the tray.

0.20 to

citrate, p

drop and mixed approximately five times by aspiration. The cover slip was inverted and placed over one chamber of the Linbro plate, containing 0.5 mL of appropriate reservoir solution. The chamber was sealed by carefully pressing and twisting the cover slip into the ring of vacuum grease.

Screening for new PGHS-1 crystallization conditions

Crystal Screen I (CSI) and Crystal Screen II (CSII) sparse matrix crystallization kits (Tables 1 and 2) and Linbro trays were purchased from Hampton Research. CSI contains 50 unique crystallization solutions (at least two reagents were not used), while CSII contains 48 (Reagents 5, 8 and 44 were excluded). The hanging drop vapor diffusion method was employed, as described above, however only 0.3 mL of each crystallization solution was used per reservoir, and drops were set up by mixing 2 µL of each Crystal Screen solution with 2 µL of protein.

Crystallization of PGHS-1 in the orthorhombic form, using sodium citrate as precipitant

Crystallization is achieved with the sitting drop vapor diffusion method, using Cryschem crystallization trays (Hampton Research). For the reservoirs, six stock solutions are prepared, one for each column in the tray. The reservoir solutions cover a range of sodium citrate concentrations, typically from 0.68 to 0.88 M, at pH 6.5, and also contain 1 mM sodium azide. Four drop stock solutions are prepared, one for each row of the tray. The drop stock solutions cover a range of β-OG concentrations, typically from 0.20 to 0.45 % (w/v). The drop stocks also contain 1 mM sodium azide and sodium citrate, pH 6.5, at a concentration matching that of the least concentrated reservoir. First,

Solutions in Crystal Screen I

Table 1

Solutions in Crystal Screen I

#	Component(s)
1	30% v/v 2-Methyl-2,4-pentanediol, 1 M Sodium Acetate trihydrate pH 4.6, 0.02 M Calcium Chloride dihydrate
2	0.4 M Potassium Sodium Tartrate tetrahydrate
3	0.4 M mono-Ammonium dihydrogen Phosphate
4	2.0 M Ammonium Sulfate, 0.1 M Tris Hydrochloride pH 8.5
5	30% v/v 2-Methyl-2,4-pentanediol, 0.1 M HEPES – Na pH 7.5, 0.2 M tri-Sodium Citrate dihydrate
6	30% w/v PEG 4000, 0.1 M Tris Hydrochloride pH 8.5, 0.2 M MgCl2 hexahydrate
7	1.4 M Sodium Acetate trihydrate, 0.1 M Sodium Cacodylate pH 6.5
8	30% v/v iso-Propanol, 0.1 M Sodium Cacodylate pH 6.5, 0.2 M tri-Sodium Citrate dihydrate
9	30% w/v PEG 4000, 0.1 M tri-Sodium Citrate dihydrate pH 5.6, 0.2 M Ammonium Acetate
10	30% w/v PEG 4000, 0.1 M Sodium Acetate trihydrate pH 4.6, 0.2 M Ammonium Acetate
11	1.0 M mono-Ammonium dihydrogen Phosphate, 0.1 M tri-Sodium Citrate dihydrate pH 5.6
12	30% v/v iso-Propanol, 0.1 M HEPES - Na pH 7.5, 0.2 M MgCl2 hexahydrate
13	30% v/v PEG 400, 0.1 M Tris Hydrochloride pH 8.5, 0.2 M tri-Sodium Citrate dihydrate
14	28% v/v PEG 400, 0.1 M HEPES – Na pH 7.5, 0.2 M Calcium Chloride dihydrate
15	30% w/v PEG 8000, 0.1 M Sodium Cacodylate pH 6.5, 0.2 M Ammonium Sulfate
16	1.5 M Lithium Sulfate monohydrate, 0.1 M HEPES - Na pH 7.5
17	30% PEG 4000, 0.1 M Tris Hydrochloride pH 8.5, 0.2 M Lithium Sulfate, monohydrate
18	20% PEG 8000, 0.1 M Sodium Cacodylate pH 6.5, 0.2 M Magnesium Acetate tetrahydrate
19	30% v/v iso-Propanol, 0.1 M Tris Hydrochloride pH 8.5, 0.2 M Ammonium Acetate
20	25% w/v PEG 4000, 0.1 M Sodium Acetate trihydrate pH 4.6, 0.2 M Ammonium Sulfate
21	30% v/v 2-Methyl-2,4-pentanediol, 0.1 M Sodium Cacodylate pH 6.5, 0.2 M Magnesium Acetate tetrahydrate
22	30% w/v PEG 4000, 0.1 M Tris Hydrochloride pH 8.5, 0.2 M Sodium Acetate trihydrate
23	30% v/v PEG 400, 0.1 M HEPES - Na pH 7.5, 0.2 M Magnesium chloride hexahydrate
24	20% v/v iso-Propanol, 0.1 M Sodium Acetate trihydrate pH 4.6, 0.2 M Calcium Chloride dihydrate
25	1.0 M Sodium Acetate trihydrate, 0.1 M Imidazole pH 6.5

Components(s)

30 % v/v 2-Methyl-2,4-pentanediol, 0.1 M tri-Sodium Citrate dihydrate pH 5.6, 0.2 M Ammonium Acetate

Table 1 continued

#	Component(s)
26	30 % v/v 2-Methyl-2,4-pentanediol, 0.1 M tri-Sodium Citrate dihydrate pH 5.6, 0.2 M Ammonium Acetate
27	20% v/v iso-Propanol, 0.1 M HEPES - Na pH 7.5, 0.2 M tri-Sodium Citrate dihydrate
28	30% w/v PEG 8000, 0.1 M Sodium Cacodylate pH 6.5, 0.2 M Sodium Acetate trihydrate
29	0.8 M Potassium Sodium Tartrate tetrahydrate, 0.1 M HEPES - Na pH 7.5
30	30% w/v PEG 8000, 0.2 M Ammonium Sulfate
31	30% w/v PEG 4000, 0.2 M Ammonium Sulfate
32	2.0 M Ammonium Sulfate
33	4.0 M Sodium Formate
34	2.0 M Sodium Formate, 0.1 M Sodium Acetate trihydrate pH 4.6
35	0.8 M mono-Sodium dihydrogen phosphate, 8 M Potassium dihydrogen phosphate, 0.1 M HEPES, pH 7.5
36	8% w/v PEG 8000, 0.1 M Tris Hydrochloride pH 8.5
37	8% w/v PEG 4000, 0.1 M Sodium Acetate trihydrate pH 4.6
38	1.4 M tri-Sodium Citrate dihydrate, 0.1 M HEPES - Na pH 7.5
39	2% v/v PEG 400, 2.0 M Ammonium Sulfate, 0.1 M HEPES - Na pH 7.5
40	20% v/v iso-Propanol, 20% w/v PEG 4000, 0.1 M tri-Sodium Citrate dihydrate pH 5.6
41	10% v/v iso-Propanol, 20% w/v PEG 4000, 0.1 M HEPES - Na pH 7.5
42	20% w/v PEG 8000, 0.05 M mono-Potassium dihydrogen Phosphate
43	30% w/v PEG 1500
44	0.2 M Magnesium Formate
45	18% w/v PEG 8000, 0.1 M Sodium Cacodylate pH 6.5, 0.2 M Zinc Acetate dihydrate
46	18% w/v PEG 8000, 0.1 M Sodium Cacodylate pH 6.5, 0.2 M Calcium Acetate hydrate
47	2.0 M Ammonium Sulfate, 0.1 M Sodium Acetate trihydrate pH 4.6
48	2.0 M mono-Ammonium dihydrogen Phosphate, 0.1 M Tris Hydrochloride pH 8.5
49	2% w/v PEG 8000, 1.0 M Lithium Sulfate monohydrate
50	15% w/v PEG 8000, 0.5 M Lithium Sulfate monohydrate

Table 2

Solutions in Crystal Screen II

#	Component(s)
1	10% w/v PEG 6000, 2.0 M NaCl
2	0.5 M NaCl, 0.01 M MgCl2 hexahydrate, 0.01 M Hexadecyltrimethylammonium Bromide
3	25% v/v Ethylene Glycol
4	35% v/v Dioxane
5	5% v/v iso-Propanol, 2.0 M Ammonium Sulfate
6	1.0 M Imidazole pH 7.0
7	10% w/v PEG 1000, 10% w/v PEG 8000
8	10% v/v Ethanol, 1.5 M NaCl
9	2.0 M NaCl, 0.1 M Sodium Acetate trihydrate pH 4.6
10	30% v/v MPD, 0.1 M Sodium Acetate trihydrate pH 4.6, 0.2 M NaCl
11	1.0 M 1,6 Hexanediol, 0.1 M Sodium Acetate trihydrate pH 4.6, 0.01 M Cobaltous Chloride hexahydrate
12	30% v/v PEG 400, 0.1 M Sodium Acetate trihydrate pH 4.6, 0.1 Cadmium Chloride dihydrate
13	30% w/v PEG Monomethyl Ether 2000, 0.1 M Sodium Acetate trihydrate pH 4.6, 0.2 M Ammonium Sulfate
14	2.0 M (NH$_4$)$_2$SO$_4$, 0.1 M tri-Sodium Citrate dihydrate pH 5.6, 0.2 M Potassium Sodium Tartrate tetrahydrate
15	1.0 M Lithium Sulfate monohydrate, 0.1 M tri-Sodium Citrate dihydrate pH 5.6, 0.5 M Ammonium Sulfate
16	2% v/v Ethylene Imine Polymer, 0.1 M tri-Sodium Citrate dihydrate pH 5.6, 0.5 M NaCl
17	35% v/v tert-Butanol, 0.1 M tri-Sodium Citrate dihydrate pH 5.6
18	10% v/v Jeffamine M-600®, 0.1 M tri-Sodium Citrate dihydrate pH 5.6, 0.01 M Ferric Chloride hexahydrate
19	2.5 M 1,6 Hexanediol, 0.1 M tri-Sodium Citrate dihydrate pH 5.6
20	1.6 M Magnesium Sulfate heptahydrate, 0.1 M MES pH 6.5
21	2.0 M NaCl, 0.1 M MES pH 6.5, 0.1 M Sodium dihydrogen phosphate, 0.1 M Potassium dihydrogen Phosphate
22	12% w/v PEG 20,000, 0.1 M MES pH 6.5
23	10% v/v Dioxane, 0.1 M MES pH 6.5, 1.6 M Ammonium Sulfate
24	30% v/v Jeffamine M-600®, 0.1 M MES pH 6.5, 0.05 M Cesium Chloride

27

Table 2 continued

#	Component(s)
25	1.8 M Ammonium Sulfate, 0.1 M MES pH 6.5, 0.01 M Cobaltous Chloride hexahydrate
26	30% w/v PEG Monomethyl Ether 5000, 0.1 M MES pH 6.5, 0.2 M Ammonium Sulfate
27	25% v/v PEG Monomethyl Ether 550, 0.1 M MES pH 6.5, 0.01 M Zinc Sulfate heptahydrate
28	1.6 M tri-Sodium Citrate dihydrate pH 6.5
29	30% v/v MPD
30	10% w/v PEG 6000, 5% v/v MPD, 0.1 M HEPES pH 7.5
31	20% v/v Jeffamine M-600®, 0.1 M HEPES pH 7.5
32	1.6 M Ammonium Sulfate, 0.1 M HEPES pH 7.5, 0.1 M NaCl
33	2.0 M Ammonium Formate, 0.1 M HEPES pH 7.5
34	1.0 M Sodium Acetate, 0.1 M HEPES pH 7.5, 0.05 M Cadmium Sulfate hydrate
35	70% v/v MPD, 0.1 M HEPES pH 7.5
36	4.3 M NaCl, 0.1 M HEPES pH 7.5
37	10% w/v PEG 8000, 8% v/v Ethylene Glycol, 0.1 M HEPES pH 7.5
38	20% w/v PEG 10,000, 0.1 M HEPES pH 7.5
39	3.4 M 1,6 Hexanediol, 0.1 M TRIS pH 8.5, 0.2 M MgCl2 hexahydrate
40	25% v/v tert-Butanol, 0.1 M TRIS pH 8.5
41	1.0 M Lithium Sulfate monohydrate, 0.1 M TRIS pH 8.5, 0.01 M Nickel(II) Chloride hexahydrate
42	12% v/v Glycerol anhydrous, 0.1 M TRIS pH 8.5, 1.5 M Ammonium Sulfate
43	50% v/v MPD, 0.1 M TRIS pH 8.5, 0.2 M mono Ammonium dihydrogen Phosphate
44	20% v/v Ethanol, 0.1 M TRIS pH 8.5
45	20% w/v PEG Monomethyl Ether 2000, 0.1 M TRIS pH 8.5, 0.01 M Nickel(II) Chloride hexahydrate
46	20% w/v PEG Monomethyl Ether 550, 0.1 M Bicine pH 9.0, 0.1 M Sodium Chloride
47	2.0 M MgCl2 hexahydrate, 0.1 M Bicine pH 9.0
48	10% w/v PEG 20,000, 0.1 M Bicine pH 9.0, 2% v/v Dioxane

one mL of reservoir solution is added to the appropriate well. Next, a 3 μL aliquot of drop stock solution is placed on the sitting drop post. An equal volume of PGHS-1 stock is added to the sitting drop post and mixed with the drop stock solution by aspiration with a pipette. Finally, the chamber is covered with a 22 mm-diameter glass cover slip, with a tight seal maintained by a ring of vacuum grease. The tray is incubated in a temperature-controlled room at approximately 20°C. Crystals are detected by visual inspection with a dissecting microscope.

Collection and processing of X-ray diffraction data

Diffraction data from PGHS-1 crystals were collected and processed in the following ways:

1) A Rigaku RU200H generator with a rotating copper anode, operated at 50 kV and 100 mA with a 0.3 mm filament, was used to produce primarily Cu K_α (λ = 1.5418 Å) radiation. The radiation was further monochromated and focused with either a Molecular Structure Corporation (MSC, The Woodlands, Texas) mirror system or Osmic (Troy, Michigan) multilayer confocal optics. The crystalline sample, mounted on a goniometer with rotatable φ- and 2θ-axes (χ=0°, ω=φ), was left at room temperature or cooled to approximately 0°C with a stream of nitrogen vapor produced by an MSC low temperature device. The position and intensities of diffracted X-rays were measured by either an MSC R-AXIS IIc imaging plate detector or an MSC R-AXIS IV++ imaging plate detector. The HKL suite (XDisplayF, Denzo and Scalepack) was used both to index the diffraction pattern and to integrate, scale and average the spot intensities (23). The fully

processed intensities were converted to structure factor amplitudes using TRUNCATE and other utilities from the CCP4 suite of programs (24).

2) A Bruker rotating copper anode X-ray generator, operated at 50 kV and 100 mA with a 0.3 mm filament, was used to produce primarily Cu K_α radiation. The radiation was monochromated and focused with Osmic multilayer confocal optics. The crystalline sample, mounted on a goniometer with rotatable φ- and 2θ-axes ($\chi=0°$, $\omega=\varphi$) and a fixed χ of 54.74°, was left at room temperature or cooled to approximately 0°C with a stream of nitrogen vapor. Initially a Bruker low temperature device was used, but this was later replaced by an MSC low temperature device. The position and intensities of diffracted X-rays were measured by a Bruker HI-STAR multiwire area detector. The Bruker programs SADIE and SAINT were used to index the diffraction pattern, integrate, scale and average the spot intensities, and convert to structure factor amplitudes.

3) The Advanced Photon Source (Argonne National Laboratory, Illinois), beamline 19-ID, with an operating current of 60-100 mA and coupled to an undulator, produced polychromatic synchrotron radiation. The radiation was monochromated to 1.03221 Å (an energy of 12 keV) with a sagitally-focusing silicon (111) double crystal and a vertically focusing mirror. Crystals were kept at a temperature of 100-110K by a low-temperature device. The position and intensities of diffracted X-rays were measured by a custom-built 3x3 CCD-array detector (SBC2). HKL2000 was used to index the diffraction pattern and integrate the spot intensities, while scaling of integrated intensities and averaging of symmetry-related reflections was done with Scalepack, from the HKL suite (23).

Cryoprotection of crystals for low-temperature data collection

Cryoloops were purchased from Hampton Research and glued to cryopins from the Gibbs Instrument Shop (Yale University, New Haven, Connecticut). For attempts made to flash-freeze PGHS-1 crystals encased in a protective layer of oil, both mineral oil and Paratone-N were tried, as well as mixtures of the two. The crystals were first moved from mother liquor or stabilization buffer to a drop of oil. Next, as much aqueous solution as possible was removed from the surface of the crystal by a combination of pulling the crystal through the oil and wicking remaining moisture away with a small strip of filter paper. Finally, the crystal was picked up in a cryoloop on a cryopin, bringing along a covering layer of oil, and flash-frozen in a stream of cold nitrogen vapor or in liquid propane. Diffraction data were measured as described above.

For cryoprotection of crystals with LiCl and sucrose, a crystal first was removed from its crystallization drop to stabilization buffer (0.9 M sodium citrate, pH 6.5, 1.0 M LiCl, 0.15% w/v β-OG). After a brief incubation (< 2 minutes), the crystal was transferred to cryoprotectant buffer (0.9 M sodium citrate, pH 6.5, 1.0 M LiCl, 24% w/v sucrose, 0.15% w/v β-OG) and shortly (< 30 seconds) thereafter flash-cooled by plunging into a vial of liquid propane. Data were then collected as described above.

their

Tweer

The c

the in

micro

conce

condu

perox

and

("PO.

1) hig

lipids

the c

condi

mater

(an ir

of 40

subse

Results

Detergent Optimization

Three detergents, each at a range of different concentrations, were evaluated for their effectiveness in solubilizing PGHS-1 from ram seminal microsomes (RSMs): Tween® 20, decyl maltoside ($C_{10}M$) and heptaethylene glycol monodecyl ether ($C_{10}E_7$). The concentration of each detergent was varied, as well as the amount of RSMs, and thus the initial protein concentration. The volume of clear supernatant solution from each microscale solubilization was recorded, then assays for peroxidase activity, protein concentration and phosphate levels (an indicator of phospholipid content) were conducted. The efficacy of extraction was judged on the basis of 1) recovery of initial peroxidase activity ("% Units Solubilized"), 2) the specific activity ("Units/mg protein") and 3) the level of phosphate (phospholipids) contamination relative to protein ("PO_4/PGHS monomer"). The results are depicted in Figure 4.

Under the conditions described above, $C_{10}E_7$ resulted in the best combination of 1) high-yield extraction of PGHS-1 from the RSMs and 2) low extraction of protein and lipids contaminants. The optimal concentration of $C_{10}E_7$ was felt to be 0.75% w/v, and the optimal protein concentration 15 mg/mL. The average results under these trial conditions were 102 % of the total peroxidase activity solubilized, with the solubilized material having a specific activity of 6.8 U/mg, and with 3400 molecules of phosphate (an indicator of phospholipid) per monomer of PGHS, assuming a "pure" specific activity of 40 U/mg. Decyl maltoside ($C_{10}M$) and Tween® 20 performed less well, and were not subsequently used in the work described here. A complicating factor, which has not been

Figure 4. Results of trial solubilizations of ovine PGHS-1. Experiments were carried out as a matrix of initial protein concentration (5, 10, 15 and 20 mg/mL) *versus* detergent concentration (0.125 to 2.000 % w/v). Each row (a, b or c) represents the same type of measurement, carried out with three different detergents. Row "a" depicts the percent of peroxidase activity extracted from each sample, which is taken as a measure of the yield of PGHS. Row "b" shows the specific activity of the solubilized material, a measure of the success of removing contaminating proteins. Row "c" gives the molar ratio of phosphate (approximately equal to the amount of phospholipid) to PGHS monomers, as a measure of the amount of "lipid contamination". For each datum, the magnitude is indicated by a specific color. The numerical ranges of the colors are given to right of each row. Blues represent less desirable characteristics (low yield, low specific activity or high phosphate/PGHS monomer). Yellows indicate more desirable states (high yield, high specific activity or low phosphate/PGHS monomer). Reds are intermediate. Where data were not collected, gray areas are drawn.
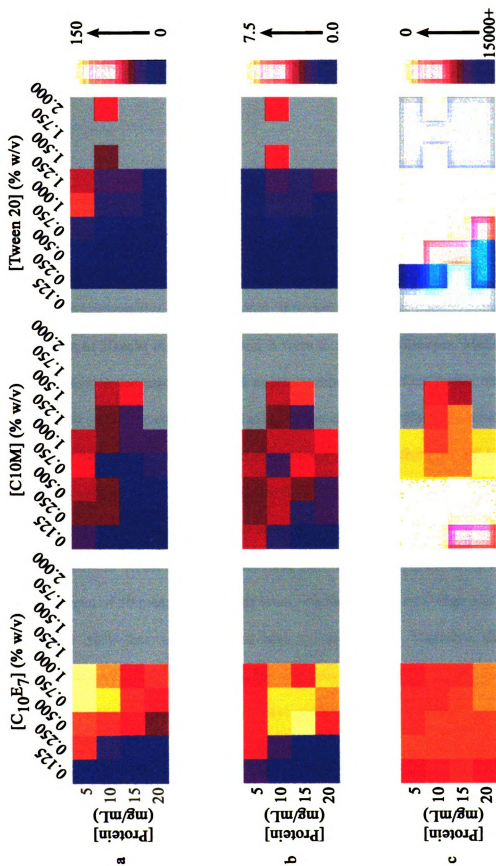
Figure 4

34

addressed, is that the type of detergent has a specific effect on enzyme activity. Therefore, statistics involving measures of activity may not be directly comparable between different detergents.

Purification

Few alterations were made to previously-established procedures for preparing RSMs or for subsequent solubilization, with the exception of the use of $C_{10}E_7$ instead of $C_{10}M$. More changes were adopted for later steps in purification. For DEAE anion exchange chromatography, an automated program was developed. Initial buffer concentrations of 20 mM in Buffers A and B were found by a colleague, Melissa Harris, to be insufficient to decrease the real pH as programmed. Therefore, buffer strength was increased to 40 mM. The addition of 20 mM sodium chloride to Buffer B, which initially had contained only buffer, was found to ease release of PGHS from the DEAE column. An interesting problem arose when $C_{10}E_6$ was used instead of $C_{10}E_7$ for solubilization and chromatography, in that PGHS could no longer be eluted from the DEAE column. Dr. Michael Malkowski serendipitously discovered that using 200 mM sodium chloride in Buffer B, instead of 20 mM, resolved this issue. Unfortunately, this "high salt" Buffer B caused about 50% loss of peroxidase activity overnight. Therefore the pooled, concentrated DEAE fractions were loaded immediately onto the S300 gel filtration column, rather than waiting for the next day, and the column was then run overnight. This eliminated the stability problems and had the added benefits of 1) improving separation due to the low flow rate and 2) reducing the duration of the entire purification procedure from three to two days. Throughout the purification, greater speed and ease of

concentratio

rather than

dialysis was

than standar

The

went directi

working we

500 g of R

RSMs from

preparation

for three su

the RSMs.

measured H

that achiev

reduced. a

purificatio

assay are

interferen

the results

when the

RSMs. It

which wa

concentration were achieved by using Millipore Ultrafree centrifugal concentrators, rather than an Amicon concentration cell pressurized with nitrogen gas. Likewise, dialysis was made easier by the use of Slide-a-Lyzer dialysis cassettes (Pierce), rather than standard dialysis tubing.

The purification protocol used for the original PGHS-1 structure determination went directly from RSVs to purified protein, involved four column steps and took one working week to finish. Typically, 40-50 mg of purified protein could be obtained from 500 g of RSVs. The current protocol is divided into two segments: 1) preparation of RSMs from RSVs, and 2) preparation of purified protein from stored RSMs. The RSM preparation takes one day and, from 350 g of RSVs, generally provides enough material for three subsequent protein purifications. The total yield of purified protein from all of the RSMs, and thus from the 350 g of RSVs, is usually 40-50 mg. Specific activity, as measured by the peroxidase activity assay and the BCA protein assay, is at least equal to that achieved with the original purification procedure. Levels of bound lipid appear to be reduced, as estimated by visual comparison of thin layer chromatograms to those of purifications carried out at the University of Chicago. Data from the Ames phosphate assay are complicated by interference from the heme group of PGHS. The reason for this interference is unclear, as neither ferrous ($FeCl_2$) nor ferric ($FeCl_3$) iron compounds affect the results. The Ames assay was useful for estimating phospholipid concentration only when the ratio of lipid to PGHS was high, for example directly after solubilization from RSMs. It was not useful for determining residual phospholipid contamination of protein which was more purified, and hence more extensively delipidated.

Orthorhombic rod crystals from PEG 4000/NaCl

The original crystal form (Figure 5a) was reproduced using the PEG4000/NaCl precipitant conditions described above. Crystals typically appeared within days or weeks and had the shape of long, brown rods, as previously observed. The best crystallization conditions had reservoir solutions with components in the range of 4-9% w/v PEG 4000, 120-540 mM NaCl, 32-72 mM sodium phosphate, pH 6.7, and 1 mM NaN$_3$, with 0.5% w/v β-OG in the initial drops. The crystals from PEG4000/NaCl were somewhat difficult to grow on a regular basis, which could have been due to variation in early versions of the new purification procedure, as well as inherent properties of the crystallization system.

Sparse matrix screening for new crystallization conditions

Sparse matrix screening identified several promising new crystallization conditions (Table 3) with a variety of precipitants, including ammonium sulfate, lithium sulfate, sodium formate, sodium citrate and dioxane. The sitting-drop vapor diffusion method was used for crystallization subsequent work, rather than the hanging-drop method.

Orthorhombic rod crystals from sodium citrate

Using sodium citrate as precipitant resulted in crystals having the same morphology as those grown from PEG4000/NaCl (Figure 5a). However, rods from sodium citrate were more easily reproduced than those from PEG4000/NaCl. The best

Table 3

Results of sparse matrix crystallization screening with ovine PGHS-1

Crystal Screen Number	Reagent Number	Reagent Composition	Appearance of protein/reagent drop
I	4	2.0 M $(NH_4)_2SO_4$, 0.1 M Tris pH 8.5	Phase separation globules, possibly containing microcrystals.
I	16	1.5 M $Li_2SO_4 \cdot H_2O$, 0.1 M HEPES pH 7.5	Phase separation globules, possibly containing microcrystals.
I	32	2.0 M $(NH_4)_2SO_4$	Phase separation globules, possibly containing microcrystals.
I	33	4.0 M Sodium Formate	Phase separation globules, possibly containing microcrystals.
I	39	2% v/v PEG 400, 2.0 M $(NH_4)_2SO_4$, 0.1 M HEPES pH 7.5	Phase separation globules, possibly containing microcrystals.
II	14	2.0 M $(NH_4)_2SO_4$, 0.1 M tri-Sodium Citrate dihydrate pH 5.6, 0.2 M Potassium Sodium Tartrate tetrahydrate	Phase separation globules, possibly containing microcrystals.
II	23	10% v/v Dioxane, 0.1 M MES pH 6.5, 1.6 M $(NH_4)_2SO_4$	Grayish, granular precipitate with microcrystal clusters.
II	25	1.8 M $(NH_4)_2SO_4$, 0.1 M MES pH 6.5, 0.01 M $CoCl_2 \cdot 6H_2O$	Early on had dark brown microcrystal clusters, later phase separation globules, possibly containing microcrystals.
II	28	1.6 M tri-Sodium Citrate dihydrate pH 6.5	Amorphous gray precipitate with microcrystals.
II	32	1.6 M $(NH_4)_2SO_4$, 0.1 M HEPES pH 7.5, 0.1 M NaCl	Many tiny brown microcrystals.

38

Figure 5. Different ovine PGHS-1 crystal forms. The figure is in shades of gray, but the crystals are actually colored brown. a) Orthorhombic rod, in this case grown from solutions containing sodium citrate. b) Hexagonal prism, grown from solutions containing sodium citrate and lithium chloride. c) "Rhombohedral" rods, grown from solutions containing PEG MME 550, sodium chloride and 1-butanol.
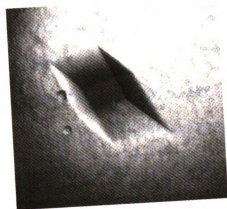
a
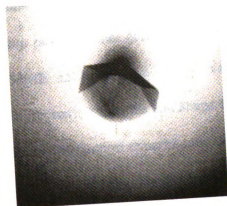
b

c

Figure 5

conditio

0.88 M

0.20-0.

all thro

or perh

when

Growi

At lea

bromo

"Rho

mole

cryst

of 2

larg

fror

cry

ran

2.0

55

cry

conditions for growing PGHS-1 crystals from sodium citrate were reservoirs with 0.68-0.88 M sodium citrate, pH 6.5, a drop stock with 0.68-0.77 M sodium citrate, pH 6.5, and 0.20-0.45 % (w/v) β-OG, protein stock with 15-20 mg/mL PGHS-1, and 1 mM NaN$_3$ in all throughout. Nonyl maltoside (C$_9$M) was tried as an additive and gave crystals as good or perhaps better than with β-OG alone. Glycerol sometimes improved crystal quality when used in the range of 0.5-2.0 % (w/v) in both the reservoir and drop stocks. Growing crystals in the presence of cyanide caused many small needle crystals to form. At least once, orthorhombic crystals grew in the presence of an AHA inhibitor, 3-(4-bromobenzyloxy)-benzohydroxamic acid.

"Rhombohedral" rod crystals from PEG MME 550/sodium chloride/1-butanol

Solutions containing polyethylene glycol monomethyl ether of 550 average molecular weight (PEG MME 550) with NaCl and NaH$_2$PO$_4$ gave smaller, brown crystals. A breakthrough in improving the size and shape these crystals was the addition of 2% (v/v) 1-butanol to the crystallization experiments, which resulted in the growth of larger, better-faceted crystals (Figure 5c). These crystals had a morphology different from either the PEG4000/NaCl or the sodium citrate crystals, but typical of rhombohedral crystal forms. The best crystals from this system grew with reservoir solutions in the range of 15-25% w/v PEG MME 550, 0-135 mM NaCl, 0-55 mM NaH$_2$PO$_4$, pH 6.7, and 2.0-2.5% v/v 1-butanol, with drops having 0.50-0.55% w/v β-OG. The PEG MME 550/NaCl/NaPO$_4$/1-butanol crystals were less easily reproduced than the sodium citrate crystals.

Hexagonal crystals from sodium citrate/lithium chloride

While attempting to grow rod crystals from solutions containing sodium citrate as precipitant and LiCl as a cryoprotectant, a new crystal morphology with the shape of small, hexagonal rods was unexpectedly discovered. However, it should be noted that in at least one case hexagonal crystals appeared in the absence of lithium chloride. Thus, lithium chloride favors the growth of hexagonal crystals, but is not absolutely required. Based on low-resolution diffraction, crystals with this morphology were tentatively assigned a hexagonal space group. This was later confirmed by the work of a colleague, Dr. Michael Malkowski (see below). Because the crystals were small, only diffracted to a resolution of approximately 4 Å, and were perhaps more radiation-sensitive than orthorhombic crystals, this author discontinued further work with this form.

Refinement of conditions for growing hexagonal crystals

In a separate line of investigation, Dr. Malkowski had developed a modified purification protocol to completely remove heme from PGHS-1. The method removed most heme by using $C_{10}M$ for all steps after extraction from RSMs. Residual heme was extracted with a glutathione affinity column. The purpose of this procedure was to allow replacement of the native heme with an inert cobalt-protoporphyrin IX (CoPPIX). PGHS whose heme had been removed and replaced with an exogenous metal-protoporphyrin IX would only crystallize in the hexagonal form, even when LiCl was omitted. Dr. Malkowski optimized a regime of citrate/LiCl crystallization solutions for CoPPIX PGHS-1 that produced large, hexagonal prisms, often grew close to 1 mm in diameter (Figure 5b) (25). The conditions which most reliably produced good hexagonal crystals

42

are 0

The

phot
of th
with
flux
prot
diff

X-r

diff
Å v
cry
suit
the
or n

cryc
cryc
glu

are 0.64–0.88 M sodium citrate, pH 6.5, 0.3-0.6 M LiCl and 1 mM NaN$_3$.

The effects of upgrading the X-ray focusing mirrors

The use of Osmic mirrors for focusing the incident X-ray beam increased the photon flux to the crystals, enhancing the intensity of the diffracted radiation. In the case of the Bruker HI-STAR system, the flux to the crystal was about fivefold higher than with the original Francks mirrors. With the MSC system, the Osmic mirrors improved flux about threefold over the Yale mirror system. By directing more X-ray photons at the protein crystals, these Osmic mirrors have allowed the collection of higher-quality diffraction data in shorter amounts of time.

X-ray diffraction by, and unsuccessful cryoprotection of, orthorhombic crystals

Orthorhombic crystals mostly diffracted to about 3.5 Å, though sometimes diffraction data could be observed to 2.7 Å. However, data of resolution greater than 3.1 Å were always too weak to measure reliably. Typically, 5 to 10% of the mounted crystals diffracted well enough, in terms of resolution, mosaicity and spot shape, to be suitable for data collection. Despite cooling to approximately 0°C, radiation damage to the crystals generally allowed only two hours of data collection per crystal, and thus five or more well-diffracting crystals would be needed for a complete dataset.

Over the course of almost three years, attempts were made to find conditions for cryoprotecting and flash-cooling orthorhombic "citrate" crystals. Numerous different cryoprotectants were tried, including glycerol, lithium chloride, sucrose, trehalose, glucose, xylose, sorbitol, lyxose, lactose (which was insoluble), maltose and glycyl

betai

chlori

an alt

vitrif

conce

cryst

crack

cryo

mixi

inter

ther

cryo

400

cryo

loss

stre

diff

Typ

the

con

X-r

betaine. The concentrations of cryoprotectant also were varied. Combinations of lithium chloride and sucrose were tested. Some solutions were made up with potassium citrate as an alternative to sodium citrate. Interestingly, it was found that β-OG tends to prevent vitrification during flash-cooling, necessitating the use of higher cryoprotectant concentrations. It was thought that lithium chloride might be causing damage to the crystals by altering the pH. However, tight control of solution pH did not reduce cracking of the crystals. Different protocols for introducing the crystals into cryoprotectant buffer were tried. For example, intermediate solutions were made by mixing stabilization buffer and cryobuffer in different proportions. The number of intermediate solutions was varied, as well the rate at which crystals were moved between them. Microdialysis was also attempted as a gentle way to equilibrate the crystals into cryobuffer. Some crystals grown in sodium citrate were moved to solutions with PEG 4000 and sodium chloride, which caused the crystals to develop large cracks. Attempts at cryoprotecting citrate-grown orthorhombic PGHS-1 crystals with a film of oil resulted in loss of all diffraction. Finally, flash-cooling the crystals in both liquid propane and in a stream of cold nitrogen vapor were tried. In all cases, the procedures degraded the diffraction pattern so much that the data could not be used for structure determination. Typical problems were lowered diffraction resolution, increased mosaicity, smearing of the diffracted rays into uninterpretable streaks, the formation of salt or ice rings or complete loss of diffraction.

X-ray diffraction by, and unsuccessful cryoprotection of, "rhombohedral" crystals

The crystals grown using PEG MME 550 as precipitant, of which approximately

20 were moun

to 5 Å. As a

PGHS crysta

some cryopr

crystals in s

flash-cooled.

eliminated d

X-ray diffrac

With

typically diff

even more r

sufficient to

above. Sinc

suspended.

The

would some

higher-resol

truncated a

molecular r

structure, th

hexagonal

solutions co

20 were mounted for room-temperature data collection, never diffracted X-rays beyond 4 to 5 Å. As a result, it was not possible to determine their space group. Flash-cooling PGHS crystals grown from PEG MME 550 in their mother liquor, which should offer some cryoprotective effect, resulted in a complete lack of diffraction. Soaking the crystals in solutions with 33 % (w/v) PEG MME 550, which will form a glass when flash-cooled, either degraded the resolution of diffraction to about 20 Å, or completely eliminated diffraction.

X-ray diffraction by, and successful cryoprotection of, hexagonal crystals

With X-rays from rotating anode generators, hexagonal-shaped PGHS-1 crystals typically diffracted to better than 5 Å. At room temperature, hexagonal crystals decayed even more rapidly than orthorhombic crystals. The limited data collected were only sufficient to tentatively assign the crystals to a hexagonal space group, as mentioned above. Since this crystal form appeared unpromising, further work by this author was suspended.

The larger crystals grown under Dr. Michael Malkowski's optimized conditions would sometimes diffract X-rays to 3.5 Å, the edge of useable resolution. However, the higher-resolution data were extremely weak, so that even the best data sets had to be truncated at 4.0-4.5 Å resolution. Nonetheless, Dr. Malkowski demonstrated by molecular replacement, using a search model derived from a monomer of the original structure, that the space group was in fact $P6_522$. Dr. Malkowski successfully prepared hexagonal crystals for low-temperature data collection by briefly soaking them in solutions containing sucrose and LiCl as cryoprotectants, followed by flash-cooling in

liquid p

showed

tempera

Advan

from h

occasi

produ

conta

prep

reas

disc

4-(

De

re

U

m

w

w

a

v

i

r

liquid propane (25). Hexagonal crystals kept at cryogenic temperatures no longer showed radiation decay, but also did not diffract to higher resolution than at room temperature. Using the very intense radiation available at beamline 19-ID of the Advanced Photon Source (APS), Dr. Malkowski observed higher-resolution diffraction from hexagonal PGHS-1 crystals, with a typical cutoff for useable resolution of 3.1 Å, or occasionally 2.9 Å. On average, 10% of the crystals prepared for data collection produced datasets suitable for refinement of the structure.

A number of hexagonal crystals were soaked by this author in solutions containing inhibitors, including cyanide and various arylhydroxamic acids (AHAs), and prepared for cryogenic data collection at beamline 19-ID of the APS. For unknown reasons, all but one of them either did not extend to useable resolution or were too badly disordered to be successfully processed. One crystal (designated "mjt_f21"), soaked with 4-(3-chlorobenzyloxy)-BHA to form a putative complex, did show diffraction to 2.7 Å. Despite high crystal mosaicity (1.2°), poor spot shape and detector overloading by lower-resolution spots, integration of intensities by HKL2000 proceeded smoothly. Unfortunately, scaling and averaging with Scalepack revealed that the data were poorly measured. Fully measured reflections (those measured over their entire angular width), were absent due to the narrow image width (0.5°) and high mosaicity (1.2°). The result was wild variations in frame-to-frame scale factors. This could not be rectified by applying restraints to B-factor and scale factor refinement because almost all reflections were then rejected. Overall completeness was 80.2% at 2.7 Å resolution, but much less in the lower-resolution shells (4.0-30.0 Å). The overall R_{sym} was 14.9% and increased markedly after 2.9 Å; the overall $I/\sigma(I)$ was 9.4. The data from 30.0 to 2.9 Å resolution

were of insu

replacement

from 46 to

calculated us

signal for th

Further work

gather a us

following th

with oil did

described ab

were of insufficient quality to independently reproduce Dr. Malkowski's molecular replacement solution. When the data were used for refinement in X-PLOR, R decreased from 46 to 38%, but R_{free} increased slightly from 48 to 49%. Electron density maps calculated using the diffraction data and phases from the protein model did not show a signal for the heme iron, which is the most electron-dense feature of the structure. Further work with this dataset was discontinued. So far, this author has been unable to gather a useable diffraction dataset from any hexagonal PGHS-1 crystal, despite following the exact conditions refined by Dr. Malkowski. Hexagonal crystals coated with oil did diffract X-rays, but not as well as when simply soaked in sucrose/LiCl, as described above.

techni

protei

struct

becau

they

that

mer

sta

pr

m

A

b

l

Discussion

Crystallography with integral membrane proteins continues to be very challenging technically, which has limited the rate of structure solution to a level typical for soluble protein work a generation ago. The Protein Data Bank currently holds over 16,000 structures, yet only about 1% of these are of integral membrane proteins. Nonetheless, because membrane proteins are predicted to account for 20 to 40% of genes, and because they are moreover some of the most pharmacologically relevant proteins, it is imperative that their crystal structures continue to be solved. Since much of the difficulty of membrane protein structure projects stems from the purification and crystallization stages, it is perhaps especially important, compared to what is common for soluble proteins, that these protocols be optimized. For example, the effect of detergent on microsomes could be imagined to depend on the specific detergent concentration used. At low concentrations, most of the detergent would intercalate into the lipid bilayer, thus being of little use for protein extraction. At medium concentrations, proteins and some lipid are liberated from the membrane, which is ideal for protein solubilization. At high concentrations of detergent, the membrane is seriously disrupted, so that much lipid is released, perhaps with deleterious effects for further purification and crystallization of the solubilized protein. On the other hand, one should keep in mind that specifically-bound lipids may benefit crystallization. In the case of *Paracoccus denitrificans* cytochrome *c* oxidase, an ordered molecule of phosphatidyl choline was observed in the crystal structure (26). In the bovine cytochrome *c* oxidase structure, fully eight lipid molecules of various types were seen for each holoenzyme complex (27).

The cu

structure deter

amount of act

Research) is

large amount

useful in redu

instead of C

protein. espe

number of cl

loss, and al

human-intro

S300 gel fil

very low fl

requires one

protein prep

would have

purified PG

method.

The

improved.

rather than

the deterge

excessively

The current PGHS-1 purification procedure, compared to that used in the original structure determination, is improved in a number of aspects. First, it should be noted that amount of activity in a given amount RSV tissue from our supplier (Oxford Biomedical Research) is superior to that of our previous supplier (Antech). Second, preparation of large amounts of stored RSMs, sufficient for several individual protein purifications, was useful in reducing the overall amount of time and labor needed. Third, the use of $C_{10}E_7$ instead of $C_{10}M$ for extraction from the RSMs improved the quality and yield of the protein, especially in terms of having less lipid contamination. Fourth, by reducing the number of chromatographic steps from four to three, we eliminated a source of sample loss, and also accelerated the protocol. Fifth, use of automated equipment limited human-introduced variations between batches of purified protein. Finally, running the S300 gel filtration column overnight not only saved time, but also allowed us to use a very low flow rate, which enhances peak separation. Overall, the new purification requires one day for RSM preparation, typically yielding enough material for three small protein preparations, each needing two days. With the original protocol, one large batch would have been produced in approximately the same time. Because of the instability of purified PGHS, purification in several small, easily-consumed batches is the preferred method.

The crystallization methods for PGHS have also been substantially changed and improved. The switch from the sitting-drop vapor diffusion method for crystallization, rather than the hanging-drop method, was made for several reasons. First, spreading of the detergent-containing hanging drop, even when the cover slip had been siliconized, excessively accelerated loss of vapor to the reservoir. Second, the smaller surface area

exposed in a sitting drop, due to its being in a shallow depression (compared to a hanging drop on a flat cover slip), led to slower vapor loss. Finally, it is easier to extract crystals from a sitting drop. The hexagonal crystal form currently is the most useful, because it is easily reproduced, can be cryoprotected and has high symmetry. If orthorhombic PGHS-1 crystals grown from citrate could be cryoprotected, they would probably yield higher-resolution data than hexagonal crystals, based on experience with rotating anode X-ray generators. Indeed, orthorhombic crystals grown from PEG4000/NaCl have recently been shown to diffract synchrotron X-rays to a useable resolution of 2.61 Å, much better than the 2.9 Å which is best resolution for a hexagonal crystal (28,29).

Clearly, to be achieved with a more reasonable expenditure of effort, projects involving determining large numbers of PGHS-1 crystal structures required a better system for purification, crystallization and data collection. The work discussed above, through extensive, incremental improvements, has resulted in just such a system. Achieving this level of technical optimization has opened the way to more extensive crystallographic studies of PGHS/ligand complexes than were previously possible. The best example of this is the solution of structures of an inert form of PGHS-1 in complex with AA and a number of alternative substrates (25,29,30). Future studies of other complexes, perhaps including those with AHAs, are now much more feasible.

The

uni

nor

and

nor

Mu

op

in

inc

ar

an

SQ

lin

o

pr

m

o

an

or

Introduction

The biological role of sulfolipid

SQDG (6-sulfo-α-D-quinovosyl diacylglycerol, or simply "sulfolipid") is a nearly universal component of photosynthetic membranes, and may be the most abundant nonpeptidic sulfur-containing compound in the biosphere (31). SQDG is found in plants and most cyanobacteria, various other photosynthetic bacteria, and even some nonphotosynthetic bacteria such as *Rhizobium meliloti* and *Bacillus acidocaldarius* (32). Mutants defective in the biosynthesis of SQDG suffer surprisingly few ill effects under optimal growth conditions (33,34). In wild-type organisms, phosphate limitation results in a decrease in phospholipid in the thylakoid membranes, while the level of SQDG increases (35,36). More specifically, the increase in SQDG levels corresponds in molar amount to the loss of phosphatidyl glycerol (PG). Since PG and SQDG are the only anionic lipids known to exist in thylakoid membranes (37), it has been proposed that SQDG is critical for maintaining proper membrane charge balance when phosphate limitation reduces the amount of available PG (32,33,35).

A lack of anionic lipids also may affect protein trafficking, as suggested by work of Inoue *et al.* with an N-terminal fragment of the transit peptide for Toc75, a membrane protein of the chloroplast stroma (38). This fragment was found to insert well into monolayers formed of anionic lipids (SQDG or PG), to a lesser degree into monolayers of zwitterionic lipids (phosphatidylethanolamine, PE, but not phosphatidylcholine, PC), and not at all into monolayers of neutral lipids (monogalactosyl diacylglycerol, MGDG, or digalactosyl diacylglycerol, DGDG). This suggests that only SQDG can replace

phos

some

cyan

whic

depe

phos

phot

func

is nc

be d

carb

of s

cytc

(42

the

pro

has

ann

wi

rev

tha

(44

phospholipids in maintaining the proper membrane characteristics needed for insertion of some proteins. In another interesting case, Sato et $al.$ isolated mutants of the cyanobacterium $Synechocystis$ sp. PCC6803 which are deficient in PG biosynthesis, but which do not make compensating amount of sulfolipid (39,40). These mutants are dependent for survival on supplementation with exogenous PG. When exogenous phospholipid is removed from the growth medium, they experience difficulties with photosynthesis, particularly in the proper accumulation of chlorophyll and in the functioning of photosystem II (PSII). This suggests that reduction of phospholipid levels is not tolerable in the absence of compensating sulfolipid biosynthesis.

Besides its role in anabolism of photosynthetic membranes, sulfolipid is known to be degraded by a number of microorganisms, several of which can use it as their sole carbon source (41). Although sulfoquinovose is found most commonly as the head group of sulfolipid, in at least one case it forms part of a glycosyl group attached to a protein, cytochrome $b_{558/566}$ of the archaebacterium $Sulfolobus$ $acidocaldarius$ ($S.$ $acidocaldarius$) (42). The resistance of the carbon-sulfur sulfonyl bond to nonenzymatic hydrolysis under the highly acidic extracellular conditions experienced by $S.$ $acidocaldarius$ has been proposed as a reason why this moiety is present in the glycosyl group. Finally, SQDG has also shown promise for treatment of several human diseases. SQDG binds and antagonizes the platelet-activating factor (PAF) receptor, which is involved in psoriasis, with an estimated IC_{50} of 2 to 10 μM (43). Inhibition of DNA polymerases and retroviral reverse transcriptases with IC_{50}'s in the micromolar range has been reported, suggesting that sulfolipids could be useful as anti-tumorigenic or anti-retroviral therapeutic agents (44-50). In fact, treatment of cultured gastric cancer cells with 0.1-1.0 mM SQDG

inhibits proli[

Biosynthesis

Prior

investigatio[

of sulfolipid

steps (52).

unidentified

sulfoquinov[

molecule, th[

identified s[

therefore m[

Rhodobact[

sulfolipid b[

similarity t[

protein pro[

catalyzes t[

sqdD in *R[*

results in

similarity

SQDG sy[

biosynthe[

the inabili[

inhibits proliferation and causes apoptosis (51).

Biosynthesis of SQDG

Prior to the work described in this dissertation, mutational and biochemical investigations had already partially elucidated the so-called "sugar nucleotide" pathway of sulfolipid biosynthesis. The pathway, first proposed in detail by Pugh *et al.*, has two steps (52). The first is the conversion of UDP-glucose to UDP-sulfoquinovose, with an unidentified "sulfur donor" presumed to contribute the sulfonyl group. Second, the sulfoquinovose portion of UDP-sulfoquinovose is donated to a diacylglycerol (DAG) molecule, thus releasing UDP and forming the final product, SQDG. Mutational studies identified several genes which are important for sulfolipid biosynthesis, and which therefore might catalyze the reactions described above. Inactivation of the *sqdB* gene in *Rhodobacter sphaeroides* (*R. sphaeroides*) or in *Synechococcus* sp. PCC7942 eliminates sulfolipid biosynthesis (53,54). Based on the *sqdB⁻* mutant phenotype and on sequence similarity to UDP-galactose 4′-epimerases and nucleotide-hexose 4′,6′-dehydratases, the protein product of *sqdB* was hypothesized to be the UDP-sulfoquinovose synthase which catalyzes the first step in the sulfolipid biosynthetic pathway. Inactivation of the gene *sqdD* in *R. sphaeroides* likewise eliminates sulfolipid production. However, it also results in accumulation of UDP-sulfoquinovose (55). The sequence of *sqdD* also has similarity to known glucosyl transferases. Therefore, *sqdD* was believed to encode the SQDG synthase, which catalyzes the second step in the pathway of sulfolipid biosynthesis. Loss of glycosyl transferase activity upon *sqdD* disruption would explain the inability of *sqdD⁻* mutants to form SQDG from UDP-sulfoquinovose and DAG. More

53

recently, a gene essential for SQDG synthase activity in *Synechococcus* sp. PCC7942, *sqdX*, has been characterized (56). Interestingly, *sqdX* seems unrelated in sequence to *sqdD*, although the various *sqdB* sequences are very similar.

If the sugar-nucleotide hypothesis for SQDG biosynthesis is biologically relevant, then the proper substrates should be available to the pathway enzymes *in vivo*. Free UDP-glucose, the presumed starting material, is found at negligible levels in the chloroplast (57). While intact chloroplasts had been shown to incorporate external, UDP-[^{14}C]glucose into SQDG, it was later revealed that the efficiency is extremely low (52,58,59). The efficiency *in vivo* could be increased by delivering UDP-glucose to the appropriate enzyme in the chloroplast by some kind of transport mechanism. A number of potential sulfur donors were shown to be incorporated into SQDG by intact, isolated chloroplasts, including sulfate, sulfite, and 3'-phosphoadenosine-5'-phosphosulfate (PAPS) (60). Depending on species, DAG for SQDG biosynthesis is derived either from both the cytoplasm and chloroplast, or from the cytoplasm alone (61). While intact chloroplasts can carry out full SQDG biosynthesis, broken chloroplasts can only catalyze the addition of sulfoquinovose to DAG. This suggests that proteins involved in SQDG biosynthesis either require a special chemical environment provided by the chloroplast, or that the components are spatially organized by the intact organelle. Because it was not possible at this point to reconstitute the full pathway outside the chloroplast, the question of which compounds feed into SQDG biosynthesis could not be definitively determined.

Characteristics of the protein SQD1

In *Arabidopsis thaliana* (*A. thal.*), both SQD1 (the homolog of SQDB) and SQDG

synthase are

sequence is s

and overexpr

85-amino ac

acids contai

cloned prote

of NAD$^+$ an

it was predi

enzymes (6

of the nucle

in this sub

dehydratas

4′,6′-dehyd

reductase (

(69) and G

A c

suggested

catalytic t

negatively

positive ci

step in tr

Intermedi

O4′-hydr

synthase are localized to the chloroplast (32,35). SQD1, whose deduced amino acid sequence is shown in Figure 6, had previously been cloned into *Escherichia coli* (*E. coli*) and overexpressed. In the cloned form, whose sequence is shown in Figure 7, the native 85-amino acid N-terminal chloroplast-targeting signal has been replaced by 12 amino acids containing a hexahistidine-tag. The resulting calculated molecular weight of the cloned protein is 45.4 kDa. Because SQD1 was found to tightly bind equimolar amounts of NAD^+ and to have GXXGXXG and YXXXK sequences (where X is any amino acid), it was predicted to belong to the short-chain dehydrogenase/reductase (SDR) family of enzymes (62). More specifically, it was believed that SQD1 was very similar to members of the nucleotide-sugar modifying subgroup of the SDR family (Table 4). Other proteins in this subgroup include UDP-galactose 4′-epimerase (UGE) (63), CDP-glucose 4′,6′-dehydratase (CGD) (64), dTDP-glucose 4′,6′-dehydratase (dTGD) (65), GDP-mannose 4′,6′-dehydratase (GMD) (66), GDP-4′-keto-6′-deoxymannose 3′,5′-epimerase-4′-reductase (GMER) (67,68), ADP-L-glycero-α-D-mannoheptose 6′-epimerase (AGME) (69) and GDP-4′-keto-rhamnose 4′-reductase (GRR) (70).

A catalytic mechanism, modeled on those proposed for UGE and CGD, had been suggested for SQD1 (Figure 8). In these enzymes, and in most other SDRs, a conserved catalytic tyrosine is believed to be maintained prior to reaction in a deprotonated, negatively-charged tyrosinate state. This condition is stabilized by the influence of positive charges on a catalytic lysine and on NAD^+, or $NADP^+$ in some SDRs. The first step in the SQD1 mechanistic scheme is conversion of UDP-glucose to a 4′-keto Intermediate I. This is accomplished when the catalytic tyrosine moves a proton from the O4′-hydroxyl to it O_η, and NAD^+ abstracts a hydride from C4′ to its own C4. Next, a

```
                -84   -80            -70          -60        -52
                 |     |              |            |          |
                MAHL LSASCPSVIS LSSSSSKNSV KPFVSGQTF
   -51        -41         -31         -21          -11         -2
    |          |           |           |            |          |
  FNAQLLSRSS LKGLLFQEKK PRKSCVFRAT AVPITQQAPP ETSTNNSSSK
    2          11          21          31           41         50
    |          |           |           |            |          |
  PKRVMVIGGD GYCGWATALH LSKKNYEVCI VDNLVRRLFD HQLGLESLTP

   51          61          71          81           91        100
    |          |           |           |            |          |
  IASIHDRISR WKALTGKSIE LYVGDICDFE FLAESFKSFE PDSVVHFGEQ

  101        111         121         131          141        150
    |          |           |           |            |          |
  RSAPYSMIDR SRAVYTQHNN VIGTLNVLFA IKEFGEECHL VKLGTMGEYG

  151        161         171         181          191        200
    |          |           |           |            |          |
  TPNIDIEEGY ITITHNGRTD TLPYPKQASS FYHLSKVHDS HNIAFTCKAW

  201        211         221         231          241        250
    |          |           |           |            |          |
   GIRATDLNQG VVYGVKTDET EMHEELRNRL DYDAVFGTAL NRFCVQAAVG

  251        261         271         281          291        300
    |          |           |           |            |          |
  HPLTVYGKGG QTRGYLDIRD TVQCVEIAIA NPAKAGEFRV FNQFTEQFSV

  301        311         321         331          341        350
    |          |           |           |            |          |
  NELASLVTKA GSKLGLDVKK MTVPNPRVEA EEHYYNAKHT KLMELGLEPH

  351        361         371         381               394
    |          |           |           |                |
  YLSDSLLDSL LNFAVQFKDR VDTKQIMPSV SWKKIGVKTK SMTT
```

Figure 6. The deduced amino acid sequence of native SQD1 from *A. thal.*

Numbering is from the cloned form.

56

```
1
|
GSRVMV

51
|
IASIHD

101
|
RSAPYS

151
|
TPNIDI

201
|
GIRATI

251
|
HPLTV

301
|
NELAS

351
|
YLSDS
```

F

```
                                            -10         -1
                                             |           |
                                            MRGSHHHHHH

   1          11          21          31          41          50
   |          |           |           |           |           |
   GSRVMVIGGD GYCGWATALH LSKKNYEVCI VDNLVRRLFD HQLGLESLTP

   51         61          71          81          91          100
   |          |           |           |           |           |
   IASIHDRISR WKALTGKSIE LYVGDICDFE FLAESFKSFE PDSVVHFGEQ

   101        111         121         131         141         150
   |          |           |           |           |           |
   RSAPYSMIDR SRAVYTQHNN VIGTLNVLFA IKEFGEECHL VKLGTMGEYG

   151        161         171         181         191         200
   |          |           |           |           |           |
   TPNIDIEEGY ITITHNGRTD TLPYPKQASS FYHLSKVHDS HNIAFTCKAW

   201        211         221         231         241         250
   |          |           |           |           |           |
   GIRATDLNQG VVYGVKTDET EMHEELRNRL DYDAVFGTAL NRFCVQAAVG

   251        261         271         281         291         300
   |          |           |           |           |           |
   HPLTVYGKGG QTRGYLDIRD TVQCVEIAIA NPAKAGEFRV FNQFTEQFSV

   301        311         321         331         341         350
   |          |           |           |           |           |
   NELASLVTKA GSKLGLDVKK MTVPNPRVEA EEHYYNAKHT KLMELGLEPH

   351        361         371         381                     394
   |          |           |           |                       |
   YLSDSLLDSL LNFAVQFKDR VDTKQIMPSV SWKKIGVKTK S*MTT*
```

Figure 7. The amino acid sequence of cloned SQD1, expressed in E. coli.

Table 4

Nucleotide-sugar modifying SDRs

Name	Substrate	Product	Structures
SQD1	UDP-α-D-glucose	UDP-α-D-sulfoquinovose	4
UGE	UDP-galactose	UDP-glucose	21
AGME	ADP-L-glycero-D-mannoheptose	ADP-D-glycero-D-mannoheptose	1
dTGD	dTDP-glucose	dTDP-4´-keto-6´-deoxyglucose	2
GMD	GDP-mannose	GDP-4´-keto-6´-deoxymannose	1
GMER	GDP-4´-ketorhamnose	GDP-L-fucose	8
CGD	CDP-glucose	CDP-4´-keto-6´-deoxyglucose	0
GRR	GDP-4´-ketorhamnose	GDP-D-rhamnose	0

58

UDP-glucose   *Intermediate I*   **Intermediate II**
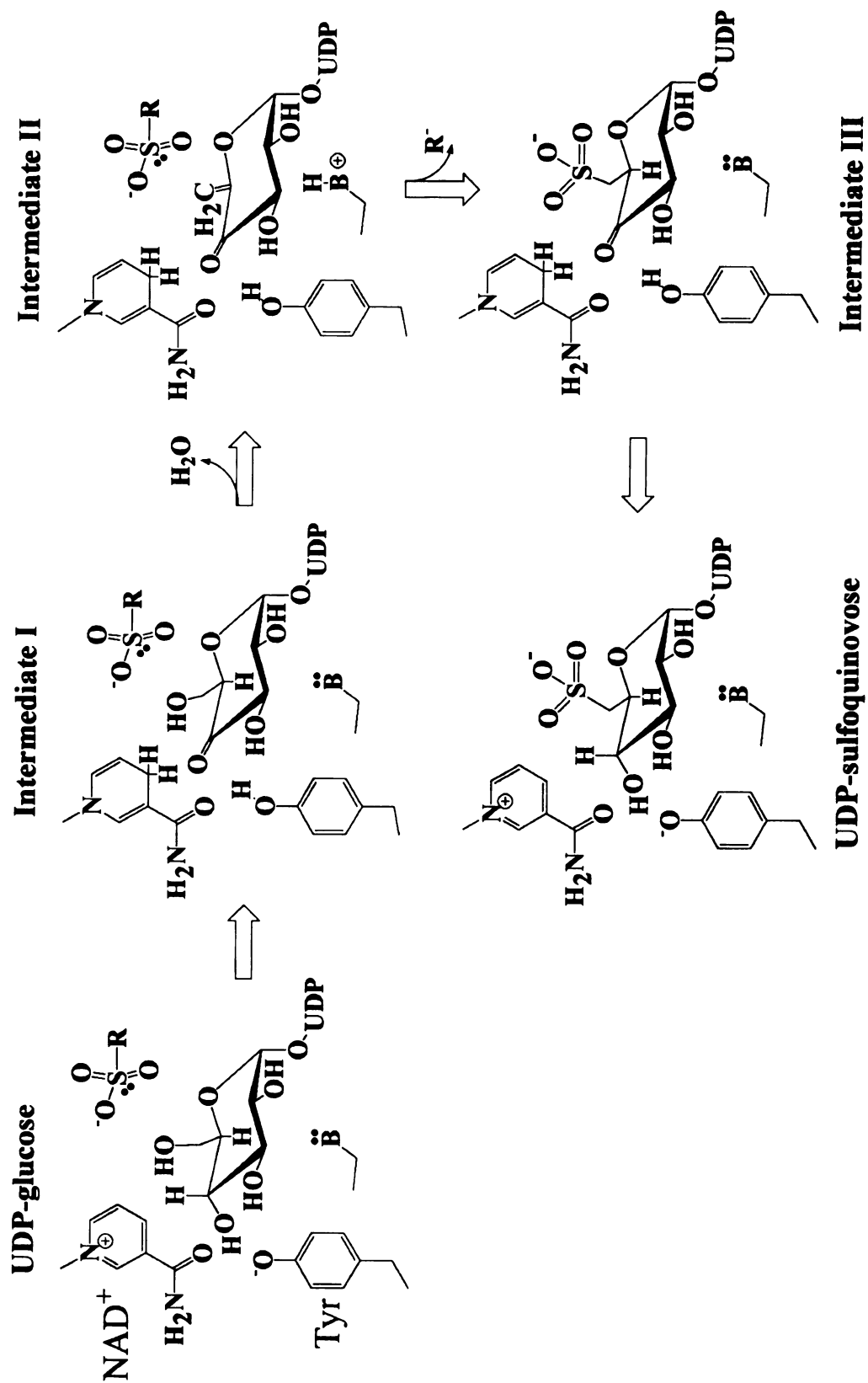
Figure 8. The early hypothetical catalytic mechanism for SQD1.

general base

hydroxyl gr

electrophili

the C5'=C

Intermediat

to C4', and

UDP-sulfo

catalysis.

Structural

The

established

now set ab

and functi

metaboliz

quaternary

the SDRs

how are

SQD1 ca

were init

ligands, v

biochemi

and led t

general base removes a proton from C5′ of the glucose ring, leading to loss of the 6′-hydroxyl group as water and formation of a 4′-keto-5′,6′-ene Intermediate II. An electrophilic sulfonyl group from the sulfur donor (depicted as R-SO$_3^-$) then adds across the C5′=C6′ double bond. The general base returns its proton to C5′, yielding Intermediate III. Finally, the reaction runs "in reverse", with NADH returning a hydride to C4′, and the catalytic tyrosine replacing a proton on O4′. Thus, the final product, UDP-sulfoquinovose, is formed and the enzyme is regenerated for another round of catalysis.

Structural biology of SQD1

The importance of SQD1 (and SQDB) in sulfolipid biosynthesis had been established and hypotheses had been made as to its structure and mechanism. We have now set about filling in the missing pieces of the puzzle. First were questions of structure and function. Is SQD1 really an SDR, and did it bind NAD$^+$? Does it bind and metabolize UDP-glucose? What are the important protein residues? What is the quaternary structure? How does SQD1 coordinate a bisubstrate reaction, uniquely among the SDRs? Second were questions of biological relevance. What is the sulfur donor, and how are substrates supplied to the enzyme? To better understand the mechanism of SQD1 catalysis and its relationship to homologous enzymes, crystallographic studies were initiated. Structures of wild-type and mutant SQD1, in complex with several ligands, were obtained. The results of these studies, in conjunction with more extensive biochemical characterization, have lent support to the hypotheses put forward for SQD1 and led to a better understanding of its biological role. Structural aspects important for

function ha

mechanisms

function have been identified, several of which have implications for the catalytic

mechanisms of other SDRs. Finally, interesting new questions have been raised.

Cell culture

The

temperature

used to inc

100 μg ml

37°C with

flask with

The 1 L c

optical der

(IPTG) is

and growt

minutes a

nitrogen f

cell pellet

Protein p

T

frozen cc

buffer (5

original

overheat

Materials and Methods

Cell culture

The procedure is largely as prescribed by Qiagen (Valencia, CA). A low-temperature stock of E. coli, harboring the pQE-30 plasmid containing the SQD1 gene, is used to inoculate a 50 mL Erlenmeyer flask holding 20 mL of LB medium, containing 100 µg/mL ampicillin and 25 µg/mL kanamycin. The inoculate is incubated overnight at 37°C with shaking at 200 rpm. The next day, the overnight culture is added to a Fernbach flask with 1 L of LB medium containing 100 µg/mL ampicillin and 25 µg/mL kanamycin. The 1 L culture is incubated at 37°C with shaking at 200 rpm for 2-3 hours, until the optical density measured at 600 nm is approximately 0.6. Isopropyl-β-D-thiogalactoside (IPTG) is added to 1 mM final concentration (238.3 mg/L) to induce SQD1 expression, and growth is continued for and additional 5 hours. The cell culture is centrifuged for 20 minutes at 4000 g, the supernatant solution is discarded, and the pellet is frozen in liquid nitrogen for storage at –80°C. Each liter of cell culture generally yields 2-3 mL of packed cell pellet.

Protein purification

The procedure is modified from that described by Qiagen. About 5-10 mL of frozen cell pellet is thawed in a room temperature water bath and suspended in Lysis buffer (50 mM HEPES, 300 mM NaCl, 10 mM imidazole, pH 8.0) to 2-3 times its original volume. The cells are broken with microtip sonication, done on ice to avoid overheating. Three 20 second bursts at 40-50% of full power are used, with a pause

be

10

sp

on

eq

Ly

m

tag

Elu

is

the

stag

ligh

con

inte

is

con

mer

con

7.5)

typi

deter

between bursts to cool down. The disrupted cells are centrifuged at 4°C and 3,000 g for 10 minutes to pellet cell debris. If desired, the pellet may be resuspended, sonicated and spun again in an effort to extract more SQD1 protein. The supernatant solution is loaded onto a column packed with about 5 mL of Ni-NTA Superflow resin (previously equilibrated with 10 volumes of Lysis buffer), followed by three column volumes of Lysis buffer. Three column volumes of Wash buffer (50 mM HEPES, 300 mM NaCl, 20 mM imidazole, pH 7.5) are passed through the column to remove weakly-binding non-tagged proteins. SQD1 is removed from the column with four column volumes of Elution buffer (50 mM HEPES, 300 mM NaCl, 200 mM imidazole, pH 7.5). The column is cleaned after use by thorough washing with 20% (v/v) ethanol, and stored at 4°C until the next purification.

SDS-PAGE gels may be run, as described above, to monitor the success of each stage of the purification. The protein concentration may be estimated from absorbance of light at 280 nm or by the Pierce BCA assay. However, the presence of imidazole complicates the results of either method because it absorbs light at 305 nm and may interfere with the BCA assay by liganding copper. For crystallization, the pooled protein is concentrated to at least 3-4 mg/mL by centrifugation using a Millipore Ultrafree concentrator with a 30 kDa nominal molecular weight limit (NMWL) ultrafiltration membrane. If desired, excess imidazole may be removed by repeated cycles of concentration and dilution with "Dialysis buffer" (25 mM HEPES, 300 mM NaCl, pH 7.5). Addition of any ligand, such as UDP-glucose or NAD^+, is done at this point, typically to concentration of 5 mM. An unusual, "sulfurous" smell, whose origin was not determined, may be given off by the protein on standing for some time. Typical yield of

pur

eac

Ge

PC

pro

CA

rea

pur

Cry

at a

the

han

Scr

cry

set

anc

pla

diff

purified protein was 3-4 mg for each mL of cell pellet, corresponding to about 8 mg for each liter of cell culture.

Generation of site-directed mutations

Site-directed mutagenesis was carried out as described by Sanda *et al.* (71). The PCR mutagenesis technique (72) was used to convert Thr145 to alanine. The PCR products were introduced into the plasmid pPCR-Script AmpSK(1) (Stratagene, La Jolla, CA) and sequenced (Michigan State University Sequencing Facility). The mutant open reading frame was inserted into pQE30 (Qiagen) and expressed in *E. coli*. The purification procedure was identical to that described above for wild-type SQD1.

Crystallization

All crystallization experiments were carried out in a temperature-controlled room at approximately 20°C. Initial crystallization conditions were identified by a member of the Benning group, Bernd Essigmann, using sparse matrix screening and employing the hanging-drop vapor diffusion method of crystallization. Crystal Screen I and Crystal Screen II sparse matrix crystallization kits (Tables 1 and 2) and VDX hanging-drop crystallization trays were purchased from Hampton. Each crystallization experiment was set up by mixing equal volumes of SQD1 protein solution and a Crystal Screen reagent and suspending the drop over a reservoir of the same reagent, in a chamber of the VDX plate.

For crystallization under the final, optimized conditions, the sitting-drop vapor diffusion method in Hampton Cryschem sitting drop plates is used. The reservoir is 1 mL

in volume.

appropriate

concentrati

versus the

0.75 M).

to prevent

Incubatio

To

mutant pr

sulfite wa

room tem

described

Collectio

I

crystals

at least

cryoprot

NaN₃ an

in a nylo

Shop, Ya

either dir

in volume, while drops are made by combining 5 μL of protein solution with 5 μL of appropriate drop stock solution. Each crystallization experiment screens the concentration of $(NH_4)_2SO_4$ in the reservoir (with an average value of about 1.5 M) versus the concentration of $(NH_4)_2SO_4$ in the drop stock solution (average value about 0.75 M). All crystallization solutions have 0.1 M MES buffer, pH 6.5, and 1 mM NaN_3 to prevent microbial growth. It is not necessary to cleave the His-tag for crystallization.

Incubation with sulfite prior to crystallization

To form the complex of T145A SQD1 with NAD^+ and UDP-sulfoquinovose, mutant protein was purified and concentrated as usual. Next, freshly-prepared sodium sulfite was added to a final concentration of 200 μM. After several hours of incubation at room temperature, the sulfite-incubated protein sample was set up for crystallization as described above.

Collection and processing of X-ray diffraction data

Initial SQD1 diffraction data were collected at room temperature from small crystals mounted in sealed capillary tubes. For routine data collection, crystals of SQD1 at least 0.2 mm in their longest dimension were transferred with fiber loops to a cryoprotectant solution typically containing 1 M $(NH_4)_2SO_4$, 0.1 M MES, pH 6.5, 1 mM NaN_3 and 30% (w/v) glycerol. A crystal was picked up from the cryoprotectant solution in a nylon fiber cryoloop (Hampton Research) attached to a cryopin (Gibbs Instrument Shop, Yale University, New Haven, Connecticut) and flash-cooled to the vitreous state, either directly in a stream of cold nitrogen, or by plunging into a vial of liquid propane.

1) ...
m...
and
sys
go...
ter
ter
eit
pla
di...
av
str
pr
2)
1(
ra
ei
m
co
lo
by
w

Diffraction data were measured and processed in one of three ways:

1) A Rigaku RU200H generator with a rotating copper anode, operated at 50 kV and 100 mA with a 0.3 mm filament, was used to produce X-radiation. The radiation was focused and monochromated to the copper K_α wavelength (1.5418 Å), either with an MSC mirror system or with Osmic multilayer confocal optics. The crystalline sample, mounted on a goniometer with rotatable φ- and 2θ-axes ($\chi=0°$, $\omega=\varphi$), was cooled to cryogenic temperatures, typically 100K, with a stream of nitrogen vapor produced by an MSC low temperature device. The position and intensities of diffracted X-rays were measured by either an MSC R-AXIS IIc imaging plate detector or an MSC R-AXIS IV++ imaging plate detector. The HKL suite (XdisplayF, Denzo and Scalepack) was used to index the diffraction pattern, integrate the spot intensities, scale the integrated intensities and average symmetry-related reflections. The fully processed intensities were converted to structure factor amplitudes using TRUNCATE and other utilities from the CCP4 suite of programs.

2) A Bruker Direct Drive generator with a rotating copper anode, operated at 50 kV and 100 mA with a 0.3 mm filament, was used to produce polychromatic radiation. The radiation was focused and monochromated to the copper K_α wavelength (1.5418 Å) with either Bruker Göbel mirrors or Osmic multilayer confocal optics. The crystalline sample, mounted on a goniometer with rotatable φ-, ω- and 2θ-axes and a fixed χ of 54.74°, was cooled to cryogenic temperatures with a stream of nitrogen vapor produced by an MSC low temperature device. The position and intensities of diffracted X-rays were measured by a Bruker HI-STAR multiwire area detector. The Bruker programs SADIE and SAINT were used to index the diffraction pattern, integrate the spot intensities, scale the

integ

amp

3) T

ID.

poly

(an

vert

tem

cus

diff

ave

De

(M

(N

he

the

we

co

de

we

Pa

integrated intensities, average symmetry-related reflections and convert to structure factor amplitudes.

3) The Advanced Photon Source (Argonne National Laboratory, Illinois), beamline 19-ID, with an operating current of 60-100 mA and coupled to an undulator, produced polychromatic synchrotron radiation. The radiation was monochromated to 1.03221 Å (an energy of 12 keV) with a sagitally-focusing silicon (111) double crystal and a vertically focusing mirror. Crystals were kept at a temperature of 100-110K by a low-temperature device. The position and intensities of diffracted X-rays were measured by a custom-built 3x3 CCD-array detector (SBC2). HKL2000 was used to index the diffraction pattern and integrate the spot intensities. Scaling of integrated intensities and averaging of symmetry-related reflections was done with Scalepack, from the HKL suite.

Determination of phases by multiple isomorphous replacement (MIR)

For phase determination by the method of multiple isomorphous replacement (MIR), formed crystals of SQD1 were transferred to cryoprotectant solution (1 M $(NH_4)_2SO_4$, 0.1 M MES, pH 6.5, 1 mM NaN_3 and 30% (w/v) glycerol) containing a heavy atom compound. The crystals were left in the solution overnight to allow time for the heavy atom compound to enter the crystal and bind to specific sites. Diffraction data were then collected from the putatively-derivatized crystal. Particular care was taken to collect highly accurate, complete, and redundant data and to measure Friedel pairs for detection of any anomalous scattering signal. Heavy atoms in successful derivatives were found with SOLVE 1.10, and their locations were confirmed by visual inspection of Patterson maps calculated with the CCP4 suite (24). SOLVE used the locations of the

hea

flat

wer

fina

À r

Mo

MI

out

am

set

ref

or

dT

par

F.

Th

der

pro

jus

wa

po

heavy atom derivatives to estimate phases for the native SQD1 reflections. After solvent flattening, initial F_o electron density maps to 2.8 Å resolution were calculated. The maps were visually evaluated with programs from the CCP4 suite and with CHAIN (73). For final model-building and refinement, a higher-resolution native dataset extending to 1.6 Å resolution was collected.

Model building, refinement and analysis

For the original SQD1 structure determination, manual model-building into the MIR electron density maps was done with CHAIN, and computer refinement was carried out with X-PLOR 3.851, using a least-squares target on the observed structure factor amplitudes (F_o) (74). For cross-validation, 5% of the reflections were reserved in a "test set". This subset was used only in calculation of the "free R-factor" (R_{free}). The reserved reflections were not used for refinement, calculation of the crystallographic R-factor (R) or electron density maps. The structures of *E. coli* UGE (PDB entry 1XEL) and *E. coli* dTGD (PDB entry 1BXK) were used as starting points (75,76). The protein model was partially built with experimental phased density maps at 2.8 Å resolution, using data with $F/\sigma(F) > 2$, and refined by simulated annealing and positional energy minimization. Thereafter, refinement continued using the 1.6 Å data with $F/\sigma(F) > 1$, and phases derived from the model. Models of NAD^+, UDP-glucose, water, sulfate and alternate protein side chain conformations were added at different points in the refinement, when justified by the $2 F_o$-F_c and F_o-F_c electron density maps. Later, a bulk solvent correction was applied and isotropic B-factors were individually refined for each atom, while positional energy minimization refinement was continued. Refinement ended when the

model could not be improved further.

Later SQD1 structures were refined with Crystallography and NMR System (CNS) 0.9a, a descendent of X-PLOR (77). The starting model in each case was the 1.6 Å wild-type structure, stripped of all nonprotein atoms and alternate conformations. B-factor values were reset to the overall value estimated from a Wilson plot by TRUNCATE. Again, 5% of the reflections from each data set were reserved for cross-validation. The same set of test reflections was chosen for each dataset, so that R and R_{free} could be compared meaningfully between all refinements. A maximum-likelihood target on structure factor amplitudes was used for refinement, and a bulk solvent correction was applied at all stages. An initial round of rigid-body refinement was used to position the model in the unit cell, followed by cycles of energy minimization of atomic positions. Manual adjustment of the model to better fit the electron density was done with the program CHAIN. In the later stages of refinement, the isotropic temperature factor of each atom was refined, but with the application of restraints. As refinement progressed, ligands, waters and alternate conformations were modeled when justified by the $2F_o$-F_c and F_o-F_c electron density maps. The stereochemical quality of the models was assessed with the program PROCHECK (78). PDBfit, from the XtalView package, was used to align 3-dimensional structures (79).

prote

resul

rema

bodi

more

refo

furth

SQD

by:

kee

Cr

of

Be

fro

O

re

1

Results

Purification of SQD1 protein

The purification protocol described above consistently produced high-quality protein in amounts sufficient to support crystallographic studies. A typical SDS-PAGE result is shown in Figure 9. As can be seen from the gel, a significant amount of SQD1 remains in the cell pellet after sonication and centrifugation, presumably as inclusion bodies; resonication of the pellet did not liberate much more SQD1. It is possible that more SQD1 protein could be recovered by purifying under denaturing conditions, then refolding the protein. However, because the amount of soluble SQD1 was sufficient for further work, attempts to achieve higher yield by these means were not pursued. Purified SQD1 was found to precipitate spontaneously from solution, a process which is retarded by: 1) increasing the ionic strength, *e.g.* by having 0.3 M NaCl in all buffers and 2) keeping the protein solutions at room temperature, rather than 4°C.

Crystallization

Small crystals of recombinant SQD1 were first observed in the former laboratory of Dr. Christoph Benning at the Institut für Genbiologische Forschung Berlin GmbH, in Berlin, Germany. At Michigan State University, we used sparse matrix screening kits from Hampton Research to identify a broader range of initial crystallization conditions. Out of 96 conditions from Crystal Screen I and Crystal Screen II (Tables 1 and 2), 35 resulted in the formation of crystals. The reagents which produced crystals were 2, 4, 7, 10, 14, 16, 29, 32-34, 36, 39, 46 and 47 from CSI and 1, 2, 5, 7, 14, 15, 20, 21, 23, 24,

1 Whole cells, sonicated
2 Supernatant (first extraction)
3 Pellet (first extraction)
4 Supernatant (second extraction)
5 Pellet (second extraction)
6 Flow-through from loading Ni-NTA column
7 Eluent from washing column with Lysis buffer
8 Eluent from washing column with Wash buffer
9 Eluent from from elution of column (purified SQD1)
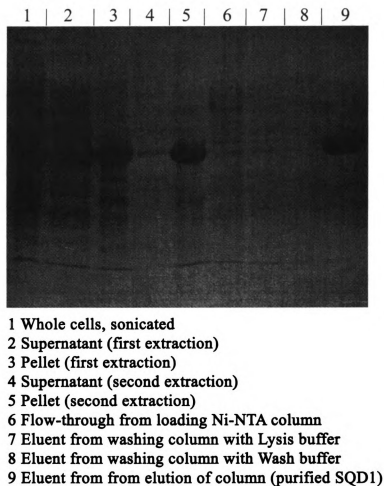
Figure 9. SDS-PAGE of samples from the course of an SQD1 purification.

28-34, 36.

bipyramid.

The best c

the precip

of exogen

the order c

approxim.

goal of g

seed crys

The large

Crystals c

In the ca

of a size

crystalli

T

disturba

liquor te

between

liquor te

diffract

observe

SQD1 c

seems tc

28-34, 36, 37, 42, and 48 from CSII. All of the crystals were colorless and all had bipyramidal morphology, with the exceptions of needle crystals in CSI-10 and CSI-14. The best crystals (Figure 10) were obtained by crystallizing with ammonium sulfate as the precipitant, as described above. The size of the crystals was improved by the addition of exogenous UDP-glucose and, to a lesser extent, NAD^+. Crystals with dimensions on the order of 0.20 x 0.20 x 0.15 mm could be grown with ease, while larger crystals up to approximately 0.30x0.30x0.20 mm were more rarely seen. Seeding experiments with the goal of growing larger crystals were not successful; in macroseeding experiments, the seed crystal did not grow, while microseeding produced only a shower of small crystals. The largest crystals grown were up to 0.6 mm long, but smaller in the other dimensions. Crystals usually appeared after days to weeks, with an average time of about two weeks. In the case of T145A mutant protein preincubated with UDP-glucose and sulfite, crystals of a size suitable for diffraction studies were not observed until six months after the crystallization experiment was set up.

The crystals are fairly resistant to physical manipulation and extremely stable to disturbances in their chemical environment. For example, crystals removed from mother liquor to distilled, unbuffered water showed no changes in morphology until some time between three and five days, when they dissolved. Crystals moved directly from mother liquor to solutions containing only sodium sulfite (about 1 M) and 30% (w/v) glycerol diffracted normally. Except when using synchrotron X-rays, no radiation decay was observed, either at ambient or at cryogenic temperatures. Despite this stability, over time SQD1 crystals change from being colorless to having a uniform brown tint. This process seems to be accelerated by the addition of exogenous NAD^+. Brown crystals do not
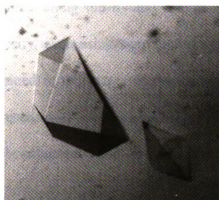
Figure 10. Typical SQD1 crystals.

diffract to as high a resolution as colorless crystals, and often contain rings of unknown origin in the diffraction pattern. Electron density maps calculated with X-ray diffraction data collected from brown crystals show no obvious structural changes. It may be that any structural changes are not well ordered or that they are purely electronic, having no effect on conformation.

SQD1 crystals with atypical morphology are sometimes seen. Very small, rod-shaped SQD1 crystals have occasionally been observed, particularly in the absence of UDP-glucose. Because of their small size, it is difficult to accurately describe their morphology, and they could even be bipyramidal crystals which have grown extensively along the c-axis and very little along the a- and b-axes. These crystals have never diffracted with useable intensity, even using synchrotron radiation, and so their internal symmetry cannot be determined in this way. Very shallow, vaguely hexagonal plates were also seen in the presence of UDP, growing from ammonium formate and ammonium sulfate/glycerol solutions, but these were too small to be further characterized.

Collection and processing of X-ray diffraction data

Bipyramidal SQD1 crystals diffract very well for their size (Table 5). Even with small crystals and using radiation from rotating anode generators, reflections to better than 3 Å resolution are almost always seen. With larger crystals reflections to 1.5 Å have been observed with the same X-ray generators. At the Advanced Photon Source, Beamline 19-ID, crystals typically diffracted to 1.4 Å, and one (designated "mjt_f12") showed spots to 1.15 Å resolution. On the basis of the diffraction patterns, the program

Denzo ass

approxima

using Sca

space gro

(described

monomer

easily es

cryoprote

P:

exception

troubles

used, as

lower-re

CCD de

on a CC

overloac

overloac

workin

HKL2(

higher

achieve

Theref

work.

Denzo assigned the bipyramidal crystals to a body-centered tetragonal space group with approximate unit cell lengths of $a=b=160$ Å and $c=99$ Å. Scaling of the diffraction data using Scalepack suggested that the crystals indeed belonged to a body-centered tetragonal space group, either I4, I4$_1$, I422 or I4$_1$22. During the course of phase determination (described below) the space group was definitively established as I4$_1$22, with a protein monomer in the asymmetric unit. Conditions for low-temperature data collection were easily established for SQD1, because the crystals are not damaged by soaking in cryoprotectant solutions, even when directly transferred from mother liquor.

Processing of SQD1 diffraction data was generally free of difficulties. An exception to this was some of the higher-resolution data from the APS. The root of those troubles was the limited dynamic range and the small active area of the CCD detector used, as well as flaws in the data processing program. The intensities of many of the lower-resolution spots in the diffraction pattern had exceeded the dynamic range of the CCD detector, and hence were not very accurately measured. Such "overloaded pixels" on a CCD detector also have the effect of disturbing measurements in neighboring, non-overloaded pixels, thus further reducing accuracy. For unknown reasons, the presence of overloads caused the spot intensity integration program, HKL2000, to repeatedly stop working. Nearly a year passed before it was possible to use an improved version of HKL2000 which was less failure-prone. Finally, because the diffraction extended to higher resolution than expected, the detector 2θ angle was not increased sufficiently to achieve adequate data completeness and redundancy in the highest-resolution ranges. Therefore, the resolution of the dataset was truncated from 1.15 Å to 1.20 Å for further work. As a rule of thumb, particular care should be taken to the planning of data

Table 5

Statistics for SQD1 diffraction datasets

Complex	WT/substrate	WT/substrate	T145A/substrate	T145A/substrate
PDB ID	1QRR	1I24	1I2C	1I2B
Wavelength (Å)	1.542	1.033	1.542	1.542
Resolution (Å)	30.00 – 1.60	20.00 – 1.15	30.00 – 1.60	30.00 – 1.75
Space group	$I4_122$	$I4_122$	$I4_122$	$I4_122$
Cell axes (Å)	$a=b=159.6, c=98.9$	$a=b=160.2, c=99.3$	$a=b=159.7, c=99.0$	$a=b=159.6, c=99.1$
Total observations	253,130	1,163,055	366,147	316,254
Unique observations	75,606 (4,965)†	196,326 (8,567)	82,759 (8,044)	63,698 (6,246)
Tot/Uni≈Redundancy	3.35	5.92	4.42	4.96
Completeness (%)	90.4 (60.3)	86.4 (38.0)	98.8 (97.6)	99.1 (98.1)
Average I/σ(I)	9.6 (0.8)	21.4 (1.7)	13.5 (1.5)	17.4 (2.0)
R_{sym} (%)	5.5 (38.4)	9.7 (36.6)	9.4 (36.2)	8.0 (33.7)

† Values in parentheses are for the 10% of data in the highest resolution shell.

76

coll

Det

deri

gluc

(MI

fact

diff

pha

sha

bou

uns

aga

res

Å "

Mo

wit

geo

φ-ψ

of a

collection when a CCD detector is used.

Determination of phases by multiple isomorphous replacement (MIR)

A molecular replacement solution could not be found for SQD1, using models derived from structures of *E. coli* UDP-galactose 4-epimerase (UGE) and *E. coli* dTDP-glucose 4,6-dehydratase (dTGD) (75,76). Instead, the multiple isomorphous replacement (MIR) technique was used to experimentally determine the phases of the structure factors. Five of the diffraction datasets collected from SQD1 crystals, derivatized with different types and concentrations of heavy atom compounds, were found to be useful for phase determination (Table 6 and Figure 11). The 10 and 20 mM KAu(CN)$_2$ derivatives shared one strongly-bound site, but the 20 mM derivative had an additionally, weakly-bound site. Data from a "pseudo-native" crystal ("Native 2" in Table 7), which had been unsuccessfully derivatized with mercury dibromofluorescein (MBF), was used for scaling against the successfully derivatized crystals. A partial model built was with the 2.8 Å resolution "Native 2" dataset, then refinement was continued and completed with the 1.6 Å "Native 1" dataset.

Model refinement and analysis

Refinement of the four SQD1 models (Table 8) produced very similar structures, with low root mean squared deviations for atomic alignment (Tables 9 and 10). The geometry of all models was very good, with at least 90% of nonglycine residues having φ-ψ angles in the allowed region (Figure 12). The largest differences were in the number of alternate conformations, the number and positions of bound water molecules, and in

Table 6

Positions of heavy atoms in SQD1 derivatives

Derivative	Site #	Heavy atom coordinates (Å)		
		x	y	z
$KAu(CN)_2$, 10 mM,	1	59.26	69.77	35.08
$KAu(CN)_2$, 20 mM	1	59.15	69.69	35.17
$KAu(CN)_2$, 10 mM,	2	74.71	81.10	43.29
$KAu(CN)_2$, 20 mM	2	74.67	81.09	43.08
EMTS	1	57.28	68.31	34.05
EMTS	2	74.51	81.53	43.20
EMTS	3	57.68	106.10	29.45
PHMBS	1	68.71	67.91	21.11
PHMBS	2	54.22	77.23	44.16
PHMBS	3	57.57	68.85	34.23
$UO_2(CH_3COO2)$	1	63.69	66.51	50.19

Figure 11. Binding sites of heavy atoms in MIR derivatives. The sites are relative to the final, refined structure. The scene is in stereo. The protein backbone is represented by a blue ribbon. NAD^+ and UDP-glucose atoms are shown as spheres, colored green and red, respectively. The heavy atoms of each derivative are shown as spheres of various colors. The yellow spheres are for the gold atoms in the $KAu(CN)_2$ derivatives, the blue spheres are mercury atoms of EMTS, the magenta spheres are mercury atoms of PHMBS and the orange sphere is uranium of $UO_2(CH_3COOH)_2$.

Figure 11

Table 7
MIR phasing statistics

Dataset	d_{min} (Å)	Unique Reflections	Completeness[†]	R_{sym}[†]	R_{merge}	Sites	$\langle F_h \rangle / \langle E \rangle$[‡]
Native 1	1.6	75,606	0.904 (0.603)	0.055 (0.384)	---	---	---
Native 2	2.8	13,952	0.908 (0.926)	0.070 (0.100)	---	---	---
KAu(CN)$_2$, 10 mM	3.0	12,621	0.972 (0.969)	0.051 (0.075)	0.145	1	0.78
KAu(CN)$_2$, 20 mM	3.0	12,620	0.969 (0.948)	0.048 (0.083)	0.220	2	0.67
EMTS, 1 mM	3.0	12,711	0.976 (0.973)	0.057 (0.089)	0.126	3	1.00
PHMBS, 1 mM	3.0	12,601	0.968 (0.960)	0.087 (0.141)	0.222	3	1.01
UO$_2$(CH$_3$COO)$_2$, 5 mM	3.0	12,767	0.980 (0.963)	0.077 (0.138)	0.097	1	0.43

[†] Values in parentheses are for the 10% of data in the highest resolution shell.
[‡] $\langle F_h \rangle$ Is the root mean squared deviation of the heavy atom scattering factor and $\langle E \rangle$ is the RMS of the lack of closure.

81

Table 8

Statistics for refinement and final stereochemistry of SQD1 models

Complex	WT/substrate	WT/substrate	T145A/substrate	T145A/product
PDB ID	1QRR	1I24	1I2C	1I2B
Number of reflections used	63,023 ($\sigma(F) \geq 1$)	184,009 ($\sigma(F) \geq 0$)	82,704 ($\sigma(F) \geq 0$)	63,693 ($\sigma(F) \geq 0$)
Working set	72,378	174,749	78,759	60,499
Test (free R) set	3228	9,260	4,125	3,194
Completeness	90.4 (60.3)	92.3 (82.1)	98.8 (97.6)	99.1 (98.1)
R (%)	17.0	19.2	17.7	18.0
R_{free} (%)	19.1	19.8	18.5	19.6
Number of residues (number of atoms)				
Total	(3481)	783 (3,622)	795 (3,542)	799 (3,539)
Protein	390 (3040)	393 (3,145)	393 (3,053)	393 (3,043)
Water	351 (351)	386 (386)	398 (399)	402 (402)
Sulfate	2 (10)	2 (10)	2 (10)	2 (10)
NAD^+	1 (44)	1 (44)	1 (44)	1 (44)
UDP-hexose	1 (36)	1 (37)	1 (36)	1 (40)
Parameters	13,924	14,488	14,168	14,160
Data/parameters	4.5	12.1	5.6	4.3
Root mean square deviations for protein stereochemistry				
Bond lengths (Å)	0.005	0.012	0.0053	0.0055
Bond angles (°)	1.37	1.58	1.29	1.27
Average B-factor (Å^2)	14.4	13.4	17.7	21.0
% with most favored φ-ψ angles	89.9	91.5	90.3	90.0
% with allowed φ-ψ angles	10.1	8.5	9.7	10.0

Parenthetic values of completeness are for the 10% of data in the highest resolution shell.

Table 9

RMSD (Å) for alignment of SQD1 crystal structures on all α-carbons

	WT/substrate 1.20 Å	T145A/substrate 1.60 Å	T145A/substrate 1.75 Å
WT/substrate 1.60 Å	0.125	0.096	0.078
WT/substrate 1.20 Å	-----	0.101	0.098
T145A/substrate 1.60 Å	-----	-----	0.052

Table 10

RMSD (Å) for alignment of SQD1 crystal structures on all protein atoms

	WT/substrate 1.20 Å	T145A/substrate 1.60 Å	T145A/substrate 1.75 Å
WT/substrate, 1.60 Å	0.252	0.251	0.239
WT/substrate 1.20 Å	-----	0.175	0.170
T145A/substrate 1.60 Å	-----	-----	0.068

Figure 12. Ramachandran plots of the four SQD1 structures. The values for nonglycine

residues are shown as black squares; those for glycines are designated by black triangles.

The most favored regions of the plot are dark gray, the allowed regions are medium gray,

the additional allowed are light gray, and the disallowed regions are white. The plots

were generated by PROCHECK 3.0.1 (78).
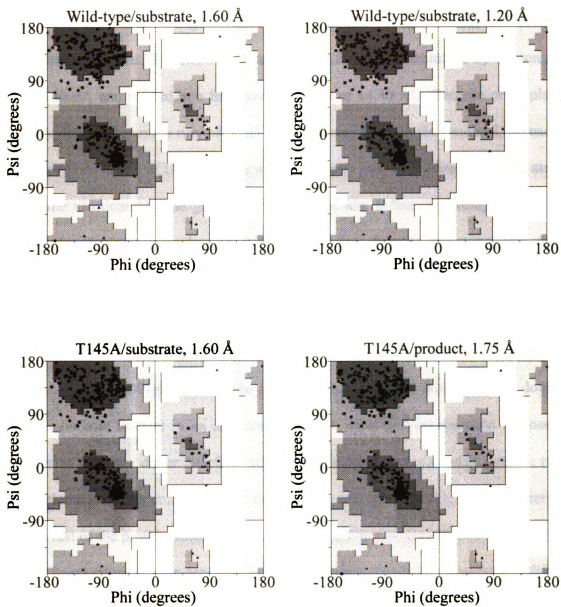
Figure 12

the UDP-hexose ligands.

The structure of wild-type SQD1 with NAD⁺ and UDP-glucose at 1.60 Å resolution

The model from the original SQD1 structure determination contains amino acid residues 2-391, NAD⁺, UDP-glucose, 2 sulfate ions and 351 (67 buried, 284 surface) water oxygens (Figure 13). The overall temperature factor was estimated by Wilson plot to be 12.40 $Å^2$, and refined to a final average value of 14.40 $Å^2$. Because of its planar geometry, the nicotinamide ring of NAD⁺ was assumed to be in the oxidized, unreacted state. The glucose ring of UDP-glucose was also clearly seen to be unreacted. The atoms of both the nicotinamide and glucose moieties have low B-factors (average values are 8.39 $Å^2$ for the nicotinamide and 9.77 $Å^2$ for the glucose, indicating that these conformational states are tightly and homogenously maintained. No candidate for a sulfur donor was observed in the crystal structure. The protein itself has two domains, a larger, modified Rossmann dinucleotide-binding fold containing NAD⁺, and a smaller domain that binds UDP-glucose (Figure 13). Two long α-helices from the large domain of each monomer interact in an antiparallel fashion with their counterparts in another monomer to form the dimer interface, which is coincident with a crystallographic two-fold rotational axis. An unusual feature is formed by residues 161-172, which project out from the rest of the protein, forming a β-ribbon that lies against the other monomer of the dimer. The coordinates were deposited at the Protein Data Bank (PDB) as entry 1QRR.

NAD⁺ binding

NAD⁺ is buried within the protein in an extended conformation. Interactions of

Figure 13. Overall structure of SQD1. A dimer, generated by crystallographic symmetry, is shown. a) The protein backbone is represented by ribbons and strands. The large domain of monomer A is dark blue, the small domain of monomer A is orange, the large domain of monomer B is light blue and the small domain of monomer B is yellow. NAD^+ is depicted as green sticks and UDP-glucose as red sticks. b) A molecular surface is drawn over all protein atoms of each monomer. The surface over monomer A is colored dark blue, while that over monomer B is colored light blue.

a

b
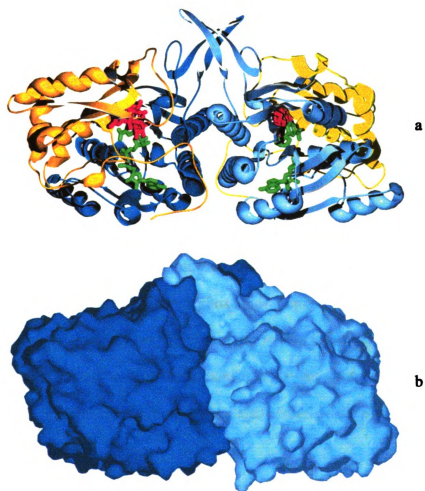
Figure 13

NAD$^+$ in the binding cleft (Figure 14, adapted from Mulichak et al. (80)), are provided by residues near the C-termini of the Rossmann fold β-strands. The NAD$^+$ pyrophosphate binds at the N-terminus of the α1 helix, with the phosphoryl groups hydrogen-bonding to backbone amide nitrogens of Tyr12 and Cys13, as well as the side chains of Arg36 and Arg101. Both hydroxyls of the NAD$^+$ adenosyl ribose are liganded by the carboxyl oxygens of Asp32, located at the base of the β2 strand. The amide group of Arg36 is also within hydrogen bonding distance of the O2' adenosyl ribose hydroxyl. The Asp75 side chain hydrogen bonds to the adenosyl amino group, whereas the main-chain amide nitrogen of Ile76 interacts with the N1 ring nitrogen. The Asn119—O$_\delta$ and —N$_\delta$ side-chain atoms make additional hydrogen bonds to the adenosyl N6 and N7 atoms, respectively.

Around the nicotinamide ribose moiety in SQD1, the conserved Tyr182 and Lys186 side chains interact with the ribose hydroxyls. The NAD$^+$ nicotinamide moiety adopts a *syn* conformation, with the carboxamide nitrogen atom within 2.8 Å of the nearest NAD$^+$ phosphoryl oxygen. The *syn* conformation may be further stabilized by an additional hydrogen bond between the carboxamide oxygen atom and the amide nitrogen of Val212 (3.2 Å). The carboxamide oxygen also makes a solvent-mediated interaction with the Val212 carbonyl oxygen.

NAD$^+$ interactions in the SQD1 binding site also include five solvent-mediated hydrogen bonds with phosphoryl oxygen atoms and one adenosyl ribose hydroxyl oxygen. Another notable interaction near the catalytic site involves WAT410 which is aligned with the plane of the nicotinamide ring and lies 3.18 Å from the C6 atom, within hydrogen-bonding distance. Although otherwise buried within the complex, WAT410 is
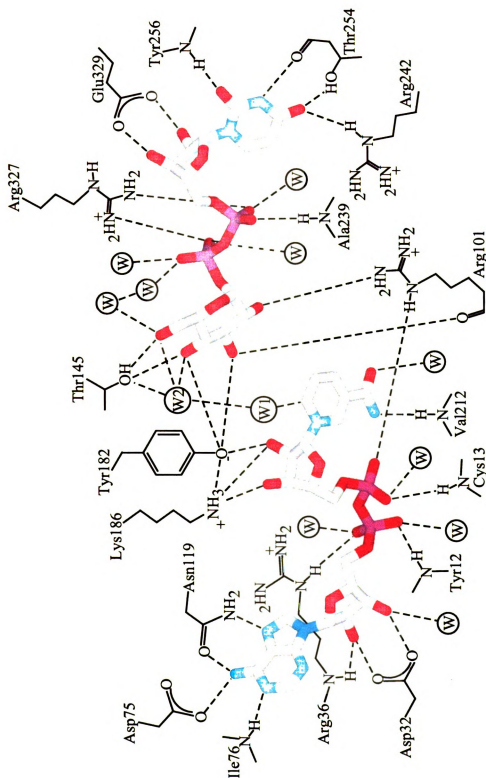
Figure 14. Binding interactions of NAD^{+} and UDP-glucose.

90

also in good hydrogen-bonding distance of both the Gln209 amide nitrogen and the Leu207 carbonyl oxygen, as well as another buried water molecule (WAT411).

UDP-Glucose Binding

The binding of the UDP pyrophosphate and ribose moieties (Figure 14) resembles the NAD^+ interactions. The pyrophosphoryl group is positioned near the N-terminus of an α-helix (residues 239-249) from the small domain and makes a hydrogen bond to the amide nitrogen of Ala239. Both phosphate groups interact with the Arg327 side chain and additionally make water-mediated interactions to main-chain atoms. The UDP-ribose hydroxyls hydrogen bond to either oxygen atom of the Glu329 carboxylate, an interaction mimicking that of the NAD^+ adenosyl ribose with Asp32. The uridine ring is hydrogen bonded by the side chain O_γ and main-chain carbonyl oxygen atoms of Thr254, the Arg242—N_ε atom, and the amide nitrogen of Tyr256. The binding of UDP-glucose is further stabilized by the parallel stacking interaction of the uridine and Tyr256 rings, with an interplanar distance of 3.5 Å.

UDP-glucose extends into the SQD1 cleft in such a way that the plane of the hexose ring is parallel to, and partially overlaps, the NAD^+ nicotinamide, with a distance of approximately 3.6 Å between the two rings (Figure 15a). The glucosyl 3'-hydroxyl is in hydrogen bonding distance (2.7 Å) of the 2'-hydroxyl from the NAD^+ nicotinyl ribose. The glucosyl ring also abuts closely against the surface of the large domain and is well stabilized by protein interactions. The O_γ hydroxyl of Thr145 makes two short hydrogen bonds (2.45 Å) with the O4' and O6' glucosyl hydroxyls (Figure 16a). WAT411, which is above the plane formed by these three atoms, makes close hydrogen bonds with

Figure 15. The position of UDP-glucose O6' in the SQD1 crystal structures. The scene is in stereo. F_o-F_c electron density maps shown (blue wire mesh), contoured at 4.25 σ, are shown. The maps were generated by first carrying out simulated annealing refinement, then omitting the UDP-hexose from further calculations. NAD$^+$ is green, with C4 colored orange. All other atoms are colored by element (white=carbon, red=oxygen, blue=nitrogen, purple=phosphorus, yellow=sulfur). a) Wild-type/substrate, 1.60 Å b) wild-type/substrate, 1.20 Å c) T145A/substrate, 1.60 Å d) T145A/product, 1.75 Å (both UDP-sulfoquinovose and UDP-glucose are shown).
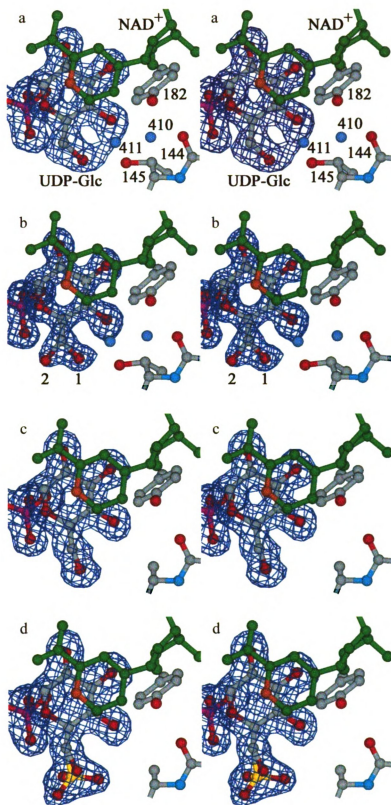
Figure 15

Figure 16. Hydrogen-bonding groups in the SQD1 active site. Molecules and their interactions are shown diagrammatically. Portions of NAD^+, UDP-glucose (UPG) and UDP-sulfoquinovose (USQ) are shown as ball-and-stick models, colored by element (gray=carbon, red=oxygen, blue=nitrogen, yellow=sulfur). Protein residues are labeled by residue type and number. Open circles represent various ordered water molecules (1=WAT410, 2=WAT411, 3=WAT461, 4=WAT463, 5=WAT470, 6=WAT475, 7=WAT466). Potential hydrogen bonds are denoted by dashed lines; those where the groups are separated by ≤ 2.5 Å are thicker. a) wild-type/substrate, 1.60 Å resolution b) wild-type/substrate, 1.20 Å resolution c) T145A/substrate, 1.60 Å resolution d) T145A/product 1.75 Å resolution (for clarity, the fraction of unreacted UDP-glucose has been omitted); The O1, O2 and O3 sulfonyl oxygens have been labeled "1", "2" and "3", respectively.

Figure 16

c

d
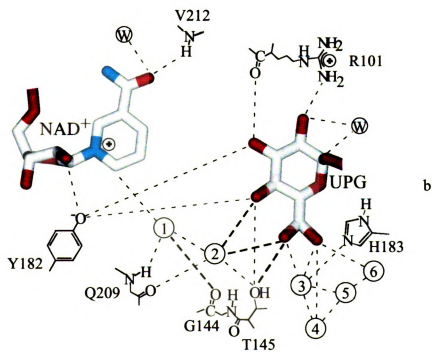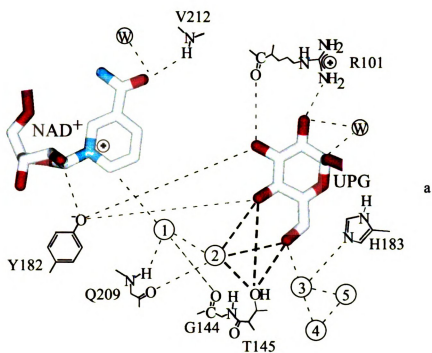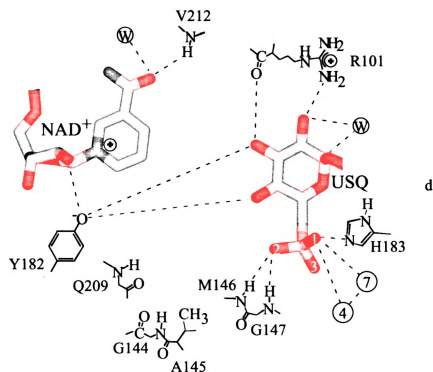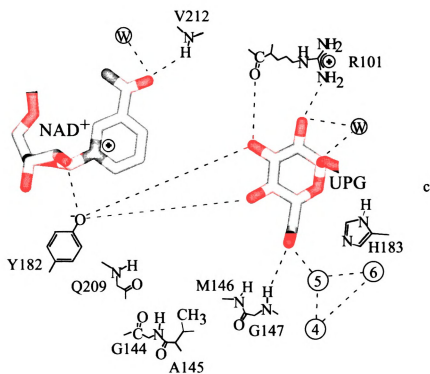
Figure 16 continued

Thr145—O$_\gamma$ (2.45 Å) and with the O4′ and O6′ hydroxyls (2.38 and 2.44 Å). WAT411 is additionally within hydrogen-bonding distance of WAT410, but is otherwise sequestered from additional solvent. The simultaneous interaction of Thr145 with both glucosyl positions forces the 6′-hydroxyl to be held in the least sterically favored rotameric orientation, placing the O6′ atom only 2.73 Å from O4′. The hydroxyl of Tyr182 is also within hydrogen bonding distance of both O4′ (2.54 Å) and O3′ (2.92 Å) glucosyl hydroxyls. Additionally, Arg101 forms hydrogen bonds with the O2′ and O3′ glucosyl hydroxyls through the guanidinium nitrogen and main-chain carbonyl oxygen atoms, respectively.

Residues 323–330 form a C-terminal flap that covers the end of the binding cleft (Figure 17). This flap is held against the rest of the protein by only one main-chain hydrogen bond (326—CO⋯HN—382) and one intraloop hydrogen bond (between Asn325⋯Glu331). Other side-chain interactions include only those of Arg327 and Glu329 with the bound UDP moiety, described above.

Sulfur-Donor Site

The Arg327 side chain on the flap also partitions off two distinct channels of buried solvent leading from the enzyme surface to the bound UDP-glucose. The first is a small channel containing eight buried water molecules that ends at the uridinyl and pyrophosphate moieties of UDP-glucose. A larger channel, designated the "sulfur donor channel", ends at a much wider solvent cavity of 9-10 Å diameter, occupied by 14 water molecules (Figure 18).

Figure 17.   The flap region of SQD1.   a) A monomer of SQD1 is shown, with a molecular surface (gray) drawn over all amino acid residues. UDP-glucose is shown as a ball-and-stick model colored by element (gray=carbon, red=oxygen); the glucose moiety is visible through the so-called sulfur donor channel (see also Figure 18). b) The same view of SQD1, with the molecular surface drawn over all amino acid residues, except those comprising the flap.   More of the UDP-glucose ligand is now exposed (purple=phosphorus).

a

b
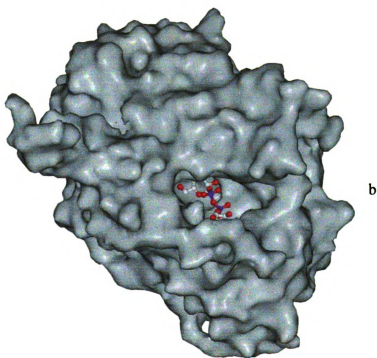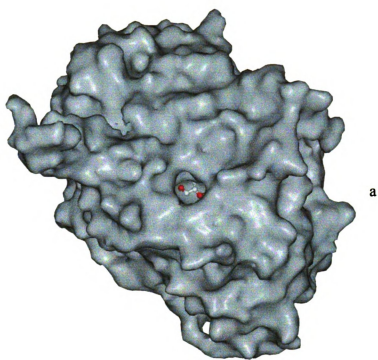
Figure 17

Figure 18. The sulfur donor channel. The scene is viewed from the protein surface. A semi-transparent molecular surface (dark gray) was drawn around all amino acid residues within 4.0 Å of waters in the channel (residues 460-474). UDP-glucose, depicted as a ball-and-stick model (gray=carbon, red=oxygen, purple=phosphorus) is glimpsed through the channel. The part of the surface which covers Arg263 is colored blue to indicate its basicity.
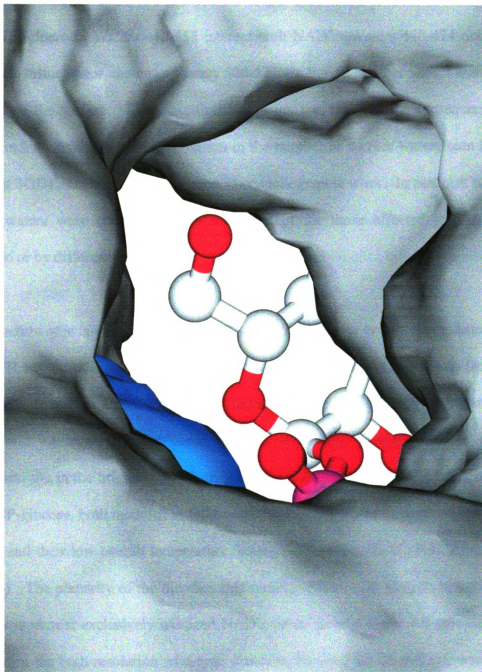
Figure 18

Bound waters

A systematic numbering scheme, based on location and interactions, was adopted for bound waters. Waters 410 and 411 are in the active site. Waters 420-427 interact with UDP-glucose. Waters 440-453 interact with NAD^+. Waters 460-474 occupy the presumed sulfur donor channel. Waters 500-528 are buried at other sites. Waters 600-885 are on the surface. This classification system was retained for subsequent SQD1 structures. A certain amount of variation in the number of surface waters seen between different SQD1 structures, as is common in crystallographic work. In contrast, nearly all buried waters were consistently observed, except for those affected by the T145A mutation or by differences in the type of bound substrate.

The structure of wild-type SQD1 with NAD^+ and UDP-glucose at 1.20 Å resolution

The electron density now supports inclusion of all amino acid residues from Gly1 to Met392, as well as a partial model of Thr393. Of these residues, 32 have partial side chains and 32 have alternate conformations, with some overlap between the two categories. As in the original crystal structure, the high-resolution model contains NAD^+ and UDP-glucose, both modeled at full occupancy because of the strength of the electron density and their low overall temperature factors (7.60 Å^2 for NAD^+, 9.92 Å^2 for UDP-glucose). The planarity of the nicotinamide moiety continues to suggest that the bound cofactor is almost exclusively oxidized NAD^+, rather than NADH. Of the 386 waters modeled in the high-resolution wild-type structure, 70 were buried and 316 were on the protein surface. Fifty-six of the waters in this structure (475-476, 529, 886-920, 922-932, 934-939 and 944) were not observed in the original structure, while 21 waters from the

original structure (714, 715, 719, 745, 781, 784, 802, 810, 815, 817, 819-820, 826, 831, 836, 846-847, 864, 873, 875, 878) were not observed. The overall B-factor, estimated as 11.59 Å^2 from a Wilson plot, refined to an average value of 13.43 Å^2. The atomic coordinates and structure factor amplitudes were deposited at the PDB as entry 1I24.

Two alternate conformations not observed in the original structure are those of Arg36 and Phe236, which may be coupled through parallel stacking interactions between the guanidinium portion of Arg36 and the phenol ring of Phe236 (separation ~ 3.5-4.0 Å). In the original structure, the N$_\varepsilon$ atom of Arg36 seemed to be involved in a hydrogen bond with NAD$^+$ (80). Because the Arg36 side chain is seen to adopt several conformers in the 1.2 Å structure, it is more likely that any hydrogen bonding interaction with NAD$^+$ is weak at best. However, the side chain interaction of Arg36 with the NAD$^+$ phosphodiester could be electrostatic in nature, and thus somewhat independent of geometry, unlike hydrogen bonding. The binding of ligands in the 1.6 and 1.2 Å structures is otherwise similar.

Two other interesting differences between the 1.2 Å structure and the 1.6 Å structure were seen. The first is in the distance between O$_\eta$ of Tyr182 and O4' of UDP-glucose. In the original, 1.6 Å structure, these two groups were separated by 2.54 Å, while in the 1.2 Å structure, they are 2.64 Å apart (Table 11). Since the longest length for an LBHB is 2.50-2.55 Å, it thus seems less likely that an LBHB has formed between these groups in the poised state of the enzyme. Second, in the 1.2 Å structure two conformations were resolved for O6' of the UDP-glucose substrate (Figures 15b and 16b), the moiety which is replaced by a sulfonyl group during catalysis. Only one conformation could be resolved in the original structure (Figure 15a), although some

extra electron density near the glucose 6′-carbon was apparent. The main conformation, modeled with an occupancy of 70%, corresponds in position to the single, strained conformation observed in the original structure. The second, more relaxed conformation seen in the high-resolution structure is generated by a 84° rotation of the O6′-C6′-C5′-C4′ dihedral angle, which displaces O6′ by 1.8 Å. As in the original structure, the major O6′ conformer is seen to hydrogen bond with Thr145-O_γ (2.29 Å), WAT411 (2.47 Å) and WAT461 (2.66 Å). The second, minor conformer interacts by hydrogen-bonding with WAT461 (2.58 Å), WAT463 (2.80 Å) and WAT475 (2.63 Å). Both O6′ conformers may also interact with WAT470, which lies 3.21 Å from the first O6′ conformer, and 2.48 Å from the second. Based on the strength of the electron density, it seems that WAT470 has low occupancy, and in fact may only be present when the major conformer is in place. In the original crystal structure, water 470 lay 4.43 Å from the O6′ hydroxyl, and so was not considered as potential hydrogen-bonding partner. Because negative F_o-F_c electron density appeared during the course of refinement on the active-site groups WAT410 and WAT411, they were subsequently modeled at occupancy levels (0.65 and 0.60, respectively) which resolved this problem. These new observations slightly modify the network of active-site hydrogen bonds identified in the original structure determination (Figure 16, Table 11).

The structure of T145A SQD1 with NAD⁺ and UDP-glucose at 1.60 Å resolution

The T145A/substrate structure contains amino acid residues 1-393, NAD⁺, UDP-glucose, two surface sulfate ions and 398 waters (65 buried, 333 surface). NAD⁺ and UDP-glucose were modeled at 100% occupancy because of the strong electron density

Table 11

Some interatomic distances (Å) in the SQD1 active site

Groups		WT/substrate, 1.60 Å	WT/substrate, 1.20 Å	T145A/substrate, 1.60 Å	T145A/product, 1.75 Å
Global coordinate error (Å)§		0.19	0.12	0.17	0.18
Tyr182—Oη	⋯ O4′—UPG	2.54	2.64	2.61	2.66
Thr145—Oγ	⋯ O4′—UPG	**2.45**	2.52	----	----
Thr145—Oγ	⋯ O6′—UPG	**2.45**	**2.29**	----	----
Thr145—Oγ	⋯ WAT411	**2.45**	2.57	----	----
UPG—O4′	⋯ O6′—UPG	2.73	2.63	3.15	3.17
USQ—O4′	⋯ O2S—USQ	----	----	----	2.99
WAT411	⋯ O4′—UPG	**2.38**	**2.49**	----	----
WAT411	⋯ O6′—UPG	**2.44**	**2.49**	----	----
WAT411	⋯ WAT410	2.86	2.90	----	----
WAT410	⋯ O=Gly144	2.57	**2.36**	----	----
WAT410	⋯ C6—NAD⁺	3.18	3.04	----	----
His183—Nε	⋯ C5′—UPG	4.21	4.25	4.12	4.02
Lys186—Nζ	⋯ Oη—Tyr182	2.97	2.88	2.86	2.87

§ The average of four CNS estimates of coordinate error: Luzzati, cross-validated Luzzati, σ(A) and cross-validated σ(A).

UPG = UDP-glucose (or UDP-sulfoquinovose, in the case of the T145A/product complex). Distances for WT/substrate at 1.2 Å resolution are for the major conformer of O6′. Distances ≤ than 2.50 Å are in boldface type.

and low temperature factors (11.11 $Å^2$ for NAD^+ and 13.89 $Å^2$ for UDP-glucose) associated with them. Of the amino acid residues, 368 are fully defined, 25 are partial and 8 have alternate conformations, although some amino acids are partially defined and also have alternate conformations. The nicotinamide moiety was again seen to be planar, suggesting that the bound cofactor is almost exclusively oxidized NAD^+, rather than NADH. Sixty-four of the waters (475-476, 886-901, 903, 905-914, 932 950 and 956-967, 969-971) were not observed in the original structure, while 16 waters (410-411, 461, 469, 709, 784, 810, 815, 817-818, 821, 828, 831, 836, 846, 878) from the original structure were not seen here. The overall B-factor was estimated as 15.24 $Å^2$ from a Wilson plot, and refined to an average value of 17.70 $Å^2$. The atomic coordinates and structure factor amplitudes were deposited at the PDB as entry 1I2C.

The overall structural effects of the T145A mutation are negligible and, as expected, all of the major changes are localized within the active site. The observed electron density at residue 145 is clearly consistent with alanine at this position. The distance between O_η of Y182 and O4′ of UDP-glucose (2.61 Å) is not significantly different from previous structures. However, the T145A mutation has markedly disturbed the hydrogen bond network around the ligands (Figure 16c, Table 11) resulting in the loss of buried waters 410, 411, 461 and 469. Hence, all short (≤ 2.5 Å) hydrogen bonds observed in the wild-type enzyme are absent in the T145A/substrate structure. In addition, the nicotinamide ring in the T145A/substrate complex shifts and rotates slightly in the direction of the UDP-glucose 4′-hydroxyl oxygen. The maximal shift between the nicotinamide rings in the mutant and wild-type structures is about 0.4 Å. This movement brings C4′ of the nicotinamide ring 4-carbon to 3.5 Å from the UDP-glucose 4′-carbon, a

position which is actually 0.2 Å closer than seen in the original and high resolution wild-type structures. The positional change of the nicotinamide ring is perhaps a result of losing the buried active site waters 410 and 411, the former of which may accept a C—H⋯O hydrogen bond from C6 of the nicotinamide ring. Finally, the absence of a liganding threonine at position 145 results in the loss of all the hydrogen- bond partners coordinating the 6′-hydroxyl of UDP-glucose in wild-type enzyme. The 6′-hydroxyl now assumes a conformation different from that seen in the wild-type structure (Figure 15c). Through a combination of a 41° change in the C4′-C5′-C6′-O6′ dihedral angle and a small shift in the glucose ring position, the 6′-oxygen is moved by 0.82 Å from the wild-type position. In this location, it now hydrogen bonds to the backbone amide nitrogen of Gly147 (3.16 Å) and to water 470 (2.81 Å), which has shifted 1.00 Å from its place in the original wild-type structure. However, WAT470 of the T145A/substrate complex has an elevated B-factor (42.31 $Å^2$) compared to the original and high resolution wild-type structures (27.76 and 27.24 $Å^2$, respectively), perhaps indicating that any hydrogen-bonding to the UDP-glucose 6′-oxygen is tenuous. In the original wild-type structure, the UDP-glucose 6′-hydroxyl oxygen was well out of hydrogen-bonding range from both the amide nitrogen of Gly147 (3.54 Å) and WAT470 (4.13 Å). Thus, the T145A mutant protein achieves extensive hydrogen bonding with UDP-glucose through shifts in water positions and in the ligand itself, without significant changes in the protein structure *per se*.

Preparing novel SQD1/ligand complexes

SQD1 crystals are approximately 64% solvent by volume, as estimated by the

refinement program CNS, and have large solvent channels. These channels allow the free diffusion of small molecules, as demonstrated by the successful derivatization during MIR work. Nonetheless, introducing ligands into the active site of SQD1 proved very difficult, particularly once it had been set up for crystallization. It is worth noting that none of the heavy atom compounds used for MIR bound in or near the active site (Figure 11). Crystallization experiments set up with UDP or UDP-phenol generally did not give a good yield of crystals of a size suitable for collection of diffraction data, whether the ligands were added to the protein stock or to the drop stock. When small, useable crystals did appear, they always were found to have UDP-glucose in the active site. Apparently, UDP-glucose from the *E. coli* overexpression host remains tightly bound in the active site of some of the SQD1 during purification. It seems that most of the protein, whether or not it bound the non-native ligand, did not crystallize. Rather, only that fraction of protein which was contaminated with UDP-glucose was able to form crystals. Addition of exogenous sulfur compounds, either during or after crystallization, likewise produced no changes. For example, crystals of wild-type SQD1, in complex with UDP-glucose and NAD^+, were soaked overnight in a solution with 0.1 M sulfite. Diffraction data from a sulfite-treated crystal (designated "mjt_f28") were collected at the APS, Beamline 19-ID, to 1.3 Å resolution. The electron density maps derived from these data showed no changes from the original 1.6 Å structure. It seems that once SQD1 enters a high ionic strength environment, and certainly after it has crystallized, its active site becomes closed. This is supported by the inverse relationship of ionic strength and catalytic activity observed for wild-type SQD1 *in vitro* (71).

The availability of the T145A mutant SQD1 protein, which had no detectable

catalytic activity under normal assay conditions, offered the possibility of preparing a complex of SQD1, its cofactor NAD$^+$ and both substrates, UDP-glucose and sulfite (71). For reasons detailed above, it was not possible to introduce sulfite during or after crystallization. Therefore, purified T145A SQD1 protein was incubated overnight in "Dialysis buffer" supplemented with 5 mM UDP-glucose and freshly-prepared sodium sulfite to 200 µM, then set up for crystallization the next morning. So far, wild-type SQD1 has not been similarly preincubated with UDP-glucose and sulfite. In additional experiments, both wild-type and T145A SQD1 protein samples were preincubated with either reduced glutathione (GSH), oxidized glutathione (GSSG), sulfoglutathione (GSO$_3$) or glutathione thiosulfonate (GSSO$_3$). However, crystallization experiments with these batches of protein produced only very small crystals. Diffraction data from the crystals of the sulfite-soaked T145A SQD1 were collected and processed as usual. The results are described in the next section.

The structure of T145A SQD1 with NAD$^+$ and UDP-sulfoquinovose at 1.75 Å resolution

The model contains amino acid residues 1-393, NAD$^+$, UDP-hexose (65% UDP-sulfoquinovose and 35% UDP-glucose), two sulfates and 402 bound waters (61 buried, 341 surface). Seventy-two waters (886-911, 915-920, 940-964, 972-986) were not seen in the original structure, while 21 waters (410-411, 461, 470-471, 474, 692, 709, 714, 751, 775, 783-784, 802, 810, 814-815, 817, 828, 831, 837) from the original structure were not included in this model. The nicotinamide moiety is planar, suggesting that the bound cofactor is almost exclusively oxidized NAD$^+$, rather than NADH. Among the amino acid residues, 361 are fully defined, 28 are partial and 5 residues have alternate

conformations (some residues have alternate conformations *and* are only partially defined). The height of the electron density and low average B-factors for NAD$^+$ (14.29 Å^2) and UDP-hexose (18.77 Å^2) again suggest near 100% occupancies of the ligands in the mutant structure. The overall B-factor was estimated as 20.04 Å^2 from a Wilson plot and refined to an average value of 21.02 Å^2. The atomic coordinates and structure factor amplitudes were deposited at the PDB as entry 1I2B.

In the active site, the O$_\eta$ of the catalytic Tyr182 remains at roughly the same distance (2.66 Å) from the UDP-hexose 4′-oxygen as in the-high resolution wild-type and T145A/substrate structures. As with the T145A/substrate structure, a number of active site waters (410, 411, 461, 470, 471, 474) are lost, although water 469 is present (Figure 16d). The nicotinamide ring of NAD$^+$ is positioned as described for the T145A/substrate complex, *i.e.* shifted more towards the glucose ring than in wild-type.

Initial refinement was carried out with only protein residues, then NAD$^+$ and a partial model of UDP-glucose lacking the O6′ hydroxyl were included. Electron density maps calculated with coefficients of the form $2F_o$-F_c and F_o-F_c showed a trilobed feature extending from the expected position of the UDP-glucose O6′. This extra density was easily fit with a model of sulfite, obtained from the Heterocompound Information Centre, Uppsala (HIC-Up), by overlaying the sulfur atom on the expected O6′ position (81). Because of the proximity of the sulfur atom to C6′ of the hexose ring, it was clear that the active site contained the product, UDP-sulfoquinovose, rather than the substrates, UDP-glucose and sulfite (Figure 15d). Later, another sulfite-incubated crystal was used to collect a separate, highly redundant dataset at the Cu K$_\alpha$ wavelength, making sure to measure a high number of Friedel pairs. Anomalous difference electron density maps,

calculated with coefficients of the form $(|F^+|-|F^-|)e^{(\varphi-90)}$ from this dataset, clearly showed a significant anomalous signal at the position after C6′. This observation is consistent with a sulfur atom, rather than an oxygen.

Initially, UDP-sulfoquinovose was modeled at 100% occupancy. During subsequent refinement, considerable negative F_o-F_c electron density was seen on the sulfonyl group, but not the rest of the hexose. The sulfonyl atoms B-factors also became elevated (average value of 28.65 Å^2) relative to those of the rest of the UDP portion of the molecule (average value of 19.37 Å^2). By comparing the level of electron density about the sulfonyl oxygens to that of oxygens elsewhere in the structure, the occupancy of the sulfonyl group was estimated to be approximately 65%. This lower limit could be an underestimate if conformational disorder lowers the average occupancy of the major conformer. For the rest of the refinement, a consensus structure was used, where UDP-sulfoquinovose was modeled at 65% occupancy and "unreacted" UDP-glucose was modeled at 35% occupancy.

In the T145A/NAD$^+$/UDP-SQ ("T145A/product") complex, the position of the sulfur atom of UDP-sulfoquinovose differs from that of the O6′ hydroxyl found in either the wild-type structure or the T145A/substrate complex structure (Figure 15). Oxygen O1 of the sulfonyl group sits essentially at the position of WAT461 in the wild-type structure and apparently displaces it, forming hydrogen bonds (Figure 16d) to H183—N$_\varepsilon$, WAT463 and WAT466 (2.99, 2.68 and 3.11 Å, respectively). Oxygen O2 forms hydrogen bonds to the backbone amide nitrogens of Met146 and Gly147 (2.86 Å and 2.59 Å). Oxygen O3 lies 3.37 Å from the nearest potential hydrogen-bonding partner (WAT467), beyond the distance considered normal for such an interaction. Interestingly,

the O2 oxygen of the sulfonyl group in the T145A/product complex structure (Figure 19a) is in a position that could not be accommodated in wild-type enzyme, because it would be only 1.63 Å from the O_γ of Thr145 (Figure 19b). Hence, the sulfonyl group must assume a slightly different conformation in the native enzyme-product complex. A rotation of 22° about the sulfoquinovose C4′-C5′-C6′-S6′ dihedral would suffice to place the O2 oxygen in the same relative position as the O6′ oxygen of UDP-glucose found in the wild-type structure (Figure 19c). In this configuration, the O1 oxygen would displace WAT463 and be 2.48 Å from a phosphodiester oxygen of the UDP-sulfoquinovose group. O2 would be 2.48 Å from the Gly147 amide nitrogen, 3.36 Å from the Met146 amide nitrogen, and 2.46 Å from the Thr145—O_γ. O3 would be 3.20 Å from WAT467. Hence, UDP-sulfoquinovose can be accommodated in the wild-type structure in a stereochemically and catalytically feasible manner.

Model stereochemistry and the nonplanarity of the Tyr182 ring

While the stereochemistry of all four SQD1 models is within the normal range for protein crystal structures (Figure 12, Table 8), a notable statistical outlier is the nonplanarity of the Tyr182 phenol rings (Table 12). Within each of the four SQD1 crystal structures, the ring of Tyr182 is always the most distorted from planarity of all 16 tyrosine residues (Figure 20a), despite the use of different methods for data collection, data processing and model refinement. Temperature factors are low for the atoms of the Tyr182 side chain (Table 12), indicating that a tight conformational state is maintained. Moreover, the RMSD from planarity of the Tyr182 ring atoms increases linearly with improving resolution, while those of noncatalytic tyrosines do not show a strong trend.

112

Figure 19. Clash between the UDP-sulfoquinovose sulfonyl group and T145—O_γ. The figure is in stereo. Molecules are shown as ball-and-stick models, colored by element (white=carbon, red=oxygen, blue=nitrogen, purple=phosphorus, yellow=sulfur). The oxygen atoms of ordered waters are represented by blue spheres. a) The arrangement in the T145A/product structure. b) UDP-sulfoquinovose from the T145A/product structure, placed into the high-resolution wild-type/product structure in the position of UDP-glucose. c) UDP-sulfoquinovose in the high-resolution wild-type structure, with the sulfonyl group moved to an acceptable binding position.
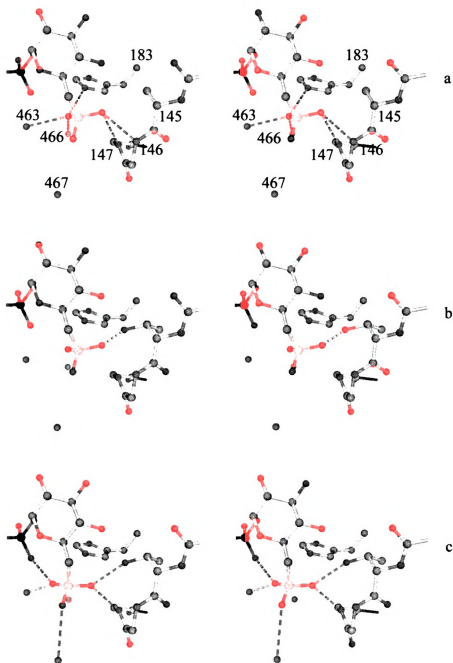
Figure 19

Table 12

Distortion of Tyr182 in SQD1 structures

Structure	d_{min} (Å)	Average B-factor (Å²)			RMS deviation of phenol ring from planarity (Å)			O_η displacement (Å)	Global coordinate error (Å)§	Displacement/ Error
		Y182 sidechain†	All atoms	Y182/ all	Y182	Avg. Tyr	Y182/ Avg Tyr			
wild-type/substrate	1.20	5.75	14.40	0.399	0.076	0.023	3.4	0.55	0.19	2.9
wild-type/substrate	1.60	7.01	13.43	0.522	0.059	0.017	3.4	0.72	0.12	6.0
T145A/substrate	1.60	10.25	17.70	0.579	0.058	0.16	3.8	0.59	0.17	3.5
T145A/product	1.75	13.01	21.01	0.619	0.054	0.15	3.7	0.55	0.18	3.1

† Atoms after C_β.

§ The average of four CNS estimates of coordinate error: Luzzati, cross-validated Luzzati, σ(A), and cross-validated σ(A).

Note: PROCHECK defines an RMSD from planarity of less than 0.030 Å to be "undistorted".

115

Figure 20. Alignment of tyrosine side chains to compare ring distortion. The tyrosines were manually aligned as follows. For each tyrosine, C_β and C_γ were first overlaid onto C_β and C_γ of an "ideal" model, then the whole side chain was manually rotated about the C_β–C_γ bond until $C_{\delta 1}$ and $C_{\delta 2}$ were equidistant from their ideal counterparts. Tyr182 is colored orange, while other tyrosines are colored by element (white=carbon, red=oxygen); each atom is labeled by name. Blue spheres with a diameter of 0.5 Å are placed at the ideal positions for a planar tyrosine side chain. a) Superimposition of tyrosine side chains from the high-resolution wild-type/substrate structure. b) Catalytic tyrosines from the four SQD1 structures and from 14 independently-refined monomers of nucleotide-sugar modifying SDRs (PDB entries 1BSV, 1BWS, 1BXK {Chains A and B}, 1DB3, 1EK5, 1EK6 {Chains A and B}, 1EQ2A {Chain A only}, 1FXS, 1GFS, 1UDA, 1UDB and 1UDC).

$C_{\delta 2}$ $C_{\epsilon 2}$

C_β C_γ $C_{\delta 1}$ $C_{\epsilon 1}$ C_ζ O_η

a

b
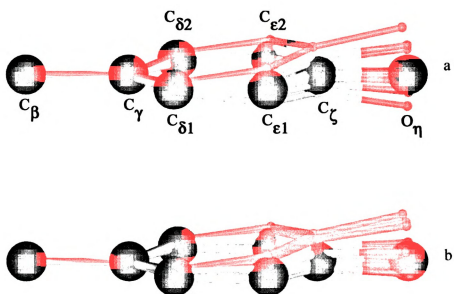
Figure 20

In the 1.2 Å structure, Tyr182 deviates by 2.4 σ from the average distortion of all tyrosine rings in that structure; the distortion of any other tyrosine was ≤ 1.5 σ from the mean. The distortion arises largely from an angular deviation of the C_β-C_γ bond from the plane formed by the atoms C_β, C_γ, $C_{\delta 1}$ and $C_{\delta 2}$. In the 1.2 Å structure, this deviation has a magnitude of 4.4°. As a result, O_η of Tyr182 is displaced 0.72 Å from its ideal position, which is approximately six times the estimated global coordinate error (Table 12). In 14 independently-refined monomers from crystal structures of other nucleotide-sugar modifying SDRs, the catalytic tyrosines were either undistorted, or less distorted than noncatalytic tyrosines.

Discussion

The overall structure

The crystal structure of SQD1 definitively established it as a member of the SDR family of enzymes, based on conservation of overall fold, protein-ligand interactions and catalytic residues, as discussed below. Crystal structures of at least 24 different kinds of SDR enzymes were available for this study. A list of the enzymes, along with some conserved catalytic residues, is shown in Table 13. Six are sugar-nucleotide modifying SDRs (Table 4). There are 37 separate crystal structures within this subgroup, comprised of 57 independently-refined monomers. The 1.20 Å wild-type/substrate SQD1 structure has the highest nominal resolution of any SDR, which is particularly impressive since it is also has one of the largest monomers. The next best resolution for an SDR is for sepiapterin reductase (PDB entry 1OAA), solved at 1.25 Å resolution (81). After SQD1, GMER has the best resolution among the sugar-nucleotide modifying SDRs, at 1.45 Å for PDB entry 1E6U (82). Because of the high quality of the 1.20 Å SQD1 model, it serves as a benchmark against which other SDR crystal structures may be compared. SQD1 is also the only crystal structure of an active, wild-type SDR in complex with its substrate. This unique situation is made possible by the poised state which is maintained in the absence of a sulfur donor. The SQD1/NAD$^+$/UDP-glucose complex is probably closer to the activated state of catalysis than any other SDR crystal structure, and so gives us an excellent chance to understand the roles of the catalytic groups.

Table 13

Some conserved catalytic residues in SDRs of known structure

Enzyme	Catalytic triad			
	Ser/Thr	Tyr	Lys	Base
SQD1	Thr145	Tyr182	Lys186	His183
dTGD (*E. coli*)	Thr134	Tyr160	Lys164	Glu136
dTGD (*S. ent.*)	Thr133	Tyr167	Lys171	Glu135
GMD	Thr132	Tyr156	Lys160	Glu134
GMER	Ser107	Tyr136	Lys140	His179
UGE (*E.coli*)	Ser124	Tyr149	Lys153	----
UGE (human)	Ser132	Tyr157	Tyr161	----
AGME	Ser116	Tyr140	Lys144	----
GDH	Ser145	Tyr158	Lys162	----
MDH	Ser149	Tyr169	Lys173	----
cBDH	Ser142	Tyr155	Lys159	----
mBDH	Ser139	Tyr152	Lys156	----
3HCDH	Ser155	Tyr168	Lys172	----
ADH (*D. mel.*)	Ser139	Tyr152	Lys156	----
ADH (*D. leb.*)	Ser138	Tyr151	Lys155	----

120

Table 13 continued

Enzyme	Catalytic triad			Base
	Ser/Thr	Tyr	Lys	
3αHDH	Ser114	Tyr155	Lys159	----
3α20βHDH	Ser139	Tyr152	Lys156	----
7αHDH	Ser146	Tyr159	Lys163	----
17βHDH	Ser142	Tyr155	Lys159	----
20βHDH	Ser139	Tyr193	Lys197	----
CR	S136	Tyr149	Lys153	----
TR-I	Ser158	Tyr171	Lys175	----
TR-II	Ser146	Tyr159	Lys163	----
PR	Asp181	Tyr194	Lys198	----
DPR	WAT320	Tyr146	Lys150	----
SR	Ser158	Tyr171	Lys175	----
triHNR	Ser164	Tyr178	Lys182	----
tetraHNR	Ser164	Tyr178	Lys182	----
βKR	Ser154	Tyr167	Lys171	----

NAD⁺ binding

The interactions between NAD^+ and SQD1 are generally similar to those of other SDRs. Interestingly, the GXXXGXG (where X is any amino acid) fingerprint sequence of the Rossmann fold at the pyrophosphate site in monodomain SDR enzymes is replaced by a GXXGXXG sequence in SQD1 and the other bidomain, sugar-nucleotide modifying SDR enzymes. The hydrogen bonding between the NAD^+ pyrophosphates and the backbone amide nitrogens of Tyr12 and Cys13 is characteristic of Rossmann folds. A hydrogen bond similar to that of Arg101 is provided by a lysine side chain in some bidomain SDRs (Lys84 in *E. coli* UGE complexes, Lys92 in human UGE and Lys178 in AGME), but not in any other SDR structure examined. Direct protein side-chain interactions with the pyrophosphate moiety of $NAD^+/NADP^+$ vary greatly among related enzymes, and are absent altogether in some cases (63,69,75,84,85).

A difference is seen between those SDRs that utilize $NAD^+/NADH$ and those that utilize $NADP^+/NADPH$. Interactions of an aspartate side chain with the ribose nearer the adenosine group, analogous to those of Asp32 in SQD1 (Figure 14), are observed for nearly all of the NAD-binding SDRs (Table 14). Only GDH lacks it, having a different fold at that part of the structure. In SDRs which utilize NADP (GMD, GMER, etc.), the phosphate group on the ribose 2′-hydroxyl makes this hydrogen-bonding interaction impossible, hence none of these SDRs retain this residue. This method of discrimination was first reported by Tanaka *et al.* (86) Highly conserved interactions with the NAD^+ adenosine moiety are also generally observed. An Asp (or more rarely an Asn) which hydrogen bonds to the adenosyl base (structurally homologous to Asp75 in SQD1) is found in all SDR enzymes. The hydrogen bond between a main-chain amide

Table 14

Residues in NAD-binding SDRs homologous to Asp32 of SQD1

Protein	Residue Number of the Aspartate
SQD1	32
UGE (*E. coli*)	31
UGE (human)	33
AGME	31
dTGD (*E. coli*)	33
dTGD (*S. ent.*)	32
GDH	--
cBDH	36
mBDH	33
3HCDH	41
ADH (*D. leb.*)	37
3αHDH	32
3α20βHDH	37
7αHDH	42
DPR	37

(Ile76 in SQD1) and the adenosyl base is also highly conserved. The hydrogen bonding between Asn119 and the adenosyl N6 and N7 is residue is seen in *E. coli* UGE (Asn99), AGME (Asn92), and has a similar counterpart in *E. coli* dTGD (Thr100), *S. ent.* dTGD (Thr99) and GMER (WAT49:Gln82). It is not otherwise widely conserved among SDRs. The interactions of Tyr182 and Lys186 with the nicotinamide ribose in SQD1 are typical of SDR enzymes.

Positioning and orientation of the nicotinamide ring

Proper positioning of the nicotinamide ring is necessary to allow hydride transfer to and from the substrate. The observed *syn* conformation of the nicotinamide group is the proper orientation for the expected B-side hydride transfer, and is seen in most other SDR structures. Of the 37 structures of nucleotide-sugar modifying SDRs available for this study, 35 contain a nicotinamide adenine dinucleotide cofactor. Five have the nicotinamide group in the *anti* conformation (GMER, PDB entries 1E6U, 1E7Q, and 1FXS, and *E. coli* UGE, PDB entries 1NAH and 2UDP), one has very disturbed cofactor binding (PDB entry 1E7S). The other 29 have nicotinamide in the *syn* conformation. In one structure of GMER (PDB entry 1BWS), the nicotinamide ring is *syn*, but is rotated away from the presumed reactive position. The two structures without a cofactor are of GMER (PDB entry 1GFS) and GMD (PDB entry 1DB3). Several factors, described below, may contribute to keeping the nicotinamide ring in the correctly positioned and in the *syn* orientation.

First, hydrogen-bonding from a main-chain amide nitrogen (Val212 in SQD1) to the carboxamide group may limit flipping of the ring to the *anti* position. The distance

from Val212—N to O7 of the nicotinamide ring is in the range of 3.03-3.19 Å in the four SQD1 structures, with an average value of 3.12 Å. The same type of arrangement is seen in dTGD (*E. coli*, Asn190, *S. ent.*, Asn197), as well as among monodomain SDRs, for example DPR (Leu181—N to O7, 2.87 Å) and GDH (Ile191—N to O7 2.86 Å). In the ten monomers of the AGME asymmetric unit, similar interaction (Val170—N to N7) ranges in distance from 3.09 to 3.60 Å, with an average value of 3.27 Å. In GMER the distances from Leu166—N to the nearest carboxamide atoms vary widely (3.25-4.58 Å). A proline at this position substitution in UGE (*E. coli*, Pro180, human, Pro188) makes such a hydrogen bond impossible.

Second, the size of residues adjacent to the nicotinamide also may have an effect position (Table 15). In SQD1, the mid-sized residues Gln209 and Val212 allow a fair amount of room. In UGE, a bulky tyrosine side chain and a proline crowd the nicotinamide ring towards the UDP-hexose by about 1.2 Å. Nearly all of the monodomain SDRs have proline in the first position, and a residue with a medium-sized side chain in the second. This general conservation of side chain size, if not identity, serves to keep the nicotinamide ring constrained to the general area of reaction by steric repulsion.

Third and lastly, C6 of the nicotinamide ring may be hydrogen-bonding, directly or indirectly, to a main-chain carbonyl oxygen of the residue before the catalytic Ser/Thr. C—H···O hydrogen bonds can occur when the carbon has some acidic character (87), as would be expected in a positively charged nicotinamide ring. In SQD1 the hydrogen bond appears to be to Gly144=O, but is bridged by WAT410 (Figure 21).. The C···O distance of 3.18 Å and C-H-O angle of 163° (based on calculated ideal H positions) agree

Table 15

Residues in SDRs abutting the nicotinamide ring

Protein	Residue 1	Residue 2
SQD1	Gln209	Val212
UGE (*E. coli*)	Tyr177	Pro180
UGE (human)	Tyr185	Pro188
AGME	Tyr167	Val170
dTGD (*E. coli*)	Cys187	Asn190
dTGD (*S. typh.*)	Cys194	Asn197
GMER	Pro163	Leu166
GMD	Leu183	His186
GDH	Pro188	Ile191
MDH	Pro199	Val202
cBDH	Ser184	Ile187
mBDH	Pro182	Val185
ADH (*D. leb.*)	Pro181	Thr184
3αHDH	Pro185	Thr188
3α20βHDH	Pro182	Thr185
7αHDH	Pro189	Ile192
17βHDH	Cys185	Val188
3HCDH	Pro198	Phe201
CR	Pro179	Val182
TR-I	Pro201	Ile204
triHNR	Pro208	Ile211
tetraHNR	Pro208	Val211
PR	Pro224	Ser227
DPR	Pro178	Leu181
βKR	Pro197	Ile200
SR	Pro199	Leu202

Table 16

Groups which may hydrogen bond to nicotinamide C6

Enzyme	NAD—C6 H-bonding	Enzyme	NAD—C6 H-bonding
SQD1	Gly144=O:WAT410	3αHDH	Ser113=O
dTGD (*E. coli*)	Ser133=O	3α20βHDH	Ser138=O
dTGD (*S. ent.*)	Ser132=O	7αHDH	Thr145=O
GMD	Ser131=O	17βHDH	Gly141=O
GMER	Gly106=O	20βHDH	Ser138=O
UGE (*E.coli*)	Ser123=O	CR	Ser135=O
UGE (human)	Ser131=O	TR-I	Ser157=O
AGME	Ser115=O	TR-II	Ser145=O
GDH	Ser144=O	PR	Val180=O
MDH	Ser148=O	DPR	Gly132=O
cBDH	Ile141=O	SR	Ser157=O
mBDH	Cys138=O	triHNR	Gly163=O
3HCDH	Ala154=O	tetraHNR	Ser163=O
ADH (*D. mel.*)	Gly138=O	βKR	Ala153=O
ADH (*D. leb.*)	Cys137=O		

Figure 21. Hydrogen-bonding of the nicotinamide 6-carbon. Coordinates from 30 different nucleotide-sugar modifying SDRs were used. Alignments were performed using backbone atoms of the two amino acids flanking the residue which putatively hydrogen bonds to C6 of the nicotinamide ring (in SQD1, these are Leu143 and Thr145, which flank Gly144). Molecules are represented as stick models; WAT410 from the two wild-type SQD1 structures is shown as spheres. Putative hydrogen-bonding in these two structures is depicted by dashed gray lines of cylinders. Hydrogen bonding in other structures would be directly between the corresponding backbone carbonyl oxygen and C6 of the nicotinamide ring, and has been omitted for clarity. a) The groups are colored by protein type: yellow is SQD1, green is dTGD, red is GMER, purple is AGME, light blue is *E. coli* UGE and dark blue is human UGE. b) The same scene, rotated 90° about the y- and z-axes.

a

b
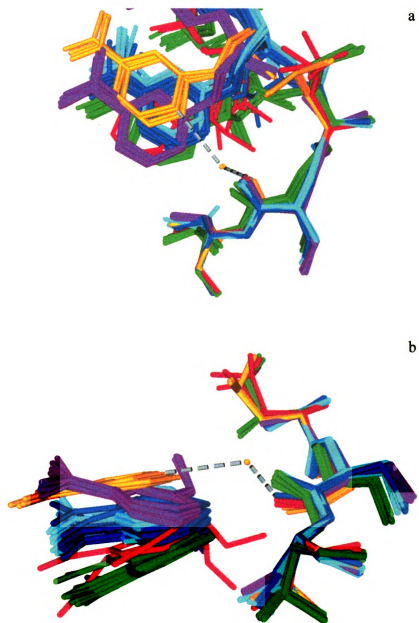
Figure 21

well with water molecules coordinated by C—H hydrogen bonds in a survey of small molecule neutron crystal structures (88), where the typical C—O distance was found to be 3.4-3.5 Å. No other structure of a sugar-nucleotide modifying SDR has a water in a position to hydrogen-bond to the nicotinamide C6. Rather, the hydrogen-bonding occurs directly between C6 the main-chain carbonyl oxygen (Table 16 and Figure 21). Hydrogen-bonding directly *versus* indirectly may be related to the timing of catalysis, as discussed below.

UDP-glucose binding and the flap region

The main-chain hydrogen bonds to UDP-glucose and the Tyr256:uridine aromatic stacking interaction are echoed in the structures of AGME and human UGE, as well as those *E. coli* UGE structures where the cofactor is reduced to NADH. In AGME, Phe201 (corresponding to Tyr256 in SQD1) stacks against the adenine group of the inhibitor ADP-glucose. Phe243 is located in a good position to stack against the other face of ADP, but its phenyl ring is tilted away. The aromatic residue in human UGE is Phe226, while in *E. coli* it is Phe218. In the *E. coli* UGE complex with UDP and NAD$^+$, the aromatic stacking was reported to be disrupted by a second conformation of the corresponding Phe218 side chain (84). Steric interference by the surrounding side chains in SQD1 would prevent the occurrence of a similar conformational change in the Tyr256 side chain.

In the SQD1 and *E. coli* UGE ternary complexes, the relative positions of the glucose ring differ significantly due to the combined effects of conformational differences in their small domains in the ligands themselves. In contrast, human UGE

(PDB entry 1EK6) is more similar to SQD1 (89). One possible reason is the substitution of a cysteine (position 307 in human UGE) for a much larger tyrosine (position 299 in *E. coli* UGE). In SQD1 the overall fold is somewhat different, so that the protein surface corresponds more closely to human UGE than to *E. coli* UGE. A second, more general reason is that the structure of human UGE is of a "clamped-down" form, where the small domain has descended against the UDP-hexose. This resembles the SQD1 complex, which enfolds the UDP-sugar very closely. The *E. coli* UGE structures are all more open.

As the bound UDP-glucose ligand is completely buried within the SQD1 structure (Figure 17), a significant conformational change of the protein must occur to allow entry and exit of substrate and product. Since the "flap" region is apparently stabilized by the presence of bound UDP-glucose, the absence of ligand may increase its flexibility and allow access to the binding site. However, this point is brought into question by comparison of temperature factors among crystal structures nucleotide-sugar modifying SDRs (Figure 22). As expected, structures containing nucleotide sugars or analogs do have lower overall B-factors than those without. Additionally, one might expect that the flap regions of structures lacking a ligand would be more mobile than the rest of those structures. However, this is not observed, as flap B-factors trend linearly with overall B-factors. A *caveat* is that B-factors for flap residues in some of the structures, particularly those of UGE, were artificially constrained to lower values, thus biasing the results. Furthermore, very high B-factors may result in electron density which is too weak for model-building, so that these data points are removed from consideration. It is not possible to draw a firm conclusion at this point.

Figure 22. Flap B-factors *versus* overall B-factors for NMSDRs. Filled circles are for structures containing substrate or an analog, while open circles are for structures lacking either. A best-fit line, calculated using all data, is also shown.
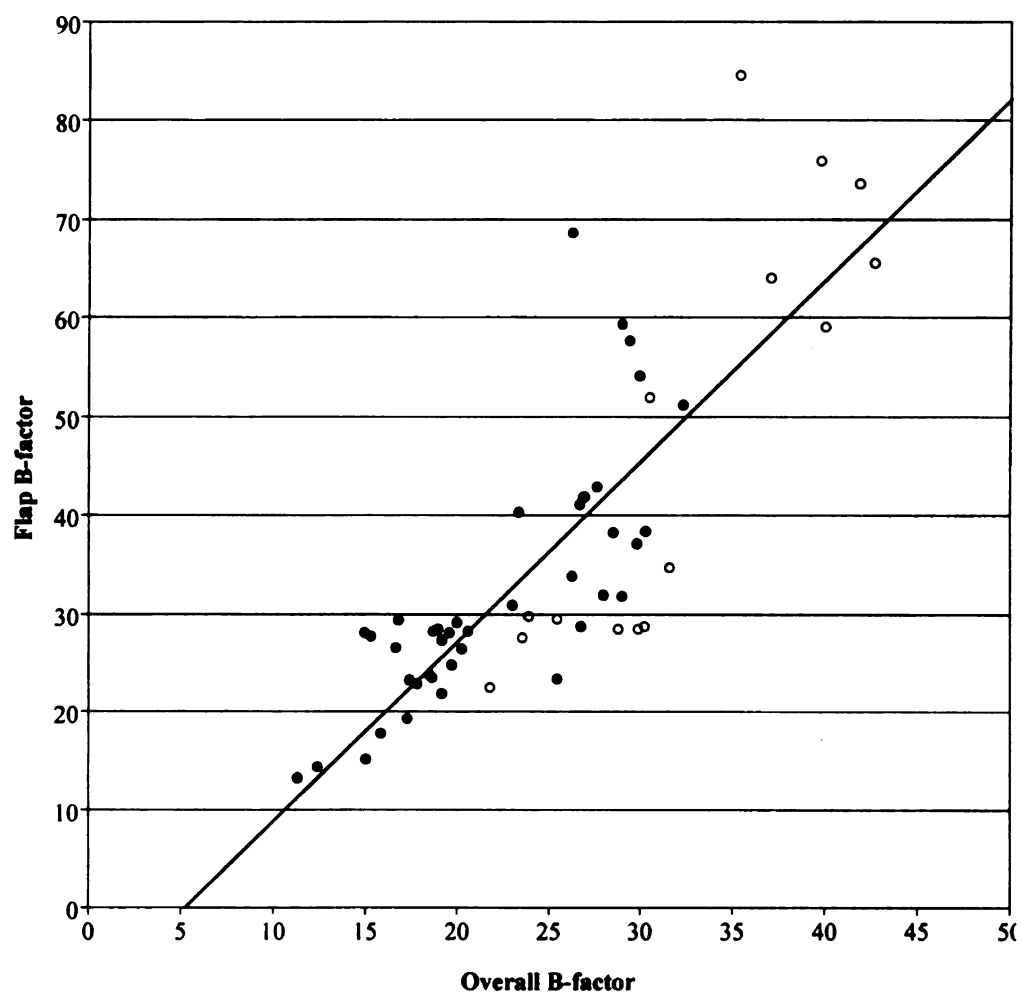
Figure 22

Sulfur-Donor Site and UDP-glucose O6′ conformations

The larger, water-filled cavity from the protein surface to the glucose ring is the presumptive binding site for the sulfur donor (Figure 18). Arg263, which extends into the center of the cavity, is an obvious candidate for potential interaction with a negatively-charged sulfonyl group on the sulfur donor. The sulfonyl group of UDP-sulfoquinovose sits at the end of the channel, suggesting that the sulfur donor does enter by this route. If this is indeed the sulfur donor channel, then the minor conformation of UDP-glucose O6′, observed only in the 1.2 Å structure, would block approach of the sulfur donor to C6′. Thus, if loss of O6′ is coordinated with addition of the sulfonyl group to C6′, holding O6′ in the major, strained conformation may be important in allowing the sulfur donor proper access to its target.

A number of possible sulfur donor compounds have been considered as potential sulfur donors, including sulfite, sulfate, thiosulfate, sulfide, glutathione (reduced and oxidized), glutathione thiosulfate, adenosine 5′-phosphosulfate (APS), and 3′-phosphoadenoine 5′-phosphosulfate (PAPS), as well as a protein sulfur donor (71). Of these, only the last could be ruled out based on the crystal structure, since the reactive glucosyl C5′ atom of bound UDP-glucose is > 10 Å from the channel entrance. The large diameter (7-9 Å) of the channel at the protein surface could potentially allow quite large compounds to enter, although whether they could react would depend on their binding position and chemical composition. Yet, despite a very empty crystal lattice (V_M=3.5; 65 % solvent content) and no crystal contacts which appear to interfere with domain movement, crystalline SQD1 has resisted all attempts at soaking sulfur ligands into its active site. Co-crystallization has likewise been unsuccessful. Even sulfate from

the crystallization medium, present at upwards of 1 M concentration, does not appear in the active site. It seems that crystalline SQD1 undergoes no conformational change(s) which would open its active site to bulk solvent. It remains unclear how and why small molecules are excluded from the SQD1 sulfur donor channel, at least under high salt conditions and after crystallization.

Revised mechanism

The hypothetical SQD1 mechanism has been modified and expanded from its original conception (Figure 23; compare to Figure 8) based on the new data. First, a poised state has been added prior to the active complex, consisting of enzyme with bound NAD^+ and UDP-glucose. Second, "catalytic" protein residues at the active site have been identified: Tyr182, Lys186, Thr145 and His183. Distortion of the catalytic Tyr182 has supported the idea that it is deprotonated on O_η. Third, the sulfur donor is now depicted as sulfite.

The catalytic active site residues: Tyr182, Lys186, Thr145, His183

Only a few residues are highly conserved throughout the entire SDR family, among them a characteristic YXXXK motif and a Ser (or Thr) residue, which together form a "catalytic triad" (see Table 13) (90). Generally among SDRs, the catalytic Tyr is absolutely conserved and the catalytic Lys nearly so. Loss of tyrosine usually causes the greatest decrease in k_{cat}. Ser/Thr appears to be less critical and is even replaced by other residues in some cases (91,92). Nonetheless, the position of the oxygen corresponding to Ser—O_γ or Thr—O_γ is conserved, including in SQD1.

135
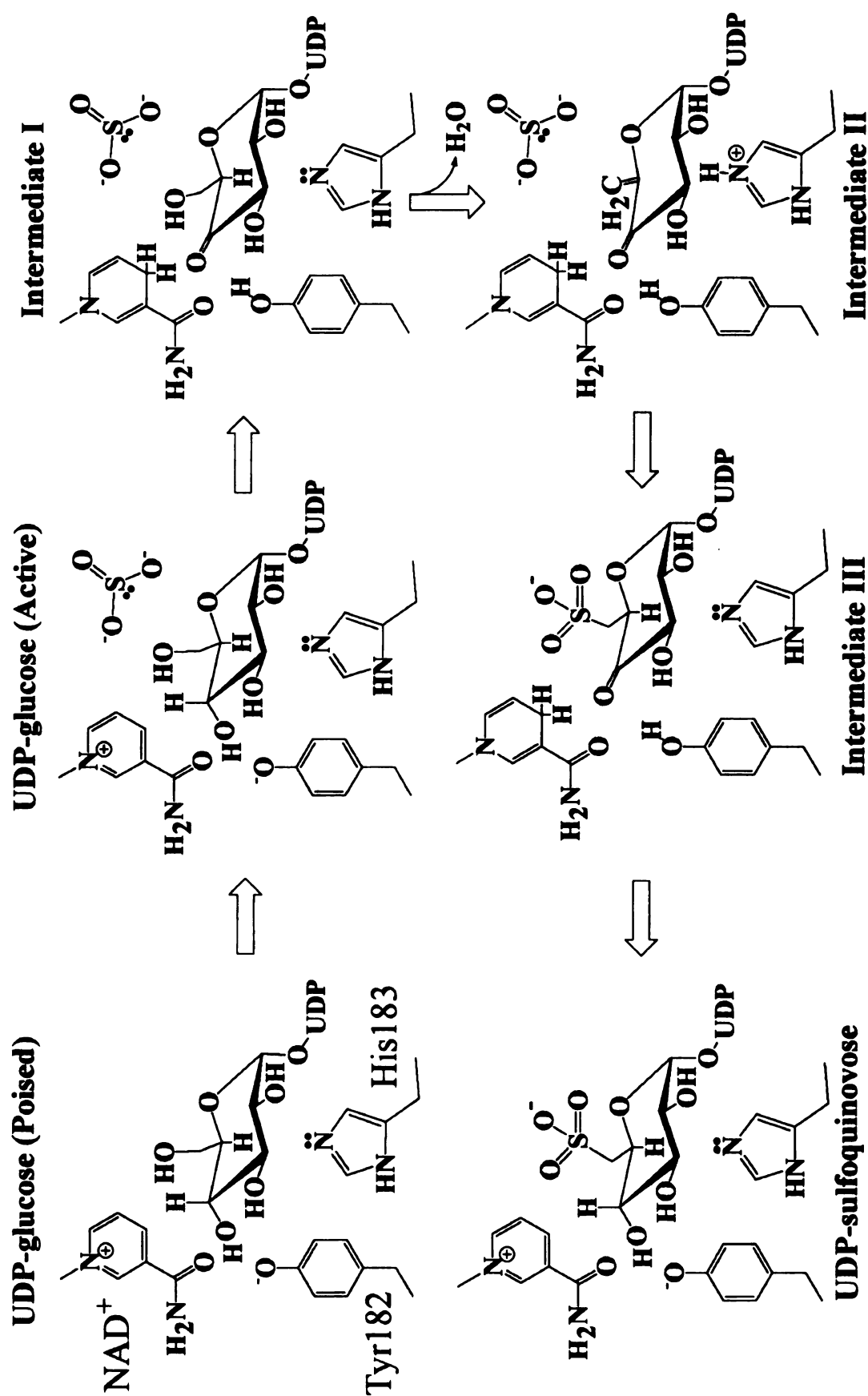
Figure 23. The later hypothetical SQD1 reaction mechanism.

136

Among the SDRs studied in this work, all conserve the catalytic tyrosine and lysine residues. Two have a residue other that serine or threonine as the first part of the triad. One is dihydropteridine reductase (DPR), which as a water in the position normally occupied by a Ser/Thr side chain hydroxyl (93). The other is pteridine reductase (PR), which has an aspartate at the same position (94). Mutational studies with SQD1 (71), *E. coli* UGE (95-97), *E. coli* dTGD (65), GMD (66), GMER (83), *D. mel.* ADH (98-100), SR (101,102), 3β17βHDH (90), human placental 15-hydroxyprostaglandin dehydrogenase (15HPDH) (103-105), rat DPR (93,106) and cBDH (107) have demonstrated the importance of these residues for catalysis (Table 17). Thr145 in SQD1 is located at the N terminus of a short segment of α-helix (residues Thr145-Tyr149), which puts the Thr145—O_γ atom within hydrogen-bonding distance (2.91-3.03 Å) of the Gly147 amide nitrogen atom. Interestingly, both the hydrogen bond and short α-helical segment are conserved in the three-dimensional structures of other SDR enzymes, suggesting that this interaction, perhaps enhanced by the helical dipole, may be important in maintaining the proper orientation of the catalytic Ser/Thr side chain.

Tyr182 distortion, Lys186 H-bonding and the tyrosinate hypothesis

A catalytic tyrosine is believed to initiate reaction in SDRs. In SQD1, Tyr182 would abstract a proton from the 4′-hydroxyl of UDP-glucose, while NAD^+ strips a hydride from C4′, to produce the 4′-keto Intermediate I (Figure 23). Chen *et al.* first suggested, for *Drosophila* alcohol dehydrogenase, that the catalytic tyrosine exists in a negatively-charged form (98). This hypothesis has since become widely accepted.

Table 17

Effect on k_{cat} of mutating residues of the SDR catalytic triad

Enzyme	Species	Substrate	k_{cat} (w.t.)	Mutation(s)	k_{cat} (mutant)	k_{cat} (w.t.)/ k_{cat} (mutant)	Ref(s)
SQD1	A. thal.	UDP-glucose, sulfite	1×10^{-1}	T145A	4×10^{-5}	3000	(71)
UGE	E. coli	UDP-galactose	4.56×10^{4}	Y149F	4.4×10^{0}	10000	(95)
				S124A	1.59×10^{1}	2870	
				S124T	1.49×10^{1}	3.06	
UGE	E. coli	UDP-galactose	1.4×10^{3}	K153A	7.2×10^{-1}	2000	(96)
				K153M	1.32×10^{0}	1091	
				T134S	1.40×10^{2}	2.0	
				T134A	1.24×10^{0}	230	
				T134V	1.3×10^{0}	240	
dTGD	E. coli	dTDP-glucose	2.9×10^{2}	Y160F	1.55×10^{0}	190	(65)
				Y160A	1.19×10^{0}	250	
				K164A	3.1×10^{0}	35	
				K164M	8.4×10^{0}	96	
GMD	E. coli	GDP-mannose	3.0×10^{2}	T133V	1.1×10^{1}	2800	(66)
GMER	E. coli	GDP-4'-keto-6'-deoxymannose	4.25×10^{2}	S107A	4.64×10^{-1}	915	(83)

k_{cat} is in units of min^{-1} N/R, not reported

Table 17 continued

Enzyme	Species	k_{cat} (w.t.)	Substrate	Mutation(s)	k_{cat} (mutant)	k_{cat} (w.t.)/ k_{cat} (mutant)	Ref(s)
ADH	D. mel.	6.12×10^2	2-propanol	Y152E	0	--	(98,99)
				Y152N	0	--	
				K156I	0	--	
				S139A	0	--	
				S139C	0	--	
				Y152F	0	--	
				Y152H	0	--	
				Y152C	0	--	
				K156I	7.2×10^0	85	
				K156R	6.6×10^1	9.3	
ADH	D. mel.	2.2×10^2	ethanol	Y152E	0	--	(98,99)
				Y152N	0	--	
				K156I	0	--	
				S139A	0	--	
				S139C	0	--	
				Y152F	0	--	
				Y152H	0	--	
				Y152C		--	
				K156I	5.2×10^{-1}	410	
				K156R	4.74×10^0	46	
ADH	D. mel.	N/R	1-propanol	S139A	0	--	(100)
				S139C	0	--	
ADH	D. mel.	N/R	1 butanol	S139A	0	--	(100)
				S139C	0	--	

Table 17 continued

Enzyme	Species	Substrate	k_{cat} (w.t.)	Mutation(s)	k_{cat} (mutant)	k_{cat} (w.t.)/ k_{cat} (mutant)	Ref(s)
cBDH	*C. test.*	*cis*-2,3-dihydro-2,3-dihydroxybiphenyl	2.5×10^3	S142A	3.3×10^1	76	(107)
				Y155F	3.1×10^0	810	
				K159A	2.3×10^2	11	
				Y155F/S142A	2.6×10^0	960	
				Y155F/K159A	6×10^{-1}	4000	
DPR	rat	quinonoid (6R)-L-*erythro*-dihydrobiopterin	1.4×10^3	A133S	1.2×10^3	1.2	(106)
				Y146H	8.34×10^3	0.17	
				Y146F	8.28×10^3	0.17	
				K150Q	1.61×10^4	0.086	
				Y146F/A133S	4.4×10^3	0.31	
				Y146F/K150Q	1×10^4	0.1	
DPR	rat	quinonoid dihydrobiopterin	9.18×10^3	A133S	8.94×10^3	1.03	(93)
				Y146F	1.0×10^2	90	
				Y146H	1.4×10^3	6.7	
				K150Q	5.4×10^3	1.7	
				K150I	3.8×10^3	2.4	
				K150M	1.6×10^3	5.9	
				Y146F/K150Q	4.6×10^3	2.0	
DPR	rat	quinonoid 6,7-dimethyldihydropteridine	9.18×10^3	A133S	9.12×10^3	1.01	(106)
				K150Q	3.1×10^3	2.9	
				Y146H	2.2×10^3	4.3	
				Y146F	1.0×10^3	9.0	
				Y146F/A133S	1×10^2	80	
				Y146F/K150Q	0	---	

140

Table 17 continued

Enzyme	Species	Substrate	k_{cat} (w.t.)	Mutation(s)	k_{cat} (mutant)	k_{cat} (w.t.)/ k_{cat} (mutant)	Ref(s)
3α17βHDH	C. test.	3β,12α-dihydroxy-5β-cholanoate	1.4×10^3	S138A S138T	0 1.5×10^3	--- 0.93	(90)
3α17βHDH	C. test.	5α-dihydrotestosterone	1×10^2	S138A S138T	0 6×10^1	--- 2	(90)
15HPDH	human	prostaglandin E_1 prostaglandin E_2 prostaglandin A_1 prostaglandin A_2 prostaglandin $F_{2\alpha}$ 6-keto prostaglandin $F_{2\alpha}$	6.61×10^2 7.13×10^2 6.26×10^2 3.80×10^2 6.48×10^2 4.49×10^2	S138A, Y151F, Y151A, Y151S, K155Q, K155L	0 0 0 0 0 0	--- --- --- --- --- ---	(103-105)
SR	rat	sepiapterin	$5.8\ 10^2$	S158D Y171V K175I S158D/Y171V	130 160 150 0	4.4 3.7 3.9 ---	(101)
SR	rat	sepiapterin	5×10^1	S158D Y171V K175I S158D/Y171V	1×10^1 1×10^1 1×10^1 0	4 4 4 ---	(102)
SR	rat	phenylpropanedione	5×10^1	S158D Y171V K175I S158D/Y171V	6×10^0 1×10^1 3×10^1 0	9 5 2 ---	(102)

Apparently, the NAD(P)$^+$ and conserved lysine (Lys186 in SQD1) surrounding the catalytic tyrosine stabilize the deprotonated, negatively-charged form of the amino acid. In *E. coli* UGE and *Drosophila lebanonensis* (*D. leb.*) ADH, it is estimated that the pK_a of the catalytic tyrosine is lowered by approximately four pH units (95,98,108) . The interaction between the Tyr/Lys pair had always been assumed to be purely electrostatic in nature, since the O_η–N_ζ distance in all determined structures of related SDR enzymes had been greater than 4 Å, well beyond hydrogen-bonding range. In the SQD1 complexes, in contrast, the Tyr182 and Lys186 side chains are 2.86-2.97 Å apart, easily within hydrogen bonding distance Figures 15 and 16, Table 11). It may be that such a Tyr⋯Lys hydrogen bond also forms in other SDRs when substrate is present.

From the close approach of Tyr182 to UDP-glucose O4′ in SQD1 crystal structures (Table 11), it appeared that this amino acid residue could abstract the 4′-hydroxyl proton directly (80). Whether direct proton abstraction occurs in most of the nucleotide-sugar modifying enzymes of the SDR superfamily was previously less clear. Work on *E. coli* UGE had led to the suggestion that proton abstraction to the catalytic Tyr149 occurred *via* a "proton shuttle" involving the catalytic Ser124 (95,97). This idea was based on a series *E. coli* UGE complex structures in which Ser124 was closer (2.6 Å) than Tyr149 (4.3 Å) to the position of the UDP-galactose O4′. On the other hand, in the SQD1 structures the reactive 4′-hydroxyl of UDP-glucose and UDP-sulfoquinovose clearly interacts directly with both the catalytic Tyr182 and Thr145. In fact, Tyr182—O_η and Thr145—O_γ are farther from one another than either is from O4′ of UDP-glucose. This is consistent with the ternary complexes of many SDR enzymes (86,109,110), in which the susceptible oxygen atoms of bound inhibitors or reaction products also make

analogous hydrogen bonds with both catalytic residues. Thus it appears that postulating a proton shuttle function for the catalytic serine in UGE was an unnecessary complication. Recent structures of human UGE in complex with either UDP-glucose or UDP-N-acetylglucosamine have shown the catalytic Tyr157 at 3.01 or 3.20 Å (in the "B" chains of PDB entries 1HZJ and 1EK6, respectively) from O4′ of substrate (85,89). These findings have strengthened the case for direct proton abstraction by the catalytic tyrosine for all related SDRs, and the proton shuttle theory has been abandoned by some groups (85), if not all (65).

The marked distortion of Tyr182 in SQD1 (Figure 20 and Table 12) is particularly interesting in light of its role in catalysis. In the observed resting state, Tyr182 of SQD1 is expected to exist largely in this O_η-deprotonated form because of its electrostatic environment (95,108). Resonance between phenolate and quinone forms could lend a partial carbanionic, sp^3 character to the mostly sp^2 electronic configuration Tyr182—C_γ (Figure 24). The conformation that would result from the electronic configurations of these two resonance states would have distortion at C_γ, as is consistently observed in all four SQD1 crystal structures. However, the ring distortion may also be influenced by steric repulsion between Tyr182 and the 4′-hydroxyl group of the UDP-hexose, which are only 2.55-2.66 Å apart in the four available SQD1 structures, and/or from favorable hydrogen-bonding and electrostatic interactions with NAD^+ O2′N (2.62-2.86 Å), UDP-glucose O3′ (2.92-3.08 Å), and Lys186—N_ζ (2.86-2.97 Å) atoms. The distorted catalytic tyrosines in the SQD1 structures, if they indeed arise from phenolate-quinone resonance, are the first structural evidence of the presence of a deprotonated catalytic tyrosine in an SDR enzyme.

While the source and importance of this distortion are not entirely certain, the observation that Tyr182 deviates more from ideality than any other tyrosine in SQD1 is intriguing. In contrast, catalytic tyrosines in structures of other SDR enzymes are not more distorted than the general population of tyrosines within each structure. These other enzymes are mostly believed to utilize a deprotonated tyrosine. If mechanism-based tyrosine distortion is observable in SQD1 at resolutions of 1.20 to 1.75 Å, then why is distortion not seen in structures of other SDRs at comparable resolutions? One reason may be the unique "poised" state maintained by SQD1, in which it is on the brink of reacting, but is somehow prevented from initiating catalysis. In contrast, in crystals of *E. coli* UGE, the conversion of the UDP-hexose to the 4′-keto intermediate is quite facile (75). Similarly, rapid mix-quench MALDI-TOF monitoring of the *E. coli* dTGD reaction on the timescale of tens of milliseconds revealed no accumulation of the 4′-keto intermediate (111). In SQD1, the 4′-keto Intermediate I is perhaps equally fleeting. Most SDRs catalyze monosubstrate reactions. For them, maintaining the catalytic tyrosine in the deprotonated state before the reactants are bound offers no advantages and could lead to untoward reactions. Since none of the other SDR crystal structures is of active enzyme with normal substrate, it is possible that their catalytic tyrosines are in the unreactive, protonated state, and thus would not display distortion due to phenolate-quinone resonance.

His183 and catalytic bases in other SDRs (dehydratases and GMER)

In the next step of the SQD1 reaction, a general base is needed to abstract a proton from the acidic glucosyl C5′ atom, forming a glucose-5′,6′-ene Intermediate IIa
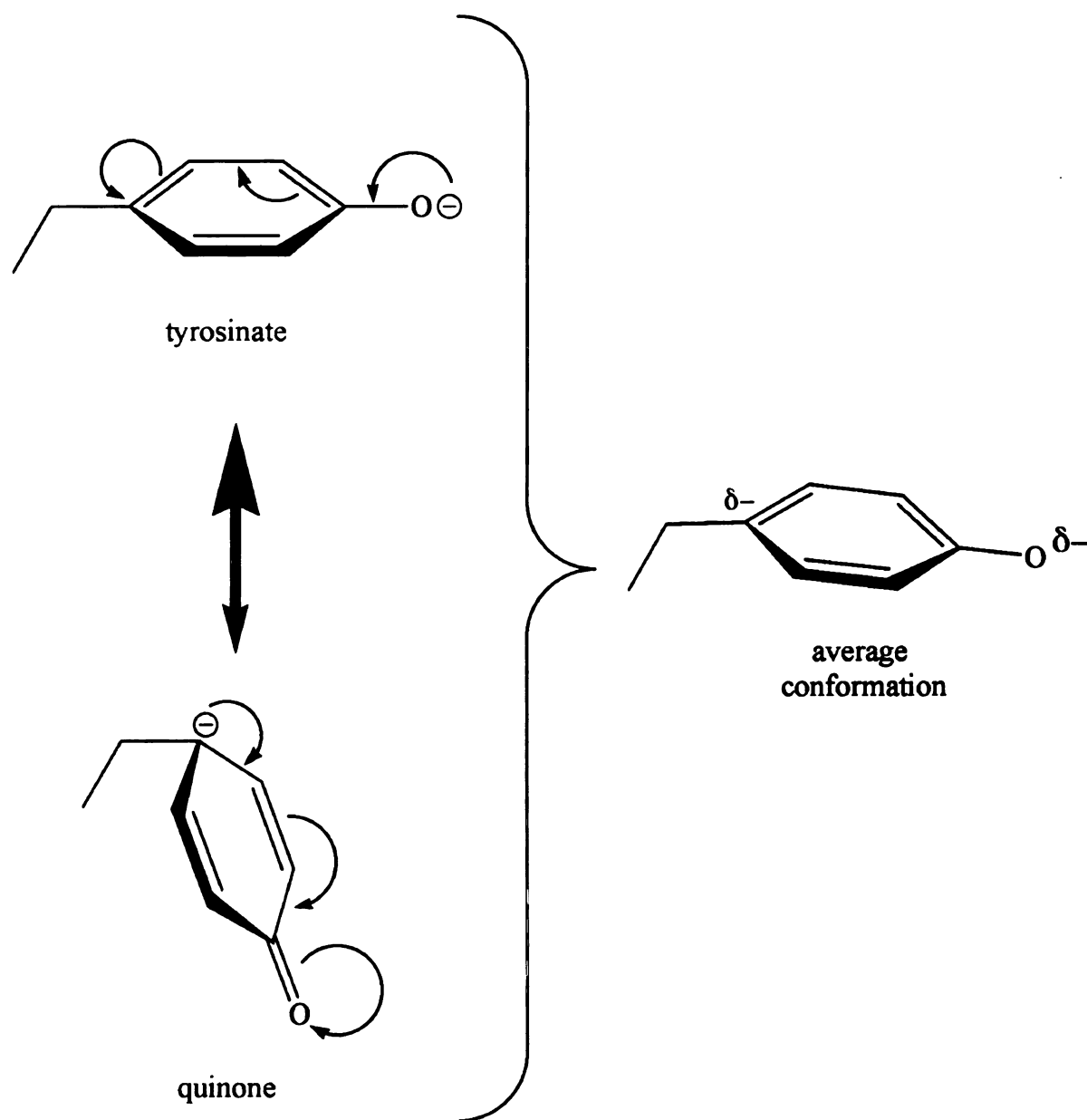
Figure 24. Possible effect of resonance in a tyrosinate side chain.

(Figure 23). Based on proposed reaction schemes, a similar proton abstraction to a general base might be expected during catalysis by CGD, dTGD, GMD, and GMER (66,67,83,111-116). His183 of SQD1, whose N_ε atom is 4.02-4.25 Å from the C5′ atom of UDP-hexose (Figures 15 and 16, Table 11), is the most likely candidate for this function. The orientation of the His183 side chain is stabilized by a hydrogen bond between its N_δ atom and the hydroxyl of Ser180. In the dehydratases, this catalytic base is a glutamate (Glu135 in GMD, Glu136 in *E. coli* dTGD and Glu135 in *S. typh.* dTGD), while in GMER it is thought to be His179.

It has been suggested (Dr. R.M. Garavito, personal communication) that histidine may be particularly suited to the SQD1 reaction because, when protonated by C5′, it would acquire a positive charge. This could help attract a negatively-charged sulfur donor towards the site of reaction. In contrast, the catalytic base of the dehydratases is negatively-charged at neutral pH, and becomes neutral when protonated. In dehydratases, no second substrate participates in the reaction. Rather, the C6′ position is simply reduced from a methylene to a methyl group by donation of a hydride from NAD(P)H. Why GMER would use His179 as its catalytic base, rather than an acidic residue, is less clear. Several intermediates in the GMER reaction could have positive charges on the hexose ring at C3′ or C5′. It may be that the positive charge on the imidazole ring could promote flipping of the hexose ring, thus exposing the opposite face to allow completion of epimerization. Ring flipping appears to be the mechanism of epimerization by UGE (117).

146

Thr145 and LBHBs

The Ser/Thr in the catalytic triad has been shown to be important, in most SDRs, for maintaining a high k_{cat}. Reasons for this have variously been supposed to substrate binding, stabilization of reaction intermediates, or in the case of *E. coli* UGE, to shuttling of protons between the substrate and the catalytic Tyr149. As described above, this last theory is now discounted. A function for Thr145 in SQD1 was suggested by the participation of its side chain hydroxyl in a network of three unusually short hydrogen bonds with the 1) glucosyl 4′-hydroxyl (2.45-2.52 Å), 2) the glucosyl 6′-hydroxyl (2.29-2.45 Å) and 3) WAT411 (2.45-2.57 Å) (Figures 15 and 16, Table 11). WAT411, which is bound above the plane of these three atoms, not only makes short hydrogen bonds with the Thr145—O_γ, but also with the O4′ (2.38-2.49 Å) and O6′ (2.44-2.49 Å) hydroxyls. Hydrogen bonds with these lengths, under the right conditions, have the potential to form "low-barrier" hydrogen bonds (LBHBs). Distinguished structurally by a heteroatom distance of ≤ 2.55 Å, these interactions are characterized by partial covalent contributions between the hydrogen and both heteroatoms (118). They can occur when the heteroatoms have similar proton affinities (*i.e.* pK_a's). Because of inherent error in macromolecular structures, a more conservative distance cutoff of ≤ 2.50 Å is usually used. Experimental determination of pK_a is not possible by X-ray crystallography, but can be estimated by NMR methods or calculated *a priori* (108) If an NAD^+:tyrosinate charge transfer band is present, the tyrosine pK_a can be estimated by observing pH-dependent changes in the nicotinamide absorbance spectrum (95).

LBHBs have been proposed to figure in the catalytic mechanisms of some enzymes by stabilizing reaction intermediates or transition states, or by lowering

energetic barriers to proton transfer. LBHBs have been invoked for stabilization of enolic species, such as could occur during formation of Intermediate II in SQD1 (Figures 23 and 25) (119,120). The unusual network observed at the reactive center of the SQD1 ternary complex suggests that LBHBs may be important in transition state stabilization, and perhaps in promoting removal of the O6′ hydroxyl.

Tyr182 may not form an LBHB

In the original SQD1 crystal structure, the separation between 182—O_η and UDP-glucose O4′ was 2.54 Å, approaching the distance cutoff of 2.50 Å commonly accepted for LBHB formation. In later SQD1 structures, this distance ranged from 2.61 to 2.66 Å (Table 11), making it somewhat less likely that a LBHB exists in the poised state of the enzyme. The differences in distance seen in the SQD1 structures are within the global coordinate error estimated from Luzzati and σ(A) plots, and so it cannot be said with confidence that the distances are significantly different. However, even a small positional change during transition to the activated state of the enzyme could bring Tyr182—O_η to within 2.50 Å of the UDP-glucose O4′. Assuming that Tyr182 already has a negative charge on O_η, such a positional shift would produce the proper conditions for creating of an LBHB, labilizing the proton on O4′ of UDP-glucose.

The kinetic and structural effects of the T145A mutation in SQD1

In other SDRs, mutation of the catalytic serine/threonine (Table 17) generally has a drastic effect on k_{cat} (65,66,83,90,93,95,100-102,105-107). Likewise, mutation of Thr145 to alanine in SQD1 greatly reduces k_{cat}, but nonetheless allows a productive cycle

Figure 25. Possible enol intermediate in the SQD1 reaction.

of catalysis to occur, as seen from kinetic data and from the T145A/product structure. Wild-type SQD1 turns over once in ten minutes with the standard assay, an endpoint product determination with an incubation time of 40 minutes. All ligands are subsequently released by denaturation of the enzyme and detected by HPLC (71). With T145A SQD1, an amount of product corresponding to 10% turnover is observed only after 46 hours of incubation. This residual activity corresponds to a k_{cat} of 19 year^{-1}. The magnitude of decrease in turnover number is in line with the effect of homologous mutations in other SDRs (Table 17).

If reduction of reaction rate is due to alterations in ligand binding, most of the effect should be seen as a change in K_m. Other mutant SDRs did not have increased K_m's relative to wild-type, which could be interpreted as meaning that the affinity of ligand binding is unchanged. With T145A SQD1, the low rate of catalysis makes estimation of this parameter difficult. Considering the results in other SDRs, it may well be similar to wild-type. The high occupancy of UDP-hexose in the T145A structures also suggests that the mutant protein binds substrate at least as tightly as wild-type protein.

The low activity of T145A SQD1 is most likely due to slow catalysis, and not to slow product release. If the mutant enzyme catalyzed product formation at the wild-type rate (0.1 min^{-1}) but released product slowly, then one quarter of the protein would be expected to turn over during the normal 40 minute assay time. The amount of product thus would be 25% of wild-type, an easily detectable quantity. Instead, no product is detected after 40 minutes, while a small but significant 10% yield is seen after 46 hours. The amount of UDP-sulfoquinovose in the T145A/product structure also does not contradict the "slow reaction" hypothesis. After an extended incubation time (6 months

after crystallization started), approximately 65% of the monomers contained product. It seems likely that sulfite must entered the enzyme active site while the protein was in solution and became trapped during crystallization. The crystallize enzyme subsequently underwent catalysis to generate the product. Since no unreacted sulfite or intermediates were seen in this structure, it seems that the reaction stopped due to lack of substrate, rather than for some other reason.

While the mutation of Thr145 to alanine in SQD1 greatly decreases the rate of catalysis, only subtle effects on the conformation of substrate UDP-glucose and essentially no changes in the overall protein structure are observed. As the T145A substrate and product structures illustrate the endpoints of a successful, albeit very slow, cycle of catalysis, we can infer that the lowering of catalytic activity in the mutant is not due to major structural perturbations of the protein and ligands. The large effect on catalytic rate is therefore most likely due to a specific chemical effect resulting from loss of the threonine side chain. One major change is that all potential LBHBs are missing in the T145A mutant structures (Figure 16, Table 11). This is due to the loss of Thr145-O_γ, WAT410 and WAT411. Another active-site water, WAT461, is also absent. Although the short hydrogen bonds are lost, an extensive network of hydrogen bonds is maintained by small rearrangements of bound waters, protein residues and the UDP-hexose atoms themselves, consistent with the maintenance of tight substrate binding.

No other significant structural changes were seen due to the T145A mutation. In particular, the distance between O_η of Tyr182 and O4' of UDP-hexose is essentially the same in all of the SQD1 structures (Table 11) at 2.54-2.66 Å. The position of His183, postulated to be involved in formation of Intermediate II, is similarly unaffected (Table

11). Thus, the low rate of catalysis in T145A SQD1 cannot be attributed to a change in these relationships. Since the only significant structural change seems to be the loss of LBHBs, while normal catalysis continues at a greatly reduced rate, it is reasonable to conclude that LBHBs (and Thr145) are responsible for accelerating catalysis in SQD1, without being absolutely necessary for reaction. LBHBs could speed up the SQD1 reaction during at least two stages of the reaction. First, removal of the proton from O4′ of UDP-glucose could be accelerated if its distance from Tyr182—O_η can be reduced slightly, to less than 2.50 Å. This result should stabilize the O4′-deprotonated form of UDP-glucose, giving NAD^+ a chance to abstract the C4′ hydride. Second, if an enol intermediate exists during the reaction, perhaps between Intermediates I and II (Figure 25), it could be stabilized by a favorable LBHB between O4′ and Thr145—O_γ. Thr145-O_γ and UDP-glucose O4′ are already at approximately the correct distance (2.45-2.52 Å) for an LBHB to occur between these atoms.

Similarly short hydrogen bonds were recently observed in crystal structures of human UDP-galactose 4′-epimerase, where the S132—O_γ is 2.40 Å (PDB entry 1EK6, monomer A), 2.47 Å (PDB entry 1EK6, monomer B) and 2.27 Å (PDB entry 1I3K, monomer B) from the substrate 4′-hydroxyl (85,121). The unusual geometry and catalytic importance of the Thr/Ser hydroxyl implicate it in formation of the 4′-keto intermediate, the common initial step between UGE, GMD, dTGD, CGD and SQD1. For SQD1 and the nucleotide-sugar 4′,6′-dehydratases GMD, dTGD and CGD, the catalytic Thr/Ser hydroxyl may also play a role in the dehydration step to form Intermediate II (Figure 23) as Thr145 coordinates not only the glucosyl 4′-hydroxyl, but also the glucosyl 6′-hydroxyl and a buried water molecule (WAT411; Figure 16). As the 4′-keto

152

group is formed (Figure 23), the O4′ atom would move away allowing Thr145—O$_\gamma$ to ligand the glucosyl 6′-hydroxyl even more strongly. The possible contributions of the hydrogen bonds to the dehydration and sulfite addition steps remains incompletely defined, yet clearly have a rate-enhancing role.

Delaying catalysis by nicotinamide orientation: possible role of H-bonding to C6

In the current SQD1 reaction scheme (Figure 23), the enzyme initially exists in the poised state, in which it binds NAD$^+$ and UDP-glucose, but does not react. It is not until the sulfur donor binds that the enzyme becomes activated and catalysis truly begins. Looking at Figure 23, one might expect the reaction to proceed spontaneously to the 4′-keto-glucose-5′,6′-ene Intermediate II, even in the absence of the sulfur donor. An obvious explanation for this delay may be that binding of the sulfur donor is required to induce a productive arrangement of NAD$^+$ and/or substrate. Indeed, the NAD$^+$ and glucosyl rings are overlapped such that the nicotinamide C4 atom is poorly aligned for abstraction of hydride from the glucosyl C4′ position (Figure 26). The nicotinamide ring is canted away from UDP-glucose so that the distance between the reacting atoms (nicotinamide C4 and UDP-glucose C4′) is 3.7 Å. In liver alcohol dehydrogenase (LADH), a well-studied model of nicotinamide hydride transfer, the distance in wild-type enzyme is 3.5 Å. In LADH mutants, catalytic efficiency decreased sharply with increasing transfer distance (122). More importantly, the angle between the nicotinamide plane and the hydrogen atom of UDP-glucose C4′ (as calculated by the PRODRG server (123)) in SQD1 is 88.6° (Figure 26). In a contrasting example, the structure of the tropinone reductase-II terminal complex, the angle is 101.4°. This is in line with the

Figure 26. Orientation of the NAD$^+$ nicotinamide ring. UDP-glucose (left) and NAD$^+$ (right) are shown as ball-and-stick models, with atoms and bonds colored by element (carbon=gray, hydrogen=dark gray, oxygen=red, nitrogen=blue, phosphorus=purple). The atoms used to calculate the "attack angle" of 88.6° (N1 and C4 of NAD$^+$ and the hydrogen on C4´) are connected by green, dashed lines.
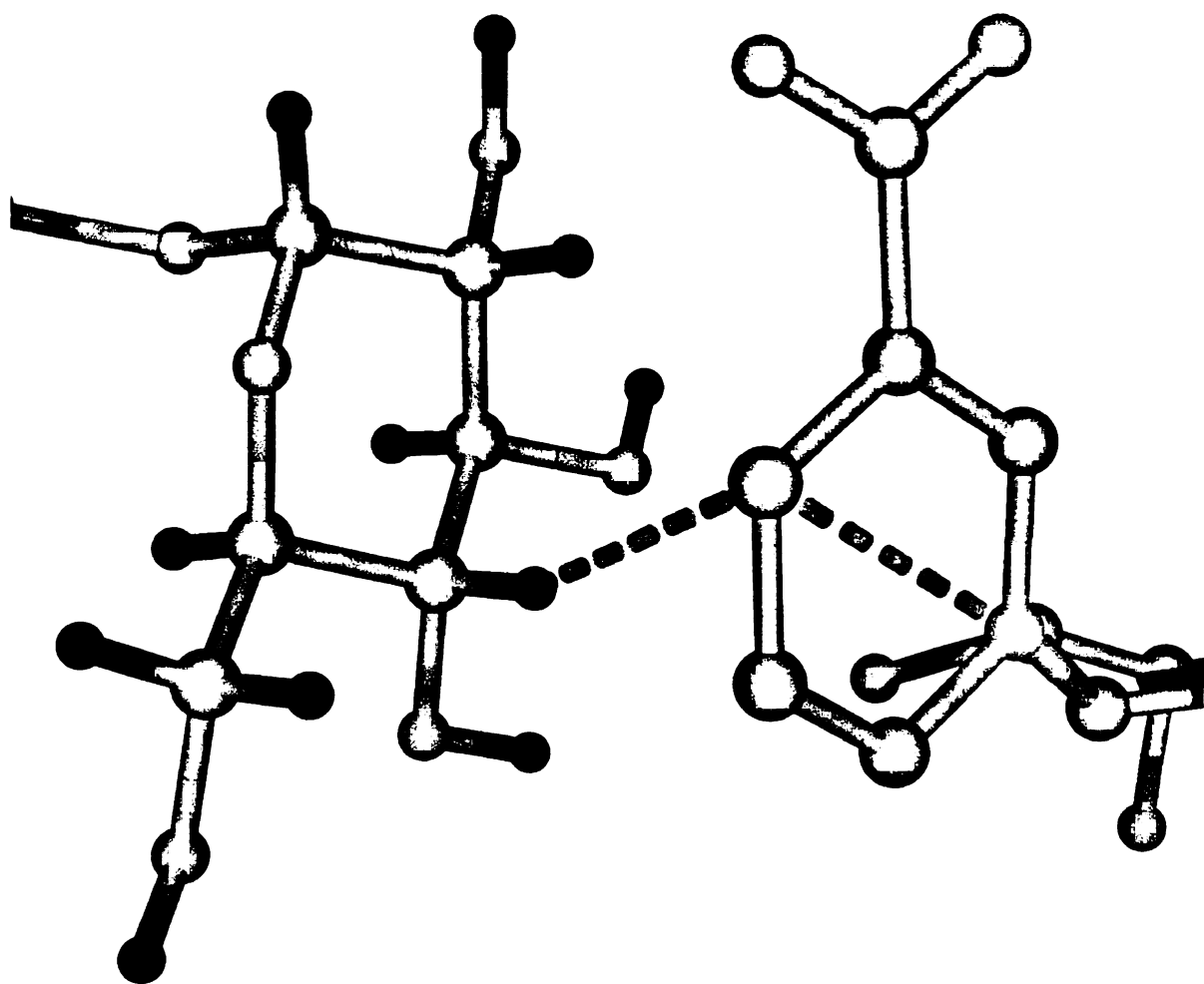
Figure 26

theoretical optimal range of 102-109° (124). It is likely that the immediate reason that the reaction does not proceed is that the nicotinamide C4 ring is at the wrong angle and too far from its target. The presence of the sulfur donor would presumably alter the active site, perhaps by changing the charge environment, in such a way that the nicotinamide ring would become properly oriented. As the sulfur donor should be rather unstable in the aqueous environment of the cell, it would be advantageous for its binding to initiate NAD^+ reduction and subsequent catalysis, in order to maximize the likelihood of achieving a successful catalytic outcome. The ability of SQD1 to tightly bind and sequester UDP-glucose and NAD^+, maintaining them in a poised state until sulfite is available, suggests that the enzyme may be adapted to limited sulfite availability *in vivo*.

One interaction which may play a role in keeping the nicotinamide canted away from the reactive position is the bridging hydrogen bond: Gly144=O···WAT410···C6—NAD^+ (Figures 15a, 15b, 16a,, 16b). WAT410 is 3.18 Å from C6 and 2.57 Å from the carbonyl oxygen. In the high-resolution wild-type/substrate structure, WAT410 is positioned only 2.36 Å from the carbonyl oxygen of Gly144. Of the nucleotide-sugar modifying SDRs with known crystal structures, five have serine at this position (*E. coli* UGE, human UGE, dTGD, AGME and GMD) and two have glycine (SQD1 and GMER) (Table 16). The identity of the Gly144 residue in SQD1 is conserved across homologs from seven other species (Personal communication from a former colleague, Dr. Sherrie Sanda). The glycine residues in SQD1 and GMER adopt φ-ψ angles that would be strained for serines, or indeed any other amino acid with a β-carbon.

This division in residues interacting with the nicotinamide C6 is paralleled by a division in mechanism. In those NMSDRs where a serine carbonyl oxygen interacts with

the nicotinamide ring, the enzymes utilize a single substrate, with participation of the nicotinamide group in forming the first intermediate. Thus they would be most efficient at catalysis if hydride abstraction occurs immediately after substrate binding. In contrast, the proposed mechanisms for SQD1 and GMER both require that the UDP-hexose substrate bind, but that hydride abstraction *not* occur, until another condition has been satisfied. In SQD1, this condition is that the sulfur donor also be present. In GMER, the prerequisite is presumably that the substrate first be epimerized at the 3′ and 5′ positions, independent of cofactor, before the 4′-carbon is reduced by NADPH. In the cases of SQD1 and GMER, premature involvement of the cofactor in the reaction could lead to untoward product formation, wasting a catalytic cycle. In other nucleotide-sugar modifying SDRs, this is not a concern.

It may be that the substitution of glycine for serine in SQD1 and GMER is a structural adaptation which permits these enzymes to bind substrate in a reactive conformation, yet delay cofactor involvement until a specific triggering event. In both the T145A mutant SQD1 structures, in which WAT410 and WAT411 are lost, the nicotinamide ring is shifted 0.2 Å *closer* to the UDP-glucose than in the two wild-type structures. Structures of GMER lack a "bridging" water (WAT410 in SQD1). This could be due to the lack of a substrate or analog in any GMER structure. Unfortunately, testing the effect of a G144S mutation in SQD1 would be difficult, because there is no additional space for a larger side chain at position 144. It would be necessary to construct a double mutant, for example G144S/E148A, to accommodate the C_β and O_γ of a serine.

Displacement of active site waters during reaction

Interestingly, besides possible displacement of WAT410 during a hypothetical realignment of the cofactor, other waters in the SQD1 active site would need to move during catalysis. WAT411 would be displaced by formation of a 4'-keto on UDP-glucose (Intermediate I), assuming that the atoms of the glucose ring remain stationary (Figure 27). Further along in the reaction, again assuming no ring movement, WAT461 would need to move when the 4'-keto-5',6'-ene Intermediate II is formed, while WAT463 likely would clash with the sulfonyl group of Intermediate III and the final product, UDP-sulfoquinovose.

Sulfite is a sulfur donor in vitro

In vitro assays using radiolabeled UDP-glucose and sulfite have demonstrated that SQD1 catalyzes UDP-sulfoquinovose formation *in vitro* (71). Radiolabeled sulfite also can be incorporated into UDP-sulfoquinovose in this assay system. In tests with various sulfur-containing compounds, inorganic sulfite was found to be at least as effective as any other substance. However, the *in vitro* reaction displays several curious kinetic properties. First, the reaction is extremely slow, with a k_{cat} of only 0.1 min^{-1}. Apparently, this is the slowest rate known for a wild-type enzyme (Dr. Christoph Benning, personal communication). Second, the maximal reaction velocity is reached at a sulfite concentration of only 100 µM. At higher concentrations an inhibitory effect, apparently due to ionic strength, reduces the amount of product formed. *In vivo*, such a level of free sulfite is not likely to be achieved, due to the cytotoxic effects, *e.g.*, sulfitolysis, lipid

Figure 27. Displacement of active-site waters by modeled reaction intermediates. The scene is in stereo. UDP-glucose, intermediates and UDP-sulfoquinovose are shown as ball and stick models, with atoms colored by element (white=carbon, red=oxygen, purple=phosphorus, yellow=sulfur). Oxygens of waters are shown as cyan spheres and labeled by residue number. Clashes are depicted by dashed pink lines. a) The poised state, with UDP-glucose and the buried waters 410, 411, 461 and 463. b) Intermediate I, with the 4'-keto oxygen clashing with WAT411. c) Intermediate II, missing WAT410 and WAT411, with the C6' of the C5'=C6' portion displacing WAT461. d). Intermediate III, missing three waters, with the sulfonyl group displacing WAT463. e) The final state, with UDP-sulfoquinovose and all four waters lost.
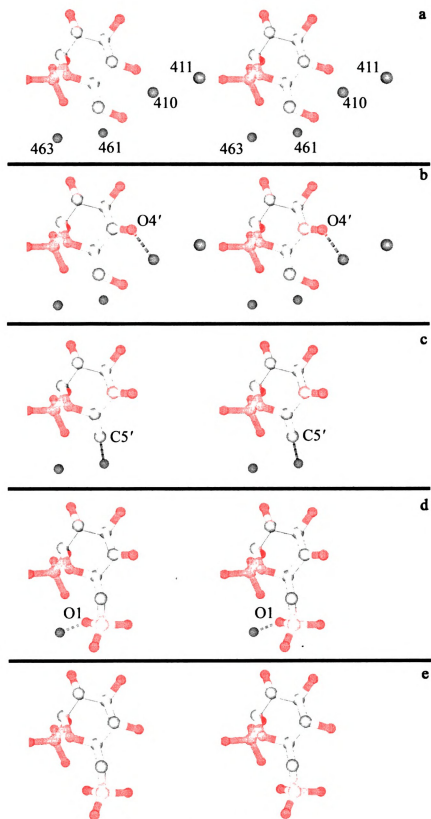
Figure 27

peroxidation, damage to nicotinamide adenine dinucleotide cofactors and inhibition of PSII activity (125-128) .

Substrate channeling

Our current hypothesis is that sulfite is also the *in vivo* sulfur donor. A difficulty with this idea is the apparent absence of free sulfite in chloroplasts, despite the presence of sulfite-producing pathways (71,129). The low rate of catalysis, as well as the difficulty of introducing molecules into the SQD1/NAD$^+$/UDP-glucose complex, has led to a supposition that substrate channeling might be necessary to efficiently introduce sulfite into the active site *in vivo*. This presumably would increase the rate of SQD1 catalysis, and would also explain the lack of free sulfite in plant chloroplasts. A sulfur donor or inorganic sulfite in the free state may be rather unstable *in vivo*. Therefore, SQD1 may have adapted by excluding bulk water from its buried active site, permitting access only through solvent channels. Since free sulfite is cytotoxic (125-128), preventing its free diffusion would be beneficial to the cell. Interestingly, the *A. thal.* chloroplast enzyme APS reductase-1 (APR1) can be used *in vitro* to "feed" sulfite to the SQD1 (71). However, the two enzymes would not necessarily have to be tightly coupled for this to work *in vitro*.

Alternatively, it may be that some condition or factor which facilitates sulfur donor binding or reaction *in vivo* has not been reproduced *in vitro*, for example an allosteric affector. Such a molecule could cause a conformational change in SQD1 leading to higher activity. This hypothesis is attractive because it could be a additional point of communication between sulfolipid biosynthesis and its proposed function in

responding to low phosphatidyl glycerol levels. However, it is known that SQD1 expression increases during phosphate deprivation (35). Protein:protein interactions could also affect the activity of SQD1.

Summary and future directions

The SQD1 structures are unique is several aspects. First, they provide information on the endpoints of reaction, using protein which is catalytically competent, albeit very slow in the case of T145A SQD1. All other SDR crystal structures are farther from the catalytically relevant state, either because they lack substrate and/or cofactor, have an inhibitor bound, are in an inappropriate oxidation state, or have been mutagenized. Second, SQD1 is the only SDR which is known to catalyze a bisubstrate reaction, this despite its high structural similarity to other SDRs. How SQD1 coordinates catalysis of two substrates, while retaining most of the structural characteristics of a class of monosubstrate enzymes, is an interesting point that could be explored in the future.

Some of the questions about SQD1 which have already been (at least partially) answered are the roles of Thr145 and other active-site residues, the identity of the sulfur donor, and how the reaction may be initiated by nicotinamide reorientation. Several issues remain. Is sulfite the *in vivo* sulfur donor, and if so, how is catalysis triggered by its binding? What are the intermediates in the SQD1 reaction? At what stage of reaction does Thr145 provide its rate-enhancing effect? Is His183 indeed responsible for abstraction of a proton from C5′? Is the reaction rate enhanced by substrate channeling, protein-protein interactions or binding of affector molecules? Finally, could SQD1 be modified in some way to produce novel sulfonated sugar compounds, for example UDP-

6′-deoxy-6′-sulfogalactose?

In the area of testing whether sulfite as the *in vivo* sulfur donor, Dr. William Smith has suggested an interesting experimental strategy (personal communication). The putative sulfur donor channel in SQD1 appears to be large enough to accommodate molecules that are more bulky than sulfite. By mutating protein residues in the channel, it might be possible to restrict its size so that only sulfite could conceivably enter. The activity of the mutant enzyme could be monitored by *in vitro* activity assays, and its structure could be checked by X-ray crystallography. This mutant could then be reintroduced into *A. thal.* lacking wild-type SQD1, to see if it can complement the deficiency. If successful, this would suggest that the biological sulfur donor is no larger than sulfite, thus eliminating from consideration many of the larger candidate biological sulfur donors.

Further insight into the chemistry and biology of SQD1 will depend on 1) determining how substrate is provided to the enzyme *in vivo*, 2) modifying the enzyme by mutagenic and chemical means, 3) solving structures of complexes between native and modified SQD1 and various molecules and 4) modeling and comparative studies. One complex which would be interesting is wild-type SQD1 with UDP-sulfoquinovose. The possibility of generating this complex would depend on the kinetics of the various steps in the SQD1 catalytic mechanism. The wild-type enzyme turns over about once every ten minutes, which includes the time for the actual reaction (k_5 in Figure 28) plus time needed for product release (k_6 in Figure 28). If crystallization could be set up before the cycle of reaction and product release is completed, and if the high salt crystallization conditions indeed "seal" the active site, preventing ligand ingress or egress, then it might

163

be possible to observe the structure of wild-type enzyme in complex with product. It is less likely, given that several weeks are generally required for sizeable crystals to grow, that intermediates would remain at the time of data collection. To obtain a complex containing both substrates in the unreacted state, it might be necessary to modify SQD1 both mutationally and chemically. For *E. coli* UGE, it was necessary to mutate both the catalytic serine (S124A) and tyrosine (Y149F), as well as to chemically reduce the cofactor. To do the same in SQD1, a double mutant (T145A and Y182F) would first have to be made and purified. NAD^+ would be reduced to NADH, and finally exogenous UDP-glucose and sulfite would be added.

Complexes which are even more interesting might be obtained by trapping the enzyme with a bound intermediate. For example, if mutation of H183 halted catalysis after formation of the 4′-keto Intermediate I, it would simultaneously confirm the role of this residue, while offering a view of any structural rearrangements necessary to accommodate the intermediate, such as loss of WAT411 and WAT410. Some intermediates may be too fleeting to be observed crystallographically. As was mentioned above, the 4′-keto species in *E. coli* dTGD could not be captured, even on the millisecond time scale (111). This suggests that this intermediate proceeds very quickly to the more stable 4′-keto-5′,6′-ene form, and so never accumulates to significant levels. If the 4′-keto intermediate in SQD1 is similarly unstable, it would never survive during the much longer timescales of X-ray crystallography. Nonetheless, with an amenable mutant enzyme and the right conditions, it might be possible. Alternatively, substrate analogs unable to complete the whole reaction cycle could be added to the enzyme to mimic an intermediate compound or a transition state.

Figure 28. A kinetic scheme for the SQD1 reaction. Crystal structures described in this work are enclosed in boxes. In keeping with the hypothesis that the SQD1 reaction is ordered, arrows which are dashed indicate a pathway which reactions which are disallowed under this system.

SQD1:NAD$^+$

+   +

UDP-glucose   sulfite

k_1 k_{-1} k_{-2} k_2

sulfite + | SQD1:NAD$^+$:UDP-glucose | SQD1:NAD$^+$:sulfite + UDP-glucose

k_3 k_{-3} k_4 k_{-4}

SQD1:NAD$^+$:UDP-glucose:sulfite

k_5 k_{-5}

| SQD1:NAD$^+$:UDP-sulfoquinovose | +   H$_2$O

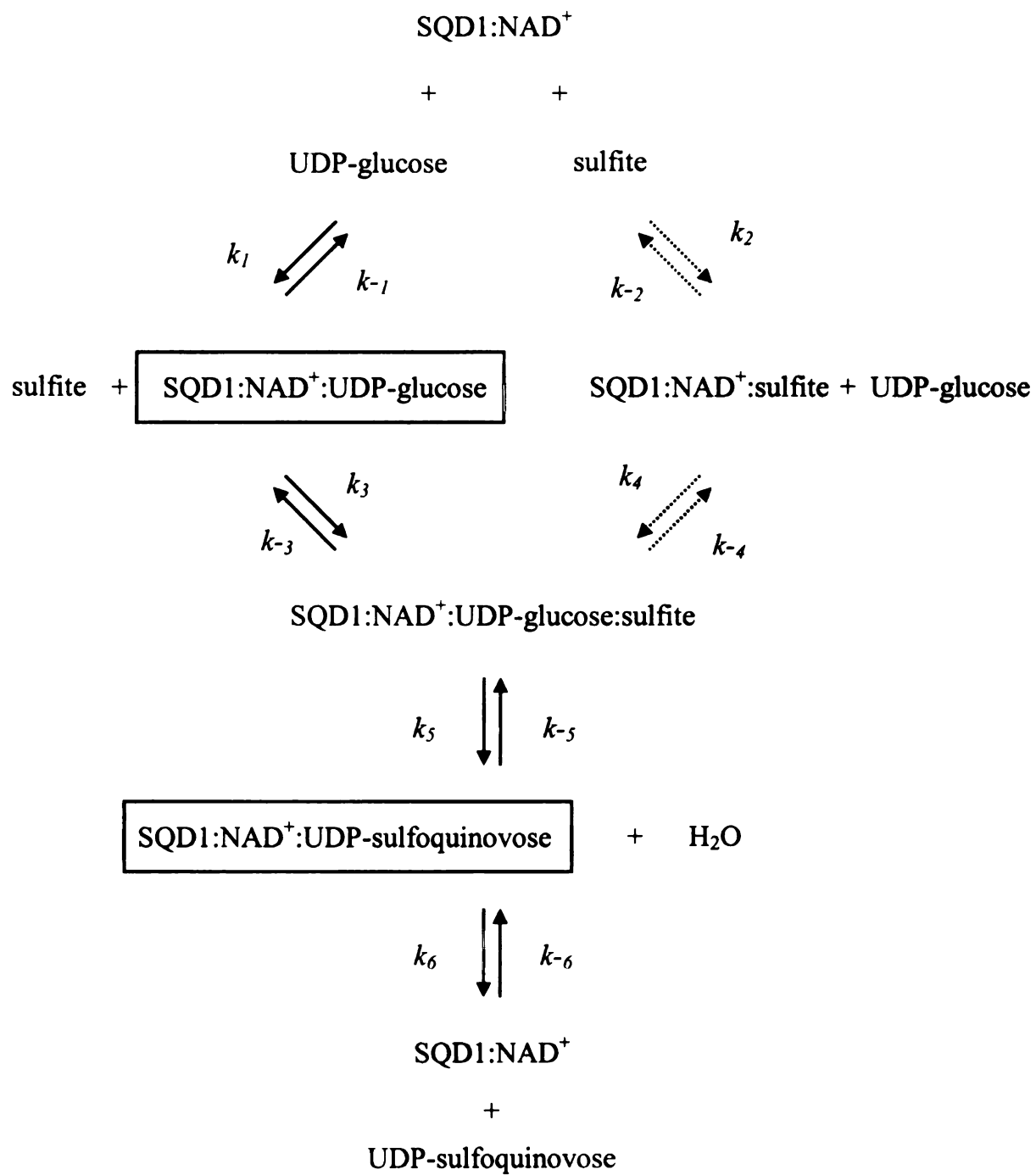k_6 k_{-6}

SQD1:NAD$^+$

+

UDP-sulfoquinovose

Figure 28

166

In order to efficiently form SQD1/ligand complexes, techniques for introducing ligands into the active site will need to be improved. A strategy to achieve this is suggested by the tight binding of His-tagged SQD1 to the Ni-NTA during affinity purification. While still bound to the Ni-NTA column, SQD1 could be incubated in a buffer containing sulfite. Presumably, any UDP-glucose present from the *E. coli* host would react to form UDP-sulfoquinovose, which would then be released from the enzyme. Afterwards, the column could be washed to remove the UDP-sulfoquinovose. Before or after elution of SQD1 from the column, the enzyme could be incubated with a different solution containing a ligand, for example UDP-xylose, or left in the unliganded state.

Comparison of SQD1 to other SDRs has already yielded some interesting contrasts. Examples of these are the relative abundance of potential LBHBs in the SQD1 active site, the distortion of Tyr182, the use of His183 as the general base, rather than an acidic residue, and the possible role of backbone carbonyl oxygens in orienting the nicotinamide ring. Further detailed comparisons could provide more information on the relationship between structure and function. Of particular interest from a biotechnology standpoint is the possibility of changing substrate specificity and reaction type. If the SQD1 active site could be mutagenized to resemble those of enzymes which utilize other substrates, it might be tailored to sulfonate a whole variety of sugars. These could form a pool of novel starting materials for further syntheses.

A final, entirely speculative avenue for investigation is related to the health implications of SQDG levels in food plants. Since levels of SQDG in plants depend on the availability of exogenous phosphorus, SQDG levels should be at a minimum in the

presence of abundant phosphorus, as is common when modern fertilizers are used. If SQDG is indeed beneficial to human health, as suggested by studies related to psoriasis, cancer and viral replication, then growing food plants with phosphorus-rich fertilizers may deprive consumers of many of these health advantages.

Literature Cited

1.   Smith, W. L., DeWitt, D. L., and Garavito, R. M. "Cyclooxygenases: Structural, Cellular, and Molecular Biology." (2000) *Annu Rev Biochem* **69,** 145-182.

2.   Otto, J. C., DeWitt, D. L., and Smith, W. L. "N-glycosylation of prostaglandin endoperoxide synthases-1 and -2 and their orientations in the endoplasmic reticulum." (1993) *J Biol Chem* **268,** 18234-18242.

3.   Spencer, A. G., Woods, J. W., Arakawa, T., Singer, I. I., and Smith, W. L. "Subcellular localization of prostaglandin endoperoxide H synthases-1 and -2 by immunoelectron microscopy." (1998) *J Biol Chem* **273,** 9886-9893.

4.   Kulmacz, R. J., and Wang, L. H. "Comparison of hydroperoxide initiator requirements for the cyclooxygenase activities of prostaglandin H synthase-1 and -2." (1995) *J Biol Chem* **270,** 24019-24023.

5.   Chen, W., Pawelek, T. R., and Kulmacz, R. J. "Hydroperoxide dependence and cooperative cyclooxygenase kinetics in prostaglandin H synthase-1 and -2." (1999) *J Biol Chem* **274,** 20301-20306.

6.   Lu, G., Tsai, A. L., Van Wart, H. E., and Kulmacz, R. J. "Comparison of the peroxidase reaction kinetics of prostaglandin H synthase-1 and -2." (1999) *J Biol Chem* **274,** 16162-16167.

7.   Picot, D., Loll, P. J., and Garavito, R. M. "The X-ray crystal structure of the membrane protein prostaglandin H_2 synthase-1." (1994) *Nature* **367,** 243-249.

8.   Spencer, A. G., Thuresson, E., Otto, J. C., Song, I., Smith, T., DeWitt, D. L., Garavito, R. M., and Smith, W. L. "The membrane binding domains of prostaglandin endoperoxide H synthases 1 and 2. Peptide mapping and mutational analysis." (1999) *J Biol Chem* **274,** 32936-32942.

9.   Kurumbail, R. G., Stevens, A. M., Gierse, J. K., McDonald, J. J., Stegeman, R. A., Pak, J. Y., Gildehaus, D., Miyashiro, J. M., Penning, T. D., Seibert, K., Isakson, P. C., and Stallings, W. C. "Structural basis for selective inhibition of cyclooxygenase-2 by anti-inflammatory agents." (1996) *Nature* **384,** 644-648.

10. Luong, C., Miller, A., Barnett, J., Chow, J., Ramesha, C., and Browner, M. F. "Flexibility of the NSAID binding site in the structure of human cyclooxygenase-2." (1996) *Nat Struct Biol* **3**, 927-933.

11. Guex, N., and Peitsch, M. C. "SWISS-MODEL and the Swiss-PdbViewer: an environment for comparative protein modeling." (1997) *Electrophoresis* **18**, 2714-2723.

12. Christopher, J. A., and Baldwin, T. O. "Real-time collaborative molecular modelling." (1998) *Journal of Molecular Graphics & Modelling* **16**, 285-285.

13. Merritt, E. A., and Bacon, D. J. "Raster3D: Photorealistic Molecular Graphics." (1997) *Methods in Enzymology* **277**, 505-524.

14. Evans, S. V. "SETOR: hardware-lighted three-dimensional solid model representations of macromolecules." (1993) *J Mol Graphics* **11**, 134-138.

15. Davey, C. A., and Fenna, R. E. "2.3 Å resolution X-ray crystal structure of the bisubstrate analogue inhibitor salicylhydroxamic acid bound to human myeloperoxidase: a model for a prereaction complex with hydrogen peroxide." (1996) *Biochemistry* **35**, 10967-10973.

16. Henriksen, A., Schuller, D. J., Meno, K., Welinder, K. G., Smith, A. T., and Gajhede, M. "Structural interactions between horseradish peroxidase C and the substrate benzhydroxamic acid determined by X-ray crystallography." (1998) *Biochemistry* **37**, 8054-8060.

17. Itakura, H., Oda, Y., Fukuyama, K., Henriksen, A., Schuller, D. J., Meno, K., Welinder, K. G., Smith, A. T., and Gajhede, M. "Binding mode of benzhydroxamic acid to *Arthromyces ramosus* peroxidase shown by X-ray crystallographic analysis of the complex at 1.6 Å resolution." (1997) *FEBS Lett* **412**, 107-110.

18. Tsukamoto, K., Itakura, H., Sato, K., Fukuyama, K., Miura, S., Takahashi, S., Ikezawa, H., and Hosoya, T. "Binding of salicylhydroxamic acid and several aromatic donor molecules to *Arthromyces ramosus* peroxidase, investigated by X-ray crystallography, optical difference spectroscopy, NMR relaxation, molecular dynamics, and kinetics." (1999) *Biochemistry* **38**, 12558-12568.

19.   Seibold, S. A., Cerda, J. F., Mulichak, A. M., Song, I., Garavito, R. M., Arakawa, T., Smith, W. L., and Babcock, G. T. "Peroxidase activity in prostaglandin endoperoxide H synthase-1 occurs with a neutral histidine proximal heme ligand." (2000) *Biochemistry* **39,** 6616-6624.

20.   Zor, T., and Selinger, Z. "Linearization of the Bradford protein assay increases its sensitivity: theoretical and experimental studies." (1996) *Anal Biochem* **236,** 302-308.

21.   Ames, B. N. (1966) in *Methods in Enzymology* Vol. 8, pp. 115-118.

22.   Ames, B. N., and Dubin, D. T. "The Role of Polyamines in the Neutralization of Bacteriophage Deoxyribonucleic Acid." (1960) *J Biol Chem* **235,** 769-775.

23.   Otwinowski, Z., and Minor, W. (1997) in *Methods in Enzymology* (Carter, C. W., Jr., and Sweet, R. M., eds) Vol. 276: Macromolecular Crystallography, part A, pp. 307-326, Academic Press, New York.

24.   Collaborative Computational Project, N. "The CCP4 Suite: Programs for Protein Crystallography." (1994) *Acta Cryst* **D50,** 760-763.

25.   Malkowski, M. G., Theisen, M. J., Scharmen, A., and Garavito, R. M. "The Formation of Stable Fatty Acid Complexes in Prostaglandin H_2 Synthase-1." (2000) *Arch Biochem Biophys* **380,** 39-45.

26.   Iwata, S., Ostermeier, C., Ludwig, B., and Michel, H. "Structure at 2.8 Å resolution of cytochrome *c* oxidase from *Paracoccus denitrificans*." (1995) *Nature* **376,** 660-669.

27.   Tsukihara, T., Aoyama, H., Yamashita, E., Tomizaki, T., Yamaguchi, H., Shinzawa-Itoh, K., Nakashima, R., Yaono, R., and Yoshikawa, S. "The whole structure of the 13-subunit oxidized cytochrome *c* oxidase at 2.8 Å." (1996) *Science* **272,** 1136-1144.

28.   Selinsky, B. S., Gupta, K., Sharkey, C. T., and Loll, P. J. "Structural analysis of NSAID binding by prostaglandin H_2 synthase: time-dependent and time-independent inhibitors elicit identical enzyme conformations." (2001) *Biochemistry* **40,** 5172-5180.

29.   Malkowski, M. G., Thuresson, E. D., Lakkides, K. M., Rieke, C. J., Micielli, R., Smith, W. L., and Garavito, R. M. "Structure of Eicosapentaenoic and Linoleic Acids in the Cyclooxygenase Site of Prostaglandin Endoperoxide H Synthase-1." (2001) *J Biol Chem* **276,** 37547-37555.

30.   Thuresson, E. D., Malkowski, M. G., Lakkides, K. M., Rieke, C. J., Mulichak, A. M., Ginell, S. L., Garavito, R. M., and Smith, W. L. "Mutational and X-ray crystallographic analysis of the interaction of dihomo-γ-linolenic acid with prostaglandin endoperoxide H synthases." (2001) *J Biol Chem* **276,** 10358-10365.

31.   Harwood, J. L., Nicholls, R. G., Nishihara, M., Yokota, K., and Kito, M. "The plant sulpholipid -- a major component of the sulphur cycle." (1979) *Biochem Soc Trans* **7,** 440-447.

32.   Benning, C. "Biosynthesis and function of the sulfolipid sulfoquinovosyl diacylglycerol." (1998) *Annu Rev Plant Physiol Plant Mol Biol* **49,** 53-75.

33.   Benning, C., Beatty, J. T., Prince, R. C., and Somerville, C. R. "The sulfolipid sulfoquinovosyldiacylglycerol is not required for photosynthetic electron transport in *Rhodobacter sphaeroides* but enhances growth under phosphate limitation." (1993) *Proc Natl Acad Sci U S A* **90,** 1561-1565.

34.   Sato, N., Tsuzuki, M., Matsuda, Y., Ehara, T., Osafune, T., and Kawaguchi, A. "Isolation and characterization of mutants affected in lipid metabolism of *Chlamydomonas reinhardtii.*" (1995) *Eur J Biochem* **230,** 987-993.

35.   Essigmann, B., Güler, S., Narang, R. A., Linke, D., and Benning, C. "Phosphate availability affects the thylakoid lipid composition and the expression of SQD1, a gene required for sulfolipid biosynthesis in *Arabidopsis thaliana.*" (1998) *Proc Natl Acad Sci USA* **95,** 1950-1955.

36.   Sato, N., Hagio, M., Wada, H., Tsuzuki, M., and Kikuchi, K. "Environmental effects on acidic lipids of thylakoid membranes." (2000) *Biochem Soc Trans* **28,** 912-914.

37.   Nishihara, M., Yokota, K., and Kito, M. "Lipid molecular species composition of thylakoid membranes." (1980) *Biochim Biophys Acta* **617,** 12-19.

38.   Inoue, K., Demel, R., de Kruijff, B., and Keegstra, K. "The N-terminal portion of the preToc75 transit peptide interacts with membrane lipids and inhibits binding and import of precursor proteins into isolated chloroplasts." (2001) *Eur J Biochem* **268**, 4036-4040 4043.

39.   Hagio, M., Gombos, Z., Varkonyi, Z., Masamoto, K., Sato, N., Tsuzuki, M., and Wada, H. "Direct evidence for requirement of phosphatidylglycerol in photosystem II of photosynthesis." (2000) *Plant Physiol* **124**, 795-804.

40.   Sato, N., Hagio, M., Wada, H., and Tsuzuki, M. "Requirement of phosphatidylglycerol for photosynthetic function in thylakoid membranes." (2000) *Proc Natl Acad Sci U S A* **97**, 10655-10660.

41.   Roy, A. B., Ellis, A. J., White, G. F., and Harwood, J. L. "Microbial degradation of the plant sulpholipid." (2000) *Biochem Soc Trans* **28**, 781-783.

42.   Zähringer, U., Moll, H., Hettmann, T., Knirel, Y. A., and Schäfer, G. "Cytochrome $b_{558/566}$ from the archaeon *Sulfolobus acidocaldarius* has a unique Asn-linked highly branched hexasaccharide chain containing 6-sulfoquinovose." (2000) *Eur J Biochem* **267**, 4144-4149.

43.   Vasänge, M., Rolfsen, W., and Bohlin, L. "A sulphonoglycolipid from the fern *Polypodium decumanum* and its effect on the platelet activating-factor receptor in human neutrophils." (1997) *J Pharm Pharmacol* **49**, 562-566.

44.   Gustafson, K. R., Cardellina, J. H., 2nd, Fuller, R. W., Weislow, O. S., Kiser, R. F., Snader, K. M., Patterson, G. M., Boyd, M. R., and Kikuchi, K. "AIDS-antiviral sulfolipids from cyanobacteria (blue-green algae)." (1989) *J Natl Cancer Inst* **81**, 1254-1258.

45.   Shirahashi, H., Murakami, N., Watanabe, M., Nagatsu, A., Sakakibara, J., Tokuda, H., Nishino, H., Iwashima, A., and Kikuchi, K. "Isolation and identification of anti-tumor-promoting principles from the fresh-water cyanobacterium *Phormidium tenue*." (1993) *Chem Pharm Bull (Tokyo)* **41**, 1664-1666.

46.   Reshef, V., Mizrachi, E., Maretzki, T., Silberstein, C., Loya, S., Hizi, A., and

Carmeli, S. "New acylated sulfoglycolipids and digalactolipids and related known glycolipids from cyanobacteria with a potential to inhibit the reverse transcriptase of HIV-1." (1997) *J Nat Prod* **60**, 1251-1260.

47.   Loya, S., Reshef, V., Mizrachi, E., Silberstein, C., Rachamim, Y., Carmeli, S., and Hizi, A. "The inhibition of the reverse transcriptase of HIV-1 by the natural sulfoglycolipids from cyanobacteria: contribution of different moieties to their high potency." (1998) *J Nat Prod* **61**, 891-895.

48.   Ohta, K., Hanashima, S., Mizushina, Y., Yamazaki, T., Saneyoshi, M., Sugawara, F., and Sakaguchi, K. "Studies on a novel DNA polymerase inhibitor group, synthetic sulfoquinovosylacylglycerols: inhibitory action on cell proliferation." (2000) *Mutation Research* **467**, 139-152.

49.   Sahara, H., Ishikawa, M., Takahashi, N., Ohtani, S., Sato, N., Gasa, S., Akino, T., and Kikuchi, K. "*In vivo* anti-tumour effect of 3'-sulphonoquinovosyl 1'-monoacylglyceride isolated from sea urchin (*Strongylocentrotus intermedius*) intestine." (1997) *Br J Cancer* **75**, 324-332.

50.   Ohta, K., Mizushina, Y., Hirata, N., Takemura, M., Sugawara, F., Matsukage, A., Yoshida, S., and Sakaguchi, K. "Sulfoquinovosyldiacylglycerol, KM043, a new potent inhibitor of eukaryotic DNA polymerases and HIV-reverse transcriptase type 1 from a marine red alga, *Gigartina tenella*." (1998) *Chem Pharm Bull Tokyo* **46**, 684-686.

51.   Quasney, M. E., Carter, L. C., Oxford, C., Watkins, S. M., Gershwin, M. E., and German, J. B. "Inhibition of proliferation and induction of apoptosis in SNU-1 human gastric cancer cells by the plant sulfolipid, sulfoquinovosyldiacylglycerol." (2001) *J Nutr Biochem* **12**, 310-315.

52.   Pugh, C. E., Roy, A. B., Hawkes, T., and Harwood, J. L. "A new pathway for the synthesis of the plant sulpholipid, sulphoquinovosyldiacylglycerol." (1995) *Biochem J* **309**, 513-519.

53.   Benning, C., and Somerville, C. R. "Identification of an operon involved in sulfolipid biosynthesis in *Rhodobacter sphaeroides*." (1992) *J Bacteriol* **174**, 6479-6487.

54.   Güler, S., Seeliger, A., Härtel, H., Renger, G., and Benning, C. "A null mutant of *Synechococcus* sp. PCC7942 deficient in the sulfolipid sulfoquinovosyl diacylglycerol."

(1996) *J Biol Chem* **271,** 7501-7507.

55. Rossak, M., Tietje, C., Heinz, E., and Benning, C. "Accumulation of UDP-sulfoquinovose in a sulfolipid-deficient mutant of *Rhodobacter sphaeroides*." (1995) *J Biol Chem* **270,** 25792-25797.

56. Güler, S., Essigmann, B., and Benning, C. "A cyanobacterial gene, *sqdX*, required for biosynthesis of the sulfolipid sulfoquinovosyldiacylglycerol." (2000) *J Bacteriol* **182,** 543-545.

57. Bligny, R., Gardestrom, P., Roby, C., and Douce, R. "^{31}P NMR studies of spinach leaves and their chloroplasts." (1990) *J Biol Chem* **265,** 1319-1326.

58. Pugh, C. E., Hawkes, T., and Harwood, J. L. "Biosynthesis of sulphoquinovosyldiacylglycerol by chloroplast fractions from pea and lettuce." (1995) *Phytochemistry* **39,** 1071-1075.

59. Roy, A. B., Harwood, J. L., and Kikuchi, K. "Re-evaluation of plant sulpholipid labelling from UDP-[^{14}C]glucose in pea chloroplasts." (1999) *Biochem J* **344,** 185-187.

60. Hoppe, W., and Schwenn, J. D. "*In vitro* Biosynthesis of the Plant Sulpholipid: On the Origin of the Sulphonate Group." (1981) *Zeitschrift für Naturforschung, Teil C* **36,** 820-826.

61. Bishop, D. G., Sparace, S. A., Mudd, J. B., and Kikuchi, K. "Biosynthesis of sulfoquinovosyldiacylglycerol in higher plants: the origin of the diacylglycerol moiety." (1985) *Arch Biochem Biophys* **240,** 851-858.

62. Essigmann, B., Hespenheide, B. M., Kuhn, L. A., and Benning, C. "Prediction and mechanistic implications of the active-site structure and binding of NAD$^+$ to the SQD1 sulfolipid biosynthetic enzyme of *Arabidopsis thaliana*." (1999) *Arch Biochem Biophys* **369,** 30-41.

63. Thoden, J. B., Frey, P. A., and Holden, H. M. "High-resolution X-ray structure of UDP-galactose 4-epimerase complexed with UDP-phenol." (1996) *Protein Sci* **5,** 2149-2161.

64. Gavini, N., Hausman, B. S., Pulakat, L., Schreiner, R. P., and Williamson, J. A. "Identification and mutational analysis of *rfbG*, the gene encoding CDP-D-glucose-4,6-dehydratase, isolated from free living soil bacterium *Azotobacter vinelandii*." (1997) *Biochem Biophys Res Commun* **240**, 153-161.

65. Gerratana, B., Cleland, W. W., and Frey, P. A. "Mechanistic Roles of Thr134, Tyr160, and Lys 164 in the Reaction Catalyzed by dTDP-Glucose 4,6-Dehydratase." (2001) *Biochemistry* **40**, 9187-9195.

66. Somoza, J. R., Menon, S., Schmidt, H., Joseph McCarthy, D., Dessen, A., Stahl, M. L., Somers, W. S., and Sullivan, F. X. "Structural and kinetic analysis of *Escherichia coli* GDP-mannose 4,6 dehydratase provides insights into the enzyme's catalytic mechanism and regulation by GDP-fucose." (2000) *Structure Fold Des* **8**, 123-135.

67. Rizzi, M., Tonetti, M., Vigevani, P., Sturla, L., Bisso, A., De Flora, A., Bordo, D., and Bolognesi, M. "GDP-4-keto-6-deoxy-D-mannose epimerase/reductase from *Escherichia coli*, a key enzyme in the biosynthesis of GDP-L-fucose, displays the structural characteristics of the RED protein homology superfamily." (1998) *Structure* **8**, 1453-1465.

68. Somers, W. S., Stahl, M. L., and Sullivan, F. X. "GDP-fucose synthetase from *Escherichia coli*: structure of a unique member of the short-chain dehydrogenase/reductase family that catalyzes two distinct reactions at the same active site." (1998) *Structure* **6**, 1601-1612.

69. Deacon, A. M., Ni, Y. S., Coleman, W. G., Jr, and Ealick, S. E. "The crystal structure of ADP-L-glycero-D-mannoheptose 6-epimerase: catalysis with a twist." (2000) *Structure Fold Des* **8**, 453-462.

70. Kneidinger, B., Graninger, M., Adam, G., Puchberger, M., Kosma, P., Zayni, S., and Messner, P. "Identification of two GDP-6-deoxy-D-lyxo-4-hexulose reductases synthesizing GDP-D-rhamnose in *Aneurinibacillus thermoaerophilus* L420-91T." (2001) *J Biol Chem* **276**, 5577-5583.

71. Sanda, S., Leustek, T., Theisen, M. J., Garavito, R. M., and Benning, C. "Recombinant *Arabidopsis* SQD1 converts UDP-glucose and sulfite to the sulfolipid head group precursor UDP-sulfoquinovose *in vitro*." (2001) *J Biol Chem* **276**, 3941-3946.

72.   Ito, W., Ishiguro, H., and Kurosawa, Y. "A general method for introducing a series of mutations into cloned DNA using the polymerase chain reaction." (1991) *Gene* **102,** 67-70.

73.   Sack, J. S. "CHAIN - A Crystallographic Modeling Program." (1988) *J Mol Graphics* **6,** 224-225.

74.   Brünger, A. T. (1992) *X-PLOR Manual*, Yale University Press, New Haven, Connecticut.

75.   Thoden, J. B., Frey, P. A., and Holden, H. M. "Molecular structure of the NADH/UDP-glucose abortive complex of UDP-galactose 4-epimerase from *Escherichia coli*: implications for the catalytic mechanism." (1996) *Biochemistry* **35,** 5137-5144.

76.   Thoden, J. B., Hegeman, A. D., Frey, P. A., and Holden, H. M. (1998) Protein Data Bank entry 1BXK.

77.   Brünger, A. T., Adams, P. D., Clore, G. M., Gros, P., Grosse–Kunstleve, R. W., Jiang, J.-S., Kuszewski, J., Nilges, N., Pannu, N. S., Read, R. J., Rice, L. M., Simonson, T., and Warren, G. L. "Crystallography and NMR system (CNS): A new software system for macromolecular structure determination." (1998) *Acta Cryst* **D54,** 905-921.

78.   Laskowski, R. A., MacArthur, M. W., Moss, D. S., and Thornton, J. M. "PROCHECK: a program to check the stereochemical quality of protein structures." (1993) *J Appl Cryst* **26,** 283-291.

79.   McRee, D. E. "XtalView: A Visual Protein Crystallographic Software System for XII/XView." (1992) *J Mol Graphics* **10,** 44-47.

80.   Mulichak, A. M., Theisen, M. J., Essigmann, B., Benning, C., and Garavito, R. M. "Crystal structure of SQD1, and enzyme involved in the biosynthesis of the plant sulfolipid headgroup UDP-sulfoquinovose." (1999) *Proc Natl Acad Sci USA* **96,** 13097-13102.

81.   Kleywegt, G. J., and Jones, T. A. "Databases in protein crystallography." (1998) *Acta Cryst* **D54,** 1119-1131.

82. Auerbach, G., Herrmann, A., Gütlich, M., Fischer, M., Jacob, U., Bacher, A., and Huber, R. "The 1.25 Å crystal structure of sepiapterin reductase reveals its binding mode to pterins and brain neurotransmitters." (1997) *EMBO J* **16**, 7219-7230.

83. Rosano, C., Bisso, A., Izzo, G., Tonetti, M., Sturla, L., De Flora, A., and Bolognesi, M. "Probing the Catalytic Mechanism of GDP-4-keto-6-deoxy-D-mannose Epimerase/Reductase by Kinetic and Crystallographic Analysis of Site-specific Mutants." (2000) *J Mol Biol* **303**, 77-91.

84. Thoden, J. B., Frey, P. A., and Holden, H. M. "Crystal structures of the oxidized and reduced forms of UDP-galactose 4-epimerase isolated from *Escherichia coli*." (1996) *Biochemistry* **35**, 2557-2566.

85. Thoden, J. B., Wohlers, T. M., Fridovich-Keil, J. L., and Holden, H. M. "Crystallographic evidence for Tyr 157 functioning as the active site base in human UDP-galactose 4-epimerase." (2000) *Biochemistry* **39**, 5691-5701.

86. Tanaka, N., Nonaka, T., Nakanishi, M., Deyashiki, Y., Hara, A., and Mitsui, Y. "Crystal structure of the ternary complex of mouse lung carbonyl reductase at 1.8 Å resolution: the structural origin of coenzyme specificity in the short-chain dehydrogenase/reductase family." (1996) *Structure* **4**, 33-45.

87. Derewenda, Z. S., Lee, L., and Derewenda, U. "The occurrence of C-H•••O hydrogen bonds in proteins." (1995) *J Mol Biol* **252**, 248-262.

88. Steiner, T., and Saenger, W. "Role of C-H•••O hydrogen bonds in the coordination of water molecules. Analysis of neutron diffraction data." (1993) *J Amer Chem Soc* **115**, 4540-4547.

89. Thoden, J. B., Wohlers, T. M., Fridovich-Keil, J. L., and Holden, H. M. "Human UDP-galactose 4-epimerase: accommodation of UDP-N-acetylglucosamine within the active site." (2001) *J Biol Chem* **276**, 15131-15136.

90. Oppermann, U. C., Filling, C., Berndt, K. D., Persson, B., Benach, J., Ladenstein, R., and Jörnvall, H. "Active site directed mutagenesis of 3β/17β-hydroxysteroid dehydrogenase establishes differential effects on short-chain dehydrogenase/reductase

reactions." (1997) *Biochemistry* **36**, 34-40.

91. Irie, S., Doi, S., Yorifuji, T., Takagi, M., and Yano, K. "Nucleotide sequencing and characterization of the genes encoding benzene oxidation enzymes of enzymes of *Pseudomonas putida*." (1987) *J Bacteriol* **169**, 5174-5179.

92. Shahbaz, M., Hoch, J. A., Trach, K. A., Hural, J. A., Webber, S., and Whiteley, J. M. "Structural studies and isolation of cDNA clones providing the complete sequence of rat liver dihydropteridine reductase." (1987) *J Biol Chem* **262**, 16412-16416.

93. Kiefer, P. M., Varughese, K. I., Su, Y., Xuong, N. H., Chang, C. F., Gupta, P., Bray, T., and Whiteley, J. M. "Altered structural and mechanistic properties of mutant dihydropteridine reductases." (1996) *J Biol Chem* **271**, 3437-3444.

94. Gourley, D. G., Schüttelkopf, A. W., Leonard, G. A., Luba, J., Hardy, L. W., Beverley, S. M., and Hunter, W. N. "Pteridine reductase mechanism correlates pterin metabolism with drug resistance in trypanosomatid parasites." (2001) *Nat Struct Biol* **8**, 521-525.

95. Liu, Y., Thoden, J. B., Kim, J., Berger, E., Gulick, A. M., Ruzicka, F. J., Holden, H. M., and Frey, P. A. "Mechanistic roles of tyrosine 149 and serine 124 in UDP-galactose 4-epimerase from *Escherichia coli*." (1997) *Biochemistry* **36**, 10675-10684.

96. Swanson, B. A., and Frey, P. A. "Identification of lysine 153 as a functionally important residue in UDP-galactose 4-epimerase from *Escherichia coli*." (1993) *Biochemistry* **32**, 13231-13236.

97. Thoden, J. B., Gulick, A. M., and Holden, H. M. "Molecular structures of the S124A, S124T, and S124V site-directed mutants of UDP-galactose 4-epimerase from *Escherichia coli*." (1997) *Biochemistry* **36**, 10685-10695.

98. Chen, Z., Jiang, J. C., Lin, Z. G., Lee, W. R., Baker, M. E., and Chang, S. H. "Site-specific mutagenesis of *Drosophila* alcohol dehydrogenase: evidence for involvement of tyrosine-152 and lysine-156 in catalysis." (1993) *Biochemistry* **32**, 3342-3346.

99. Cols, N., Marfany, G., Atrian, S., and Gonzalez-Duarte, R. "Effect of site-directed mutagenesis on conserved positions of *Drosophila* alcohol dehydrogenase." (1993) *FEBS*

Lett **319,** 90-94.

100. Cols, N., Atrian, S., Benach, J., Ladenstein, R., and Gonzalez-Duarte, R. "*Drosophila* alcohol dehydrogenase: evaluation of Ser139 site-directed mutants." (1997) *FEBS Lett* **413,** 191-193.

101. Fujimoto, K., Ichinose, H., Nagatsu, T., Nonaka, T., Mitsui, Y., and S., K. "Functionally important residues tyrosine-171 and serine-158 in sepiapterin reductase." (1999) *Biochim Biophys Acta* **1431,** 306-314.

102. Fujimoto, K., Hara, M., Yamada, H., Sakurai, M., Inaba, A., Tomomura, A., and S., K. "Role of the conserved Ser-Tyr-Lys triad of the SDR family in sepiapterin reductase." (2001) *Chem Biol Interact* **130-132,** 825-832.

103. Ensor, C. M., Tai, H. H., and Follmann, H. "Site-directed mutagenesis of the conserved tyrosine 151 of human placental NAD^+-dependent 15-hydroxyprostaglandin dehydrogenase yields a catalytically inactive enzyme." (1991) *Biochem Biophys Res Commun* **176,** 840-845.

104. Ensor, C. M., and Tai, H. H. "Bacterial expression and site-directed mutagenesis of two critical residues (tyrosine-151 and lysine-155) of human placental NAD^+-dependent 15-hydroxyprostaglandin dehydrogenase." (1994) *Biochim Biophys Acta* **1208,** 151-156.

105. Ensor, C. M., and Tai, H. H. "Site-directed mutagenesis of the conserved serine 138 of human placental NAD^+-dependent 15-hydroxyprostaglandin dehydrogenase to an alanine results in an inactive enzyme." (1996) *Biochem Biophys Res Commun* **220,** 330-333.

106. Kiefer, P. M., Grimshaw, C. E., and Whiteley, J. M. "The comparative interaction of quinonoid (6R)-dihydrobiopterin and an alternative dihydropterin substrate with wild-type and mutant rat dihydropteridine reductases." (1997) *Biochemistry* **36,** 9438-9445.

107. Vedadi, M., Barriault, D., Sylvestre, M., and Powlowski, J. "Active site residues of cis-2,3-dihydro-2,3-dihydroxybiphenyl dehydrogenase from *Comamonas testosteroni* strain B-356." (2000) *Biochemistry* **39,** 5028-5034.

108. Winberg, J. O., Brendskag, M. K., Sylte, I., Lindstad, R. I., and McKinley-McKee,

J. S. "The catalytic triad in *Drosophila* alcohol dehydrogenase: pH, temperature and molecular modelling studies." (1999) *J Mol Biol* **294,** 601-616.

109. Nakajima, K., Yamashita, A., Akama, H., Nakatsu, T., Kato, H., Hashimoto, T., Oda, J., and Yamada, Y. "Crystal structures of two tropinone reductases: different reaction stereospecificities in the same protein fold." (1998) *Proc Nat Acad Sci USA* **95,** 4876-4881.

110. Sawicki, M. W., Erman, M., Puranen, T., Vihko, P., and Ghosh, D. "Structure of the ternary complex of human 17β-hydroxysteroid dehydrogenase type 1 with 3-hydroxyestra-1,3,5,7-tetraen-17-one (equilin) and NADP." (1999) *Proc Natl Acad Sci USA* **96,** 840-845.

111. Gross, J. W., Hegeman, A. D., Vestling, M. M., and Frey, P. A. "Characterization of enzymatic processes by rapid mix-quench mass spectrometry: the case of dTDP-glucose 4,6-dehydratase." (2000) *Biochemistry* **39,** 13633-13640.

112. He, X., Thorson, J. S., and Liu, H. W. "Probing the coenzyme and substrate binding events of CDP-D-glucose 4,6-dehydratase: mechanistic implications." (1996) *Biochemistry* **35,** 4721-4731.

113. Gabriel, O., and Lindquist, L. C. "Biological mechanisms involved in the formation of deoxy sugars: IV. enzymatic conversion of thymidine diphosphoglucose-4T to thymidine diphospho-4-keto-6-deoxyglucose-6T." (1968) *J Biol Chem* **243,** 1479-1484.

114. Oths, P. J., Mayer, R. M., and Floss, H. G. "Stereochemistry and mechanism of the GDP-mannose dehydratase reaction." (1990) *Carbohydr Res* **198,** 91-100.

115. Glaser, L., and Zarkowsky, R. (1971) in *The Enzymes* (Boyer, P., ed) Vol. 5, pp. 465–480, Academic Press, New York.

116. Menon, S., Stahl, M., Kumar, R., Xu, G. Y., and Sullivan, F. "Stereochemical course and steady state mechanism of the reaction catalyzed by the GDP-fucose synthetase from *Escherichia coli*." (1999) *J Biol Chem* **274,** 26743-26750.

117. Thoden, J. B., and Holden, H. M. "Dramatic differences in the binding of UDP-galactose and UDP-glucose to UDP-galactose 4-epimerase from *Escherichia coli*."

(1998) *Biochemistry* **37**, 11469-11477.

118. Cleland, W. W. "Low-barrier hydrogen bonds and enzymatic catalysis." (2000) *Arch Biochem Biophys* **382**, 1-5.

119. Gerlt, J., Kreevoy, M., Cleland, W., and Frey, P. "Understanding enzymic catalysis: the importance of short, strong hydrogen bonds." (1997) *Chemistry & Biology* **4**, 259-267.

120. Cleland, W. W., Frey, P. A., and Gerlt, J. A. "The low barrier hydrogen bond in enzymatic catalysis." (1998) *J Biol Chem* **273**, 25529-25532.

121. Thoden, J. B., Wohlers, T. M., Fridovich-Keil, J. L., and Holden, H. M. "Molecular basis for severe epimerase-deficiency galactosemia: X-ray structure of the human V94M-substituted UDP-galactose 4-epimerase." (2001) *J Biol Chem* **276**, 20617-20623.

122. Luo, J., Kahn, K., and Bruice, T. C. "The linear dependence of $\log(k_{cat}/K_m)$ for reduction of NAD^+ by $PhCH_2OH$ on the distance between reactants when catalyzed by horse liver alcohol dehydrogenase and 203 single point mutants." (1999) *Bioorganic Chemistry* **27**, 289-296.

123. van Aalten, D. M., Bywater, R., Findlay, J. B., Hendlich, M., Hooft, R. W., and Vriend, G. "PRODRG, a program for generating molecular topologies and unique molecular descriptors from coordinates of small molecules." (1996) *J Comput Aided Mol Des* **10**, 255-262.

124. Yamashita, A., Kato, H., Wakatsuki, S., Tomizaki, T., Nakatsu, T., Nakajima, K., Hashimoto, T., Yamada, Y., and Oda, J. "Structure of tropinone reductase-II complexed with $NADP^+$ and pseudotropine at 1.9 Å resolution: implication for stereospecific substrate binding and catalysis." (1999) *Biochemistry* **38**, 7630-7637.

125. Tuazon, P. T., and Johnson, S. L. "Free radical and ionic reaction of bisulfite with reduced nicotinamide adenine dinucleotide and its analogues." (1977) *Biochemistry* **16**, 1183-1188.

126. Shimazaki, K., Nakamachi, K., Kondo, N., and Sugahara, K. "Sulfite Inhibition of Photosystem-II in Illuminated Spinach Leaves." (1984) *Plant and Cell Physiology* **25**,

337-341.

127. Lizada, M. C. C., and Yang, S. F. "Sulfite-induced Lipid Peroxidation." (1981) *Lipids* **16,** 189-194.

128. Wurfel, M., Haberlein, I., and Follmann, H. "Facile sulfitolysis of the disulfide bonds in oxidized thioredoxin and glutaredoxin." (1993) *Eur J Biochem* **211,** 609-614.

129. Leustek, T., Martin, M. N., Bick, J. A., and Davies, J. P. "Pathways and regulation of sulfur metabolism revealed through molecular and genetic studies." (2000) *Annual Review of Plant Physiology and Plant Molecular Biology* **51,** 141-165.